# An Investigation Of The Use Of Haematoporphyrin And Helium-Neon Laser Excitation For The Detection Of Cancers By Means Of Fluorescent Endoscopy

A THESIS FOR THE DEGREE OF

Master of Science

PRESENTED TO

Dublin City University

BY

Colin Joseph Kelly BSc (Hons)

School of Physical Sciences

Dublin City University

RESEARCH SUPERVISOR

Dr. W.J.M. van der Putten

September 1991

TABLE OF CONTENTS

# ABSTRACT

In this study the use of a He-Ne laser as excitation source in fluorescent endoscopy is investigated Fluorescence endoscopy is based on the principle of injecting a fluorescent tumour localiser prior to examination with a fibre-optic endoscope Tumours marked by the fluorescent localiser can then be identified by the detection of the characteristic fluorescence output of the localiser The localiser examined in this research is Haematoporphyrin or Hp

Previous studies with Hp have generally utilised the violet portion of the visible spectrum (400nm) to excite fluorescence Spectroscopic studies carried out in this project reveal that He-Ne laser light (632 8nm) can be used to excite Hp fluorescence It is shown that 632nm excitation possesses significant advantages over the use of violet light for the detection of small tumours deeply embedded in healthy tissue

One such type of tumour is early small cell carcinoma of the tracheo-bronchial (TB) tract These tumours may only be a few millimetres in extent and up to 0 5mm thick Such a small tumour will have very small amounts of the Hp marker material This combined with the fact that Hp has a very low excitation efficiency at 630nm will result in a very low fluorescent emission To detect such a low level light signal a highly efficient illumination and detection system is required Such a system has been developed and is described in chapter 3 In vitro experimentation demonstrates that the system can detect fluorescence from concentrations of Hp down to as low as 0 01 $\mu$g/ml in methanol and 0 1 $\mu$g/ml in water

A comprehensive mathematical model has been developed to predict the response of the detection system for the detection of early small cell TB tumours The model predicts that the instrument can detect tumours as low as 2 5mm in extent and 0 3mm thick embedded deep within the submucosa of the TB tract

In order to measure the response of the instrument in conditions which simulate a clinical environment a tumour-tissue phantom has been developed Experiments carried out on the phantom with the endoscopic apparatus yield results in very good agreement with those predicted by the model

In conclusion it has been shown that He-Ne laser light can be used as an effective excitation source in fluorescent endoscopy for the detection of previously undetectable tumours The use of He-Ne laser excitation in fluorescent endoscopy could then play a role in the cancer screening of high risk sections of the population

Chapter 1

# LITERATURE REVIEW

## 1 1 Introduction

Photomedicine has been defined as *the use of light in medically related activities including the prevention of disease,the preparation of pharmaceuticals, the diagnosis and treatment of disease, and the elucidation and etiology of disease* (1) In recent years research activity has expanded both in terms of fundamental research and in the clinical applications of photomedicine Modern applications of photomedicine can be divided into two categories

(i) where light is utilised alone e g the surgical application of lasers and the treatment of jaundice in premature babies by means of their exposure to ultra-violet light ,

(ii) where light is used in conjunction with a previously administered light sensitive dye

In the latter case the use of tumour-seeking agents such as Haematoporphyrin Derivative (HpD) have been used in combination with light to localise as well as treat cancer tumours The basic principles of this technique are outlined in Fig 1.1 (2). HpD in low concentration is injected intravenously It spreads quickly through the body 2-3 days later it is observed to selectively

accumulate in tumour tissue while being removed from healthy tissue by natural processes The mechanisms for this retention are still unclear

Light irradiation of the tumour bound HpD, with wavelengths corresponding to one of its excitation peaks, will result in the emission of a characteristic red fluorescence The detection of this HpD fluorescence above background serves to identify the location of the tumour If enough light energy is supplied to the tumour, light induced chemical changes triggered by the HpD molecules can occur causing eventual tumour destruction This cancer treatment is known as Photodynamic therapy (PDT) Thus a combination of light and HpD may be used in both the diagnosis and treatment of cancers

It is the aim of this project to design and test an effective system for the detection of fluorescence from a HpD marked tumour Firstly a review of the early development of photomedicine is presented It is shown how this leads to the discovery of photosensitisers and ultimately to the utilisation of the fluorescent and localising properties of HpD for the detection of tumourous areas. Subsequently recent clinical techniques for the detection of cancers using HpD are reported It is in the light of these techniques that a system is designed and tested for the detection of HpD fluorescence (see chapter 3)

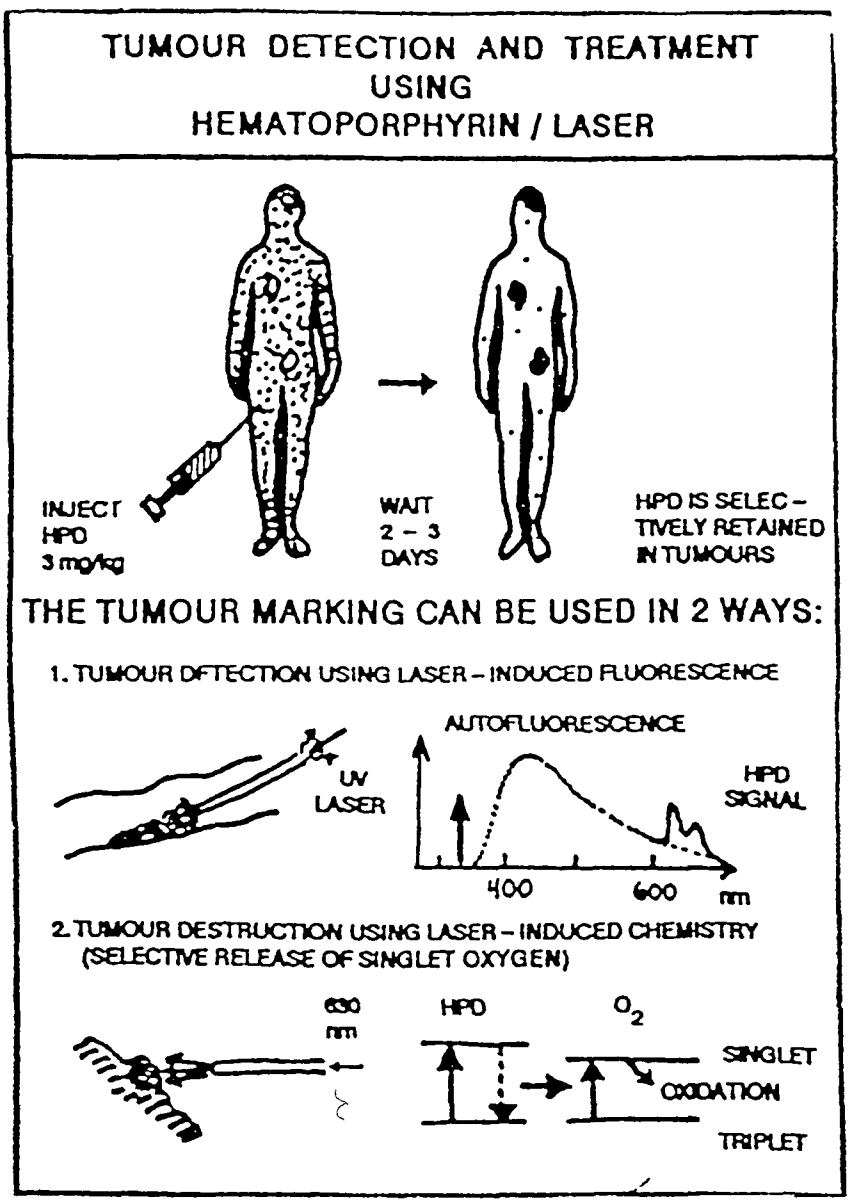


Fig 1.1 Schematic diagram of cancer detection using HpD in combination with laser irradiation (2)

1 2 Historical Background

Although evidence exists that the ancient Chinese and Egyptians (1) were aware of the medical properties of light, modern studies began only about 100 years ago when the Danish scientist Niels Finsen successfully treated the tubercular skin lesion known as lupus vulgaris This disease manifests itself by the protrusion of darkly coloured lesions on the surface of the skin and was endemic among Scandinavians during the dark winter months Finsen proposed that the disease was caused by underexposure to ultra-violet (u v) light from the sun By exposing a lesion to irradiation from a u v source he was able to trigger intrinsic chemical reactions which destroyed the lesion The process by which this occurred was then a mystery, but the disease was observed to clear up and within 10 years of Finsen commencing his treatments had all but disappeared in Scandinavian countries By this technique Finsen had established the principle that light could be used in medicine By the turn of the century photomedical techniques were being tested in the Finsen Institute in Copenhagen, and in the London Hospital Finsen received the Nobel Prize for Medicine in 1903 and the science of photomedicine was born (3)

At around the same time Oscar Raab, a medical student in Munich, found that low concentrations of acridine and other dyes demonstrated a rapid killing of small multicellular organisms such as protozoa and paramecium

upon illumination (4) During the course of the next few years his professor, Hermann Von Tappeiner, conducted a series of experiments on biological tissues He found that upon light irradiation cellular damage could be affected in the presence of a wide variety of dyes The photochemical reactions which caused cell death and necrosis only occurred when the tissue was irradiated with wavelengths of light corresponding to the absorption peaks of the dye When Von Tappeiner published his results in 1903 (5) he suggested the combined use of light and eosin as a treatment for a number of skin diseases ranging from skin cancer to herpes Von Tappeiner and Raab had discovered the existence of photosensitive dyes which were normally inactive but could be photo-activated to induce chemical reactions which could destroy tissue This added an extra dimension to photomedicine as it suggested the possibility of being able to selectively destroy tumourous areas while leaving the surrounding tissue unharmed The therapeutic prospects of such a discovery seemed very bright indeed

## 1 3 In Search of the Ideal Photosensitiser

The use of photosensitive dyes in medicine appeared very promising but early medical applications were to prove disappointing Clinical trials by von Tappeiner and Jesionek were a limited success (6) Skin tumours in 3 patients were treated using a topically applied eosin solution as photosensitiser. All 3 patients showed some improvement. Other dyes such as fluorescein, acridine orange and magdaline red were also used with similar but

with inconclusive results (6) In 1925 Copeman et al (7) attempted to treat skin tumours by painting fluorescein solutions onto the affected areas and illuminating these areas with light from a Mercury arc lamp He reported no favourable results These drawbacks served to dampen early enthusiasm for photosensitisation The momentum was regained in 1942 when Auler, Banzer and Figge focussed their attention on the photosensitising properties of a group of chemical compounds known as the porphyrins (8)

The photosensitising properties of porphyrins were first demonstrated in 1913 Meyer Betz, an Austrian chemist, injected himself with 200 mg of Haematoporphyrin (Hp) and observed that in the presence of light the exposed parts of his body became red and swollen The effect lasted for several weeks post injection (3) Auler et al (8) injected laboratory animals with a porphyrin solution and upon illumination they detected red fluorescence from surface tumours After the war, Figge continued his research and showed that Hp was the most effective porphyrin for the localisation of a wide variety of cancer types (9)

In 1961 Lipson and Baldes (10) pointed out that the fluorescent yield and the localising capability of Hp in tumours, were variable This was attributed to the varying composition of the Hp mixture which they were using Subsequently they standardised the preparation of Hp into a Haematoporphyrin Derivative (HpD) (11). HpD has been shown to be a complex mixture of various porphyrins and a full description of its preparation and constituents is outlined

in chapter 2 Lipson and Baldes (10) outlined the advantages of using HpD as follows

(1) Greater localisation in malignant cells.

(2) Less accumulation in healthy tissue

(3) Greater consistency and reproducibility in results

The excitation and fluorescent spectra of HpD are almost identical to that of Hp, although HpD has a slightly lower fluorescence yield

By the use of HpD and a sufficiently intense ultra-violet illumination source, Lipson and Baldes were able to observe good localised fluorescence for a number of tumour types The results were significantly better than those using crude Hp Clinical trials followed and by 1967 Lipson was able to report a 95% detection rate for malignant tumours in humans (12) Since then HpD and commercial variants has been the main photosensitiser in clinical use for the detection of tumours (27)

## 1 4 Instrumentation and Methods in Tumour Detection

Tumour detection using HpD relies on two main properties of porphyrins namely their high fluorescent quantum yield and their localising ability Throughout the years numerous clinical techniques have been developed to exploit the use of HpD in cancer diagnosis Recently with advances in endoscopic technology interest has increased in the use of HpD for the early detection of thin superficial tumours in the bronchial and gastro-intestinal tracts This field of interest has been termed "fluorescence endoscopy" In this section several techniques of cancer diagnosis using fluorescence endoscopy are discussed Any apparatus must include both a system for the conduction of excitation light to the porphyrin bound in the tumour and a system for the collection and detection of the resultant fluorescence In order to simplify the discussion methods of fluorescence endoscopy are reviewed in terms of whether an arc-lamp or a laser are used as excitation source

### 1 4 1 Arc Lamp Systems

Before the invention of the laser, arc-lamps were the light sources of choice in photomedicine Finsen (3) had used a carbon arc-lamp for treating lupus vulgaris and Raab and and Von Tappeiner (4) (5) had used Mercury (Hg) arc-lamps in their studies Similarly many researchers have used arc-lamps as the excitation source in fluorescence endoscopy

In 1979 Profio and Doiron (13) outlined the use of a

200 W Hg arc lamp with a fluorescent bronchoscope for the detection of tracheo-bronchial (TB) tumours An advantage of using a Hg-lamp was that use could be made of the strong Hg line at 404 7nm , which corresponds to the major excitation peak of HpD In fig 1 2 the system of Profio and Doiron is illustrated

The lamp is focussed on a narrow bandpass violet filter centred at 405nm, in order to remove any unwanted Hg emission The resultant violet light is refocused onto a specially made bundle of quartz-glass which has enhanced ultra-violet transmission This bundle carries the 405nm excitation light to the tumour site where the HpD bound to the tumour fluoresces in a broad red region of the spectrum from approximately 630nm to 690nm The fluorescent light is then focussed by means of a lens onto an imaging bundle At the proximal end of this bundle the light is passed through a red filter, in order to reject any reflected violet light which may have travelled down the imaging bundle The remaining "pure" fluorescence image is incident on the photocathode of an image intensifier and the fluorescent image from the intensifier is viewed directly Alternately, the fluorescent signal can be passed to an appropriate photodetector and amplifier and the fluorescent signal measured digitally The authors reported the detection of TB tumours in 3 of 4 patients previously known to have cancer. In a later publication (14), however, they conceded that the tumours detected were also visible by x-ray and conventional white-light bronchoscopy

The main disadvantage in the use of ultra-violet excitation light is the presence of a large healthy tissue auto-fluorescent signal which tends to mask the characteristic HpD fluorescence from the tumour The phenomenon of auto-fluorescence is caused by the excitation of intrinsic chromophores present in healthy tissue and gives rise to many false diagnoses The auto-fluorescence spectrum of HpD is contained in fig 1 1 Maximum auto-fluorescence emission is obtained for excitation at violet wavelengths (i e 400-450nm) In order for tumour detection to occur the HpD fluorescence must be detected above the auto-fluorescent signal

In 1986, Mattiello and Hetzel (15), described a similar system using a Hg-Xe lamp, and a bi-furcated fibre bundle. This bundle consisted of a quartz excitation fibre designed to transmit only light around 405nm, and a glass bundle constructed to transmit only 630nm fluorescence Excitation light is passed down the fibre to the tumour and the fluorescent signal was detected using a narrow bandpass red filter and a photomultiplier tube (PMT) situated at the end of the fluorescent bundle A chopper is used to alternately switch off the excitation signal while the white light of an illumination guide is transmitted to enable the clinician to observe the area under treatment in a normal fashion The voltage signal from the PMT is converted to frequency and used to produce an audio signal for the clinician

The use of a chopper in this set-up allows for the

detection to occur in phase with the excitation signal, and thus reduces the level of background noise detected

The papers reviewed above indicate that arc-lamps can be used in fluorescence endoscopy However several disadvantages inherent in the use of arc-lamps have become evident These disadvantages are outlined below ·

1 Heavy filtering is required to select the correct wavelength and reduce the auto-fluorescent signal from the tissue

2 The low light intensities obtained from arc-lamps at the desired wavelength necessitate the use of high wattage lamps These lamps prove expensive and the high voltages required often interfere with the detection electronics

3 It is difficult to couple arc-lamp light into single fibres. For this reason thick fibre-bundles are required to convey the excitation light This limits the locations within the body which the arc-lamp can access

In 1987, however, Anderson et al (16), described a technique which used a Hg arc lamp and avoided some of the disadvantages mentioned above Their method used a standard endoscope and involved the use of a Hg lamp to supply both

the excitation (405nm) light and the white light required for normal illumination. As in the case of Mattiello et al they used an optical chopper to alternately switch on the white light illumination while switching off the excitation light and the photodetector. In their chopper (see Fig 1.3) they incorporated a green and a red filter which allowed the detection of both the HpD fluorescence(red) and the normal tissue fluorescence (auto-fluorescence, green). This red:green ratio, when gathered electronically, was the basis for their tumour detection. Furthermore, by extrapolating the normal tissue fluorescence to the red region of the spectrum a value for the tissue auto-fluorescence, at the HpD fluorescent wavelengths was obtained. This value was subtracted electronically from the detected signal to give a true value for the fluorescent signal.

In this method tumour fluorescence was detected using a standard clinical endoscope. Its filtered chopper and ratio method of fluorescence detection reduced the problems due to auto-fluorescence and incorporated the advantages of Mattiello's system.

In 1988 Lenz (17) introduced a new concept when he described an endoscopic system whereby a chopper was used to alternately detect fluorescent signal (F) and reflected excitation light (R), from a Xenon arc lamp. The ratio F:R is then used as a measure of tumour detection. The authors claimed that this technique has the effect of reducing the effect of parameters such as distance of fibre bundle from the tumour, the power of the source, and any temporal

variations which may influence the system

The techniques mentioned in this section have increasingly maximised the efficiency of using arc lamps as excitation sources by removing the disadvantages of background signal and tissue auto-fluorescence as effectively as possible Despite this other disadvantages remain, the most serious of which is the poor coupling efficiency into single fibres In practice arc lamps are still in use The reason for this is that they are simple, relatively inexpensive, reliable, and, in the case of most research institutions and hospitals , readily available

If fluorescence endoscopy is to establish itself as a valuable method of cancer diagnosis, its success must lie in the early detection of small cancers otherwise undetectable to conventional cancer diagnostic techniques It was for this reason that attention was focussed on the laser. Lasers have a very good coupling efficiency into single fibres facilitating the use of more flexible endoscopes which can access more remote tumour sites Similarly they are monochromatic with intense emission at a single wavelength In the following section several techniques of fluorescence endoscopy using lasers are assessed

1 4 2 Laser Systems

Most of the techniques described in the arc-lamp section can be performed, with slight modifications, using a laser source The most commonly used laser is the CW Krypton ion laser which typically has a power output of circa 1 watt and can lase at 407nm (close to the main absorption peak of HpD) Other lasers that have been used are the argon-ion laser and several pumped dye lasers The reasons why lasers are not more widely used is that they are not always readily available and that they are relatively expensive with a Krypton ion laser costing circa $60-120,000

It was Profio and Doiron (1979) (18) who first proposed the use of a Krypton ion laser as excitation source They used a system similar to their earlier apparatus in which a Hg arc lamp was used. The main difference was that with the laser they could now use a single excitation fibre Consequently, the light intensity at the distal end of the fibre was higher and the entire system was more flexible, and capable of detecting more remote tumours Cortese and Kinsey (1979) (19) also described a similar endoscopic apparatus utilising a Krypton ion laser Clinical trials, however, showed that the potential of fluorescence endoscopy was limited by the large number of erroneous results obtained These errors could be classified as follows

(1) False Positive results caused by the violet light excitation of intrinsic tissue chromophores i e tissue autofluorescence

(2) False Negative results caused by tumours located under epithelial layers thick enough to absorb all of the excitation light

In order to alleviate these problems Zandomeneghi et al (20) suggested the use of He-Ne lasers for the excitation of the tumour bound HpD He-Ne lasers are cheap, reliable and easy to maintain and install They emit at 632 8nm, which corresponds to one of the minor absorption peaks of HpD

Zandomeneghi et al reported the use of an instrument for the detection of HpD fluorescence from large tumours grown on the legs of laboratory mice. A 10mW He-Ne laser was used as excitation source and the resultant fluorescence passed through an infra-red filter and detected on photographic film In this way fluorescence images of the tumour site were obtained The photographic plates were then scanned using a micro-densitometer and fluorescent readings from both tumour bearing and normal animals recorded. A ratio of these values was then obtained. By using this ratio problems due to residual noise and background auto-fluorescence were reduced Although they used a large experimental tumour the authors claimed the advantages of using red light were significant and suggested the He-Ne laser as the ideal excitation source for use in fluorescence endoscopy

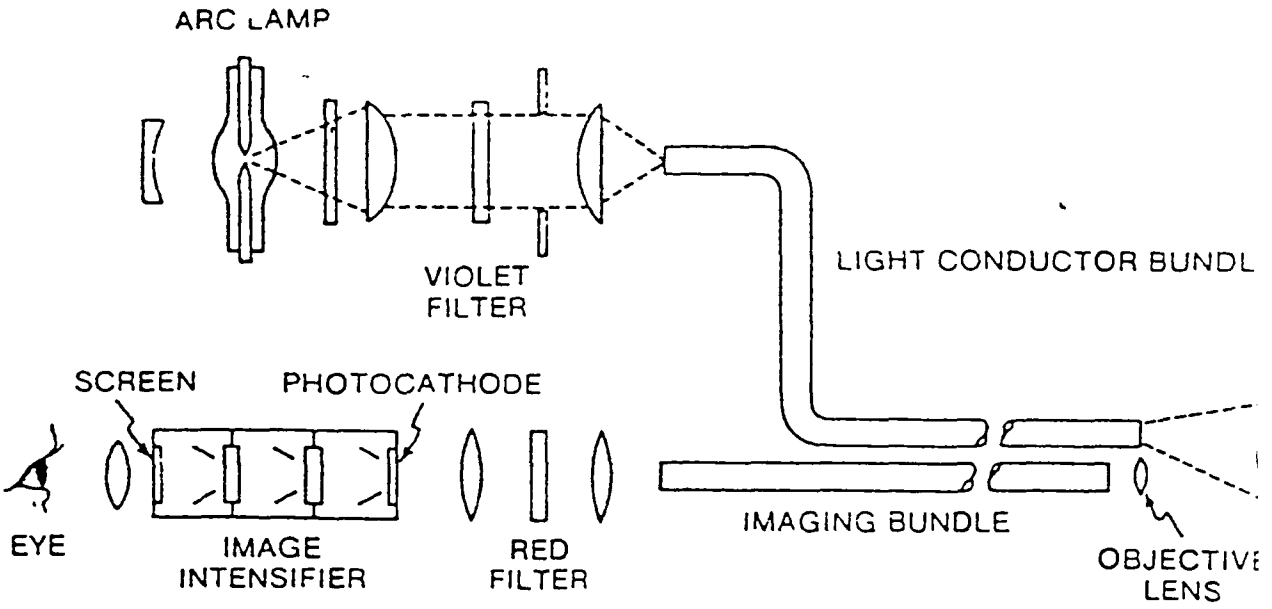


Fig 1 2 Fluorescent Broncoscope system of Profio and Doiron (1979)

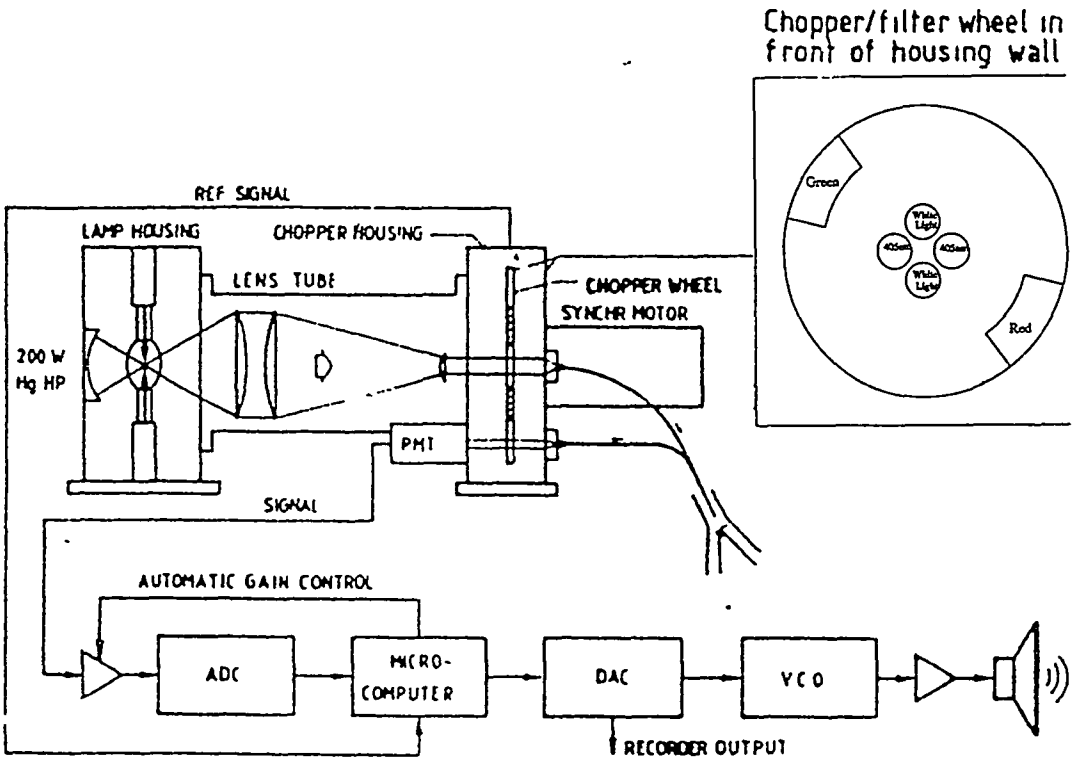


Fig 1 3 Fluorescent endoscope instrument of Andersson et al (1987)

## 1.5 Conclusion

The discovery of the fluorescent and localising properties of Hp followed by its standardisation into HpD has prompted much research into its exploitation for the early detection of tumourous areas. In the field of fluorescence endoscopy the poor coupling efficiency of arc-lamps into single fibres seems to severely limit the locations in which tumour detection can occur. Laser light however can be coupled down single fibres and access remote areas in the tracheo-bronchial (TB) and gastro-intestinal (GI) apparatus. From the literature however the use of Krypton-ion lasers have been shown to result in large numbers of false diagnoses. The use of red He-Ne laser light, as proposed by Zandomeneghi (20), seems to offer a more attractive proposition than the use of violet Krypton laser light for the following reasons

(1) red light has good penetration in tissue (significantly better than blue light penetration)

(2) red light penetration is not affected by the presence of blood while blue light is strongly absorbed by Hemoglobin

(3) autofluoresence at 630nm is negligible compared to levels recorded at blue wavelengths.

(4) 630nm is the wavelength used for therapy purposes via PDT.

The problem with using a He-Ne laser is that power outputs are low and its emission at 630nm corresponds to a minor absorption peak of HpD For this reason any system using a He-Ne laser as source must incorporate a detection system capable of detecting very small fluorescent signals

Recently the use of ratio methods of fluorescent detection have been outlined (16,20) These methods present an advantage over straight fluorescence detection in that they are claimed to reduce the effect of extraneous factors on the detection process This is a particular advantage when dealing with tumour fluorescence detection

In the light of the techniques reviewed in this chapter an instrument is developed in chapter 3 which investigates the use of a He-Ne laser for excitation and a ratio method for the detection of Hp fluorescence The sensitivity of this system is tested and its adaptability for the detection of human tumours via fluorescence endoscopy assessed

# Chapter 2

# HAEMATOPORPHYRIN

## 2 1 Introduction

A photosensitiser can be defined as *a chemical compound which is normally stable and inert but upon photostimulation initiates chemical changes in other compounds in its environment* (24) In this chapter the photosensitising dye Haematoporphyrin (Hp) is discussed Together with its photosensitising properties Haematoporphyrin has been noted to selectively accumulate in tumourous tissue (see chapter 1) This property is known as localisation Haematoporphyrin's twin properties of photosensitisation and localisation have been used in medicine to both detect and treat cancer tumours In this chapter the photosensitising and localising properties of Haematoporphyrin are described and the mechanisms by which Hp is used to both detect and treat tumours are outlined

Work is then presented on the examination of the excitation and emission spectra of Hp This work was carried out using a spectrofluorimeter and on solutions of Hp in an aqueous environment These spectra serve to locate

the excitation peaks of Hp and provide a comparison of the location and strength of fluorescent emission for each excitation peak The sensitivity limits i e the lowest detectable concentrations of Hp are then obtained for each of the excitation peaks This provides information on the feasibility of using red light over violet light as excitation source in fluorescence endoscopy

## 2 2 Porphyrins

The porphyrins are one of the oldest and most well documented of chemical families They are characterized by their bright colours and strong fluorescent properties (3) Their parent substance, porphin, is a purple crystalline solid, made up of four pyrole rings each containing four carbon atoms and one nitrogen atom linked to form a large ring (see fig 2 1) In the centre of the ring is a cavity surrounded by the four nitrogen atoms of the four rings This cavity can accommodate any one of a variety of metal ions The chemical properties of each porphyrin depend on the presence and type of metal present in the centre

Porphyrins are readily found in nature and play a vital role in the process of living Iron porphyrins called haems are found in hemoglobin and myoglobin Protohaem, the porphyrin in hemoglobin is responsible for carrying oxygen to the tissues in mammals Chlorophylls, which play a role in photosynthesis in plant cells, are porphyrins with a magnesium ion in the core.

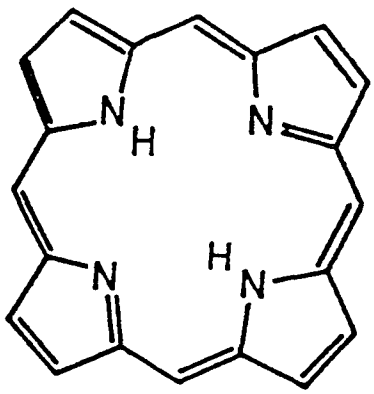


Fig 2 1 The chemical structure of porphin

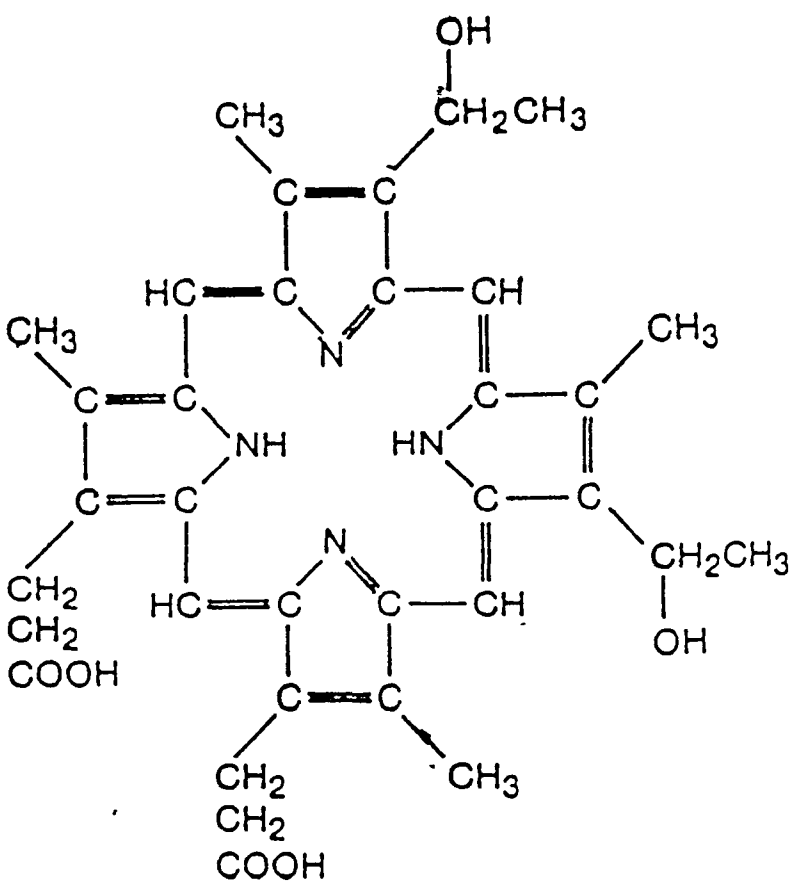


Fig 2 2 The chemical structure of Haematoporphyrin

## 2 3 Haematoporphyrin (Hp)

The first porphyrin to be synthesized artificially was Haematoporphyrin, when in 1867 J L Thudicum prepared it by treating Hemoglobin with sulfuric acid and following that with extraction with alcohol (21) Hp is characterized by the absence of a metal ion in its core and the presence of two hydroxyethyl groups, two propionic acid groups and four methyl groups attached to the four pyrole ring (see fig 2 2) Haematoporphyrin is not a naturally occurring compound and has not been isolated in nature Indeed a statement has been made in the literature (27) that a pure sample of Hp has never been produced

Since its discovery Hp has been extensively studied and analyzed (for a review see Kessel (22)) In medicine researchers became interested in Hp because of its properties of photosensitisation and localisation In 1960 Lipson and Baldes suggested that these two properties could be exploited in tandem for the detection and treatment of cancer It was not until the early 1970s (Diamond 1972 (23), Barenbaum et al 1975) that such a technique began to be used clinically In the following sections these two properties of localisation and photosensitisation are discussed in more detail.

### 2.3.1 Localisation:

No adequate explanation has yet been brought forward to explain why porphyrins localise in tumorous tissue despite the fact that it has been observed since the 1940s. In 1942 Auler, Banzer and Figge (8) discovered that mouse tumours selectively retained Hp after its disposal by healthy tissue. In 1961 Lipson and Baldes (10) reported the selective retention of Hp in human cancer cells, 2-3 days after the porphyrin was injected into the blood stream. This property of Hp localisation together with the strong fluorescent properties of Hp made it possible to locate previously undetectable tumours.

### 2.3.2 Photosensitisation

In order to understand how a photosensitiser works let us consider a system consisting of 2 chemical compounds X, Y. As this system does not contain a photosensitiser it does not exhibit any photochemical change when irradiated with light of particular wavelengths. Thus :

$$(X,\ Y) \xrightarrow{h\upsilon} (X,\ Y) \qquad \text{(no reaction)}$$

However when the photosensitiser (S) is present the photochemical reaction does occur as follows :

$$(X, Y) \xrightarrow{h\upsilon} (X, P) \quad \text{(sensitized reaction } Y \rightarrow P\text{)}$$

Hp's properties as a photosensitiser have been well known, ever since Mayer-Betz's famous 1913 experiment (25) (described in chapter 1) In this chapter the role of Hp as a photosensitising agent in biological tissue is emphasized

Most cells are rather insensitive to direct effects of visible light, (the exception being cells which contain melanin and other natural pigments), since their major organic constituents do not absorb appreciably in this wavelength range In the presence of an appropriate photosensitiser such as Hp, organisms, cells and many types of biologically important molecules can be damaged and destroyed by visible light (24)

In the case of Hp the photosensitised reaction results eventually in a change of the electronic energy of molecular oxygen ($O_2$) from its stable triplet state to a highly reactive singlet state This singlet state attacks fatty materials and cell membranes causing cell death If sufficient cells are killed tissue necrosis will occur In the next section these photosensitised reactions are discussed in more detail.

## 2.4 The Role of Hp in the Detection and Treatment of Cancer

In fig 1 1 the various stages involved in the detection and treatment of tumours using Haematoporphyrin are outlined After about 2 days post injection the Hp is seen to selectively accumulate at the tumour site while it has been removed from healthy tissue by natural processes

If the tumour is then exposed to visible light the presence of the photosensitiser will cause the following two simultaneous reactions to occur .

(1) The emission of characteristic red Hp fluorescence

(2) The conversion of oxygen molecules within the tumour from their stable triplet state to the highly reactive singlet states

The mechanism by which these reactions occur is outlined on the following pages

In order to study the mechanisms by which these photosensitised reactions occur it is important to discuss the absorption spectra of Hp The major absorption of Hp occurs in the so called Soret band peaking at 405nm and corresponding to transitions from the ground singlet state to the second excited singlet state Further minor excitation peaks at 500, 530, 570, and 630nm respectively correspond to transitions to the first excited singlet state (see fig 2.3) Regardless of how the excitation was performed the molecules are non-radiatively transferred to the lowest vibrational level of the singlet state from

where fluorescence occurs Hp exhibits a characteristic dual-peaked fluorescent light distribution in the red spectral region. The detection of this spectral finger-print serves to identify the location of the tumour

Alternatively the excited Hp molecules can transfer their acquired energy to oxygen molecules at the tumour site This transfer is mediated by the long-lived metastable triplet state to which radiationless transitions can occur. This triplet Hp state has an energy of greater than 94 kilo joules per mole above that of the ground state

Molecular oxygen requires a large energy outlay of 94 kilo joules per mole to be excited from its very stable triplet ground state to highly reactive singlet oxygen Visible light has more than enough energy to bring about the triplet-singlet transition But oxygen is transparent and thus has no way of directly absorbing that energy Triplet-singlet transition can occur however in the presence of a photosensitiser such as Hp Triplet Hp molecules transfer their acquired energy to the oxygen molecules and return to the ground state This energy is just enough to facilitate molecular oxygen triplet to singlet conversion Singlet molecular oxygen is a strong toxic agent and oxidizes the surrounding (tumour) tissue

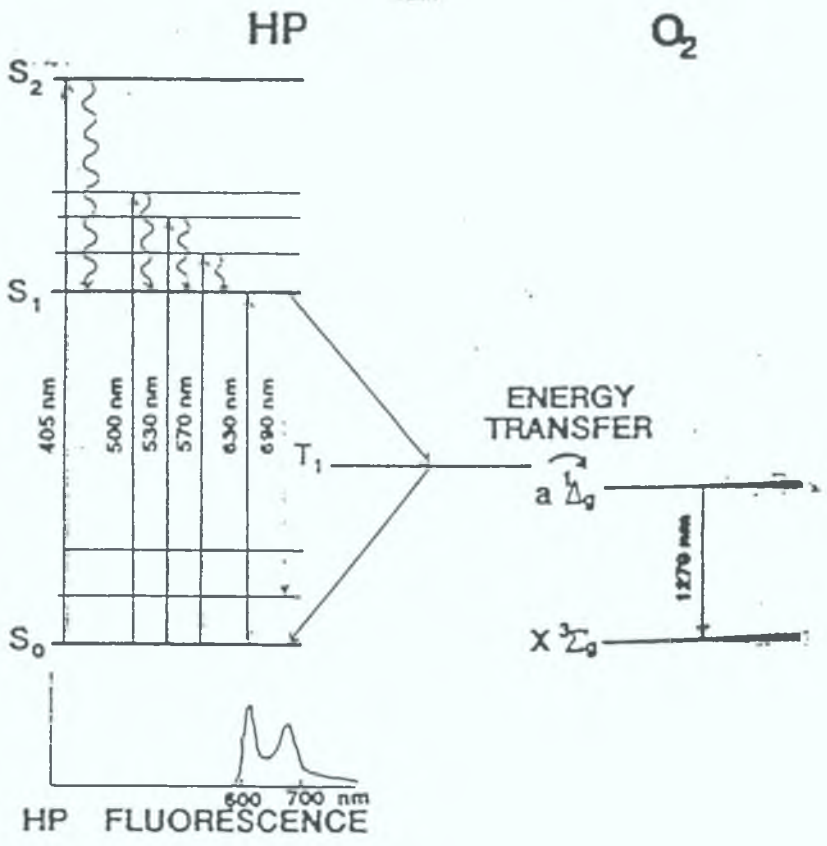


Fig 2.3 Energy level diagrams and processes relevant to photosensitised reactions involving Hp in tissue (2).

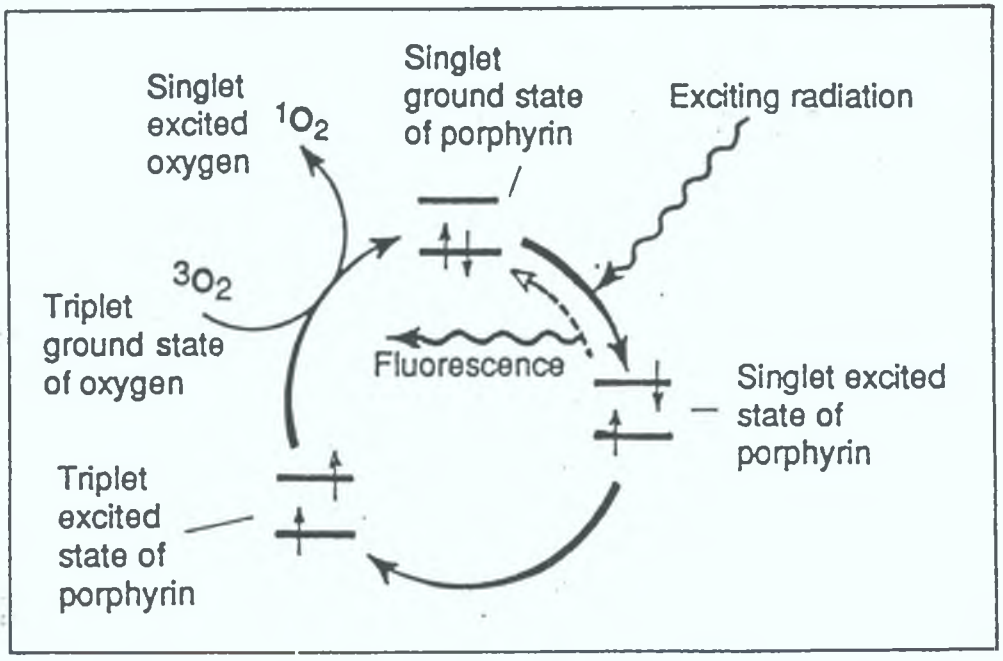


Fig 2.4 An outline of how Hp combines with light radiation to produce fluorescence and singlet oxygen (3).

Both the emission of characteristic Hp fluorescence and the production of singlet oxygen occur simultaneously in Hp marked tumours upon irradiation with light containing the correct wavelength components Jori (1987) (53) has quoted a quantum yield of 0 63 for the production of singlet oxygen by Hp in an aqueous environment upon 630nm excitation In this way both the localising and photosensitising properties of Hp can be exploited in order to detect and treat cancer tumours In fig 2 4 the mechanism (described above) by which visible light and Hp combine to produce fluorescence and singlet oxygen within tissue is schematically outlined

## 2.5 Haematoporphyrin Derivative (HpD)

In the previous section it has been shown how Haematoporphyrin (Hp) can be used in conjunction with visible light for the location and destruction of tumour tissue. In clinical circumstances however the use of Hp is problematic for the following reasons :

(1) Hp is not a naturally occurring substance and a pure sample has proven difficult to extract. Doiron (27) has reported that a pure sample of Hp has never been made available. Furthermore it has been shown by Schwarz and co-workers (27) that commercial preparations of Hp are a crude mixture of many porphyrins This was confirmed by Bonnett (28) who examined samples of available Hp using high pressure liquid chromatography (HPLC), and found an average of 10% impurities in each sample. These results cause unacceptable variability in results and make Hp difficult to control in a clinical situation.

(2) Richelli and Grossweiner (29) reported that age, temperature and pH of solution cause variation in the photochemistry of Hp.

(3) It is difficult to dissolve Hp.

Irreproducibility of results in clinical use with Hp was indeed noted by Lipson and Baldes (11). Schwarz (27) attributed this to variations in the chemical composition of the Hp samples they were using. In order to evaluate whether a more refined technique based on the accumulation

of an administered porphyrin in a tumour could be utilised for cancer detection Lipson and Baldes prepared Haematoporphyrin Derivative (HpD)

HpD is prepared by treating Haematoporphyrin dihydrochloride with a solution of sulfuric acid and acetic acid The full preparation is described fully elsewhere i.e Doiron and Bonnett (27,28) HpD is also not a pure compound HPLC studies by Moan and Summer (30) have revealed that HpD is a mixture of many compounds with at least four major components which are named 2, 4A, 4B, and 7 Component two is ascribed to free Hp while 7 is protoporphyrin and the two other components are thought to be a mixture of numerous porphyrins The results of one such HPLC study is outlined in fig 2 5

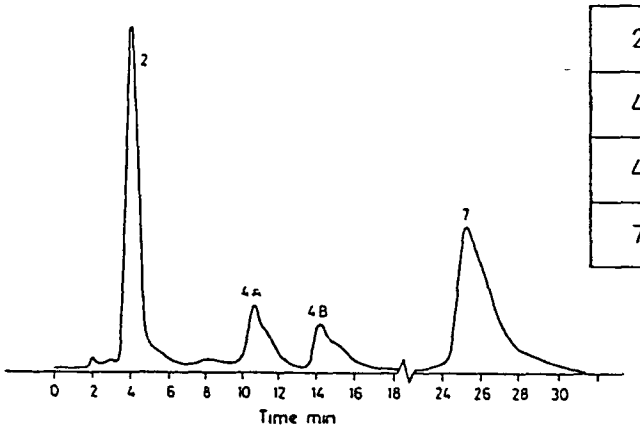


| | |
|---|---|
| 2 | 48% |
| 4A | 30% |
| 4B | 16% |
| 7 | 5% |

Fig 2 5 HPLC studies of the major constituents of HpD and their respective volumes (as reported by Moan and Summer (30))

HpD has been found to have a greater localising ability than Hp (Lipson (11)) Moan and Summer suggested this to be due to a complex formed between component 2 and component 7 The fluorescent quantum yields between Hp and HpD are comparable and the absorption spectra of HpD is red shifted 5-10nm due to increased dimerisation (Pottier et al (31))

HpD can be prepared relatively simply However extensive purification is required to obtain a relatively pure sample of the constituents with the highest tumour localising ability The standard preparation of HpD provides a compound reasonably free from impurities and with greater localising ability than Hp This is of great benefit in clinical practice At present work is in progress to further purify the derivative, and Photofrin I and Photofrin II are the commercially available purifications currently in widespread use (26) Photofrin II is the product which is currently used for clinical trials

## 2 6 Experimental Studies

In order to locate the excitation peaks of Hp and compare and contrast fluorescence emission at each peak a spectroscopic analysis of a solution of Hp + $H_2O$ was undertaken In this way the magnitude of the excitation peaks and their relative efficiency for the excitation of fluorescence from a HpD marked tumour can be assessed In chapter 1 the use of red light instead of the conventional violet excitation was proposed The spectroscopic studies carried out in this section allow a comparison to be made of the use of red over violet wavelengths for the stimulation of Hp fluorescence

Although HpD and its commercial purifications (i e Photofrin II) are used in clinical procedures it was decided to carry out these tests with Hp The reason for this is that the cost of Photofrin II is prohibitive and laboratory procedures for the extraction of Haematoporphyrin derivative (HpD) from Hp are quite complex As the photo physical properties of Hp and HpD are similar it was considered that Hp could be used as a convenient model for the clinically utilised HpD

### 2 6.1 Procedure

Emission and excitation spectra were measured with a Perkin Elmer MPF 44B spectrofluorimeter This system utilises a Xenon arc lamp as excitation source and a

Hamamatsu R928 photomultiplier tube for detection The monochromator slits were set at a width of 4 5mm for maximum signal. All of the spectra obtained were corrected for the wavelength response of the spectrofluorimeter This had been determined previously by van der Putten (54)

In section 2 5 it has been pointed out that the photo physical properties of Hp can be affected by factors such as pH, age and temperature. Similarly due to impurities, the chemical composition of one Hp solution may differ markedly from another causing a change in spectroscopic characteristics In order to obtain as great a degree of reproducibility of results as possible, a standard preparation of Hp solutions was developed Samples of anhydrous Hp were taken from a single vial. The Hp was weighed on a sensitive balance and added to 30 ml solutions of distilled water These solutions were refrigerated for 24 hours in order to preserve the samples while the dissolution process continued The resultant samples were placed in the spectrophotometer and excitation spectra obtained Fluorescent emission spectra were obtained for each of the excitation peaks The concentration of Hp in solution was progressively diluted in order to obtain the lowest concentration of Hp for which fluorescence could be detected for each of the excitation peaks. None of the Hp samples were kept for longer than 36 hours in total

2.6.2 Results

The literature (31) suggests that the main Hp fluorescence band is centred at 675nm. With the emission monochromator of the spectrophotometer centred at 675nm the excitation spectrum of Hp + $H_2O$ was obtained by scanning the excitation wavelength from 400 to 640nm and monitoring the fluorescent output at 675nm. This spectrum is shown in fig 2.6.

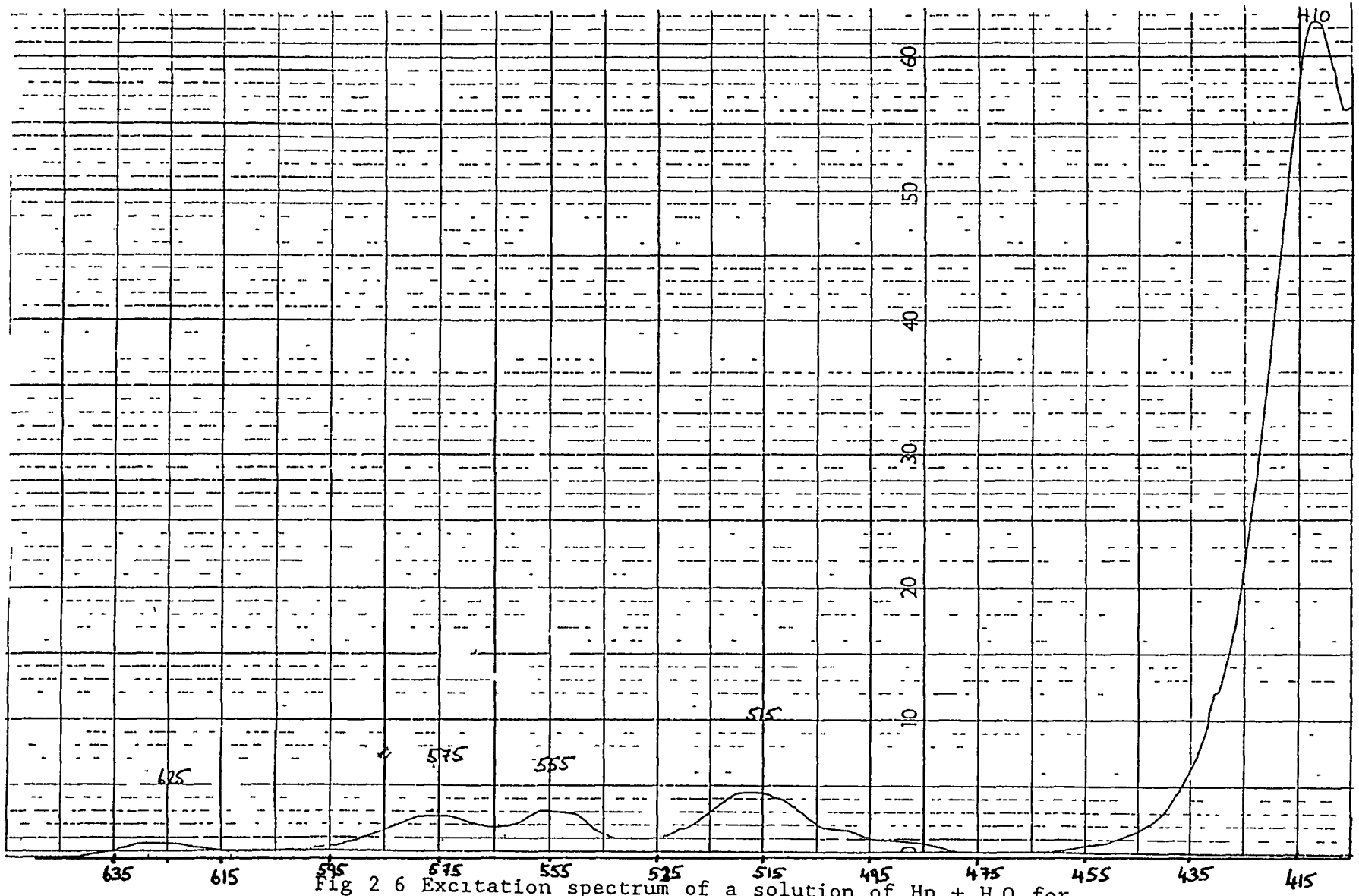


Fig 2 6 Excitation spectrum of a solution of Hp + $H_2O$ for emission at 675nm

The spectrum reveals the presence of five excitation bands centred at 410, 515, 555, 565 and 625nm respectively If the peak height of the 410nm band is taken as 100 then the relative magnitudes can be expressed as 100 4 4 6 4 8 1 8 In chapter 1 the use of He-Ne laser light to excite fluorescence from a HpD marked tumour was proposed From fig 2 6 ıt is apparent that excitation of Hp can occur at 632nm (the lasing line of the He-Ne laser) but is much less efficient in comparison to the excitation obtaınable at the commonly used 405nm

Using the same spectrophotometer the fluorescent spectra of Hp + $H_2O$ were obtained for excitation at 410, 515, 555, 565 and 632nm respectively In this way the fluorescent peaks of the Hp solution are located Comparison of the emission characteristics at these wavelengths provides informatıon on the type of excitation sources which can be used in fluorescence endoscopy In chapter 1 the use of He-Ne laser light (632nm), instead of the commonly used Kr-ion laser light (410nm), as excitation source in fluorescent endoscopy is proposed Emission spectra for 410 and 632nm excıtation were obtained in order to compare the fluorescent emission obtained at these two wavelengths The emission spectra for each of the five excitation wavelengths were obtained for increasingly dilute solutions of Hp + $H_2O$ The sensitivity limit i e the

lowest concentration of Hp for which fluorescence can be detected were found for each excitation wavelength

In fig 2 7 fluorescent spectrum obtained by exciting a solution of 1μg Hp per ml of $H_2O$, with 410nm light is shown It displays a three peak spectrum, with peaks at 585, 615 and 679nm These peaks are well documented (see Andreoni)(26) As the concentration of Hp in solution is reduced it was noticed that the 585 peak grows to be the largest peak These three peaks are also visible upon 555 excitation while 515nm and 565nm excitation yields just the 615 and 679nm peaks Upon 632nm excitation (see fig 2 8) the 679nm peak has red shifted to circa 685nm In fig 2.9 the fluorescent peaks and their sensitivity limits are outlined

| Excitation (nm) | Emission (nm) | Sens Limit (μg/ml) |
|---|---|---|
| 410 | 580 | $3\ 16x10^{-7}$ |
| | 615 | $9\ 0x10^{-8}$ |
| | 679 | $1\ 0x10^{-3}$ |
| 515 | 615 | $3\ 1x10^{-6}$ |
| | 679 | $5\ 0x10^{-3}$ |
| 555 | 580 | $1\ 7x10^{-3}$ |
| | 615 | $1\ 7x10^{-4}$ |
| | 679 | $7\ 9x10^{-3}$ |
| 575 | 615 | $1\ 0x10^{-2}$ |
| | 679 | $2\ 4x10^{-2}$ |
| 632 | 685 | 0 36 |

Fig 2 9 Table of fluorescent sensitivity levels

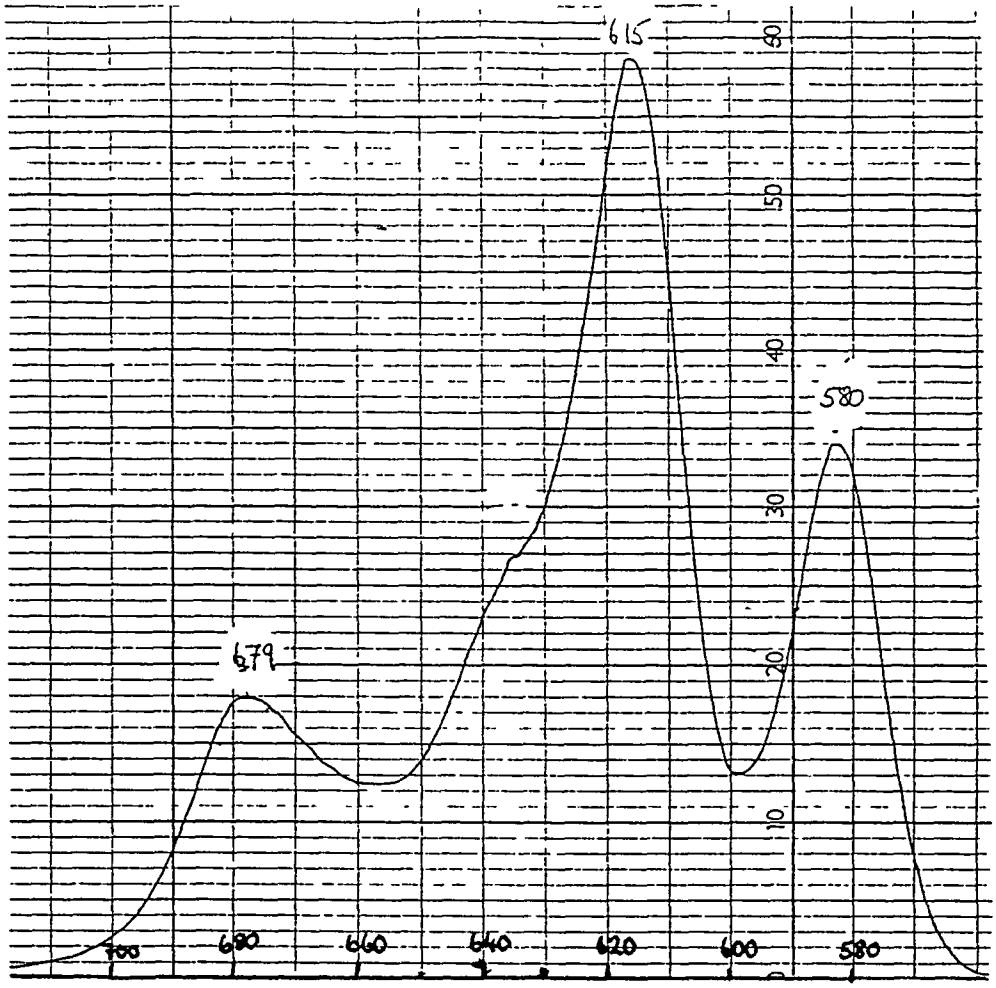


Fig 2 7 Emission Spectrum of Hp + $H_2O$
upon 410nm excitation
Concentration 1$\mu$g/ml

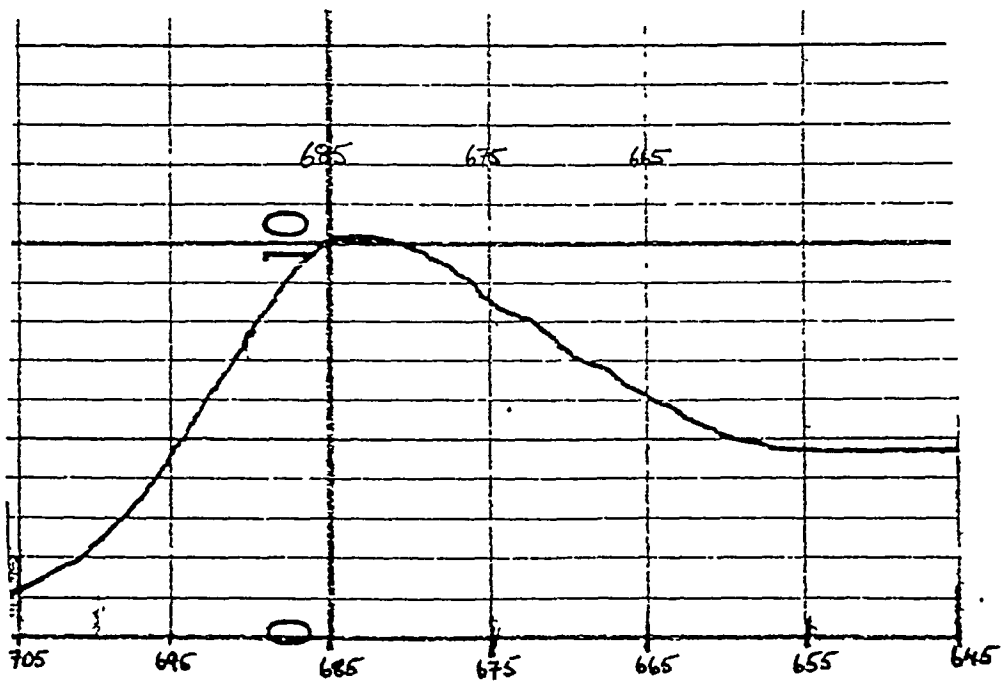


Fig 2.7 Emission Spectrum of Hp + $H_2O$
upon 632nm excitation
Concentration 10$\mu$g/ml

2 6 3 Discussion

The results obtained in fig 2 6 for the excitation spectra of Hp duplicate the results reported by Andreoni and Cubeddu in 1983 (26) Richelli and Grossweiner (29) report a similar excitation spectrum for Hp in a phosphate buffer solution As a number of outside factors such as shifts in pH, temperature and age of solution, can influence porphyrin spectra, it is not exactly valid to compare results from different authors However Andreoni (HpD in water) (26), Doiron (HpD in fetal calf serum) (27) and van der Putten (HpD in serum) (54) have all reported similar excitation spectra for HpD with a circa 5nm red shift From fig 2 6 it is apparent that the excitation band centred in the red (625nm) is about 75 times smaller than the violet excitation peak (410nm) This is due to the low absorption of Hp molecules in the red spectral region

The emission spectra obtained in this chapter reveal three fluorescent emission peaks for Hp at circa 585, 615 and 678nm The in vivo detection of these fluorescent wavelengths can thus be used for the identification of tumourous tissue in techniques such as fluorescent endoscopy The sensitivity limits obtained for these fluorescent peaks (see fig 2 9) provide an indication as to the relative efficiency of each of the excitation peaks for the detection of Hp fluorescence Concentrations of up to 1$\mu$g of HpD per gram of tumour have been reported to accumulate in tumourous tissue (27) From fig 2 9 it is

seen that sensitivity limits well below this figure are obtained for each of the excitation wavelengths Although these figures represent the detection of in-vitro fluorescence under ideal circumstances they indicate that each of the excitation wavelengths investigated could be effective for the in-vivo detection of tumours including the red 632nm wavelength proposed in chapter 1

## 2.7 Conclusion

In this chapter the photosensitising dye haematoporphyrin was discussed. Its chemical structure was briefly outlined and its properties as a localiser and photosensitiser are described The mechanisms by which it is effective for both the detection and therapy of cancer tumours upon photo-stimulation were then briefly described

Haematoporphyrin derivative as its name suggests is a derivative of the pure Hp. Both compounds have the same photo physical properties although HpD is a better localiser than Hp For this reason the commercially available form, Photofrin II, is currently the most common photosensitiser used in clinical trials Photofrin II is very expensive and the extraction of HpD from Hp is a complex chemical process. Thus it was considered that for in vitro fluorescent detection tests, Hp can be used as a model for the clinically popular HpD

In fig 2 6 five excitation peaks for Hp were located at 410, 515, 555, 575, and 625nm respectively Of these the Soret Band (405nm) is by far the largest

From table 2 9 it is obvious as to why the Soret Band is the most commonly utilised excitation wavelength in fluorescent endoscopy Extremely low concentrations of Hp in solution are detectable upon excitation at this wavelength In this regard Hg arc lamps and Kr-ion lasers have been used in clinical situations (see chapter 1) The main disadvantage with Soret Band excitation is that violet light has poor penetration in tissue This makes it impossible to detect bloody tumours or tumours beneath a layer of healthy tissue Similarly violet excitation stimulates a large auto-fluorescent signal (see chapter 1) from healthy tissue This signal known as auto-fluorescence tends to mask the HpD fluorescence and hinder the detection of tumourous tissue

The excitation peaks at 515, 555, and 575nm have better penetration in tissue than violet light Argon ion lasers with emission at 514nm and tunable dye lasers with emissions close to the 555nm and 575nm have all been investigated as possible sources for fluorescent endoscopy Indeed it can be seen from fig 2 9 that quite low concentrations of Hp can be detected using these wavelengths. These wavelengths are generally not used in clinical studies because they stimulate a considerable

auto-fluorescent signal from the healthy tissue layers surrounding the tumour

The use of He-Ne laser light (632 8nm) as excitation source in fluorescent endoscopy has been recently proposed (20) The advantages of using He-Ne light are outlined in chapter 1 and are good penetration in tissue, low auto-fluorescence, and the fact that 630nm is the wavelength used in photodynamic therapy of tumours A sensitivity limit of 0 36$\mu$g/g has been obtained in this chapter for the 632nm excitation of Hp in solution This is much higher than the limit obtained for Soret excitation This means that much lower concentrations of Hp can be detected upon violet excitation than upon He-Ne excitation. However violet light will only propagate in superficial tissue layers while 632nm light can propagate deep into tissue This suggests that He-Ne laser excitation may be effective for the detection of tumours lying deep within a healthy tissue bed One such cancer is the early small cell carcinoma of the tracheo-bronchial tract. Such tumours could not be reached by violet excitation light The sensitivity limit of He-Ne light for Hp detection at 0 36$\mu$g/ml is still lower than the 1$\mu$g/g concentration of HpD quoted to accumulate in tumourous tissue In the light of these facts it was considered that further investigation of the use of He-Ne light for the detection of deep lying tumours was justified

# Chapter 3

## SYSTEM DESIGN AND ANALYSIS

### 3 1 Introduction

In chapter 1 the topic of fluorescence endoscopy was introduced and several techniques for its use in cancer diagnosis were outlined A review of clinical procedures found that the use of blue excitation light resulted in a high proportion of false diagnoses The use of red excitation light has been suggested in a recent paper (20) The authors claimed that the use of red excitation light has significant advantages over blue light and would reduce the number of false diagnoses In this chapter the suitability of using red He-Ne laser light (632 8nm) as excitation source in fluorescence endoscopy is investigated

There are two main disadvantages inherent in the use of He-Ne excitation light Firstly, He-Ne lasers have generally very low power outputs ( typically 1-10mW ) Secondly, as has been shown in chapter 2, the excitation peak of Hp at 630nm is very small compared to that of the

most commonly utilised blue wavelength i e 405nm Similarly the Hp fluorescence stimulated with He-Ne excitation was found to be very weak in comparison to that obtained for other excitation wavelengths

In this chapter a system is developed for the detection of in-vitro Hp fluorescence using a He-Ne laser as excitation source The system is designed, on the basis of the results obtained in chapter 2, for the detection of low level fluorescence signals It is constructed using readily available pieces of laboratory equipment and although the system is designed for the detection of in-vitro Hp fluorescence it could easily form the basis of a clinical instrument for the detection of tumours via fluorescence endoscopy The system incorporates a fibre-optic bundle and fluorescent detection is achieved by means of a photomultiplier tube and lock-in amplifier , chosen for their ability to detect low level light signals In the following sections a theoretical analysis of the performance of the system is presented and experiments are carried out to determine the sensitivity limit of the system for the detection of Hp fluorescence ( i e the lowest concentration of Hp for which fluorescent detection is possible) In this manner the design and performance of the instrument can be assessed and the suitability of using a He-Ne laser as excitation source in clinical fluorescence endoscopy can be investigated

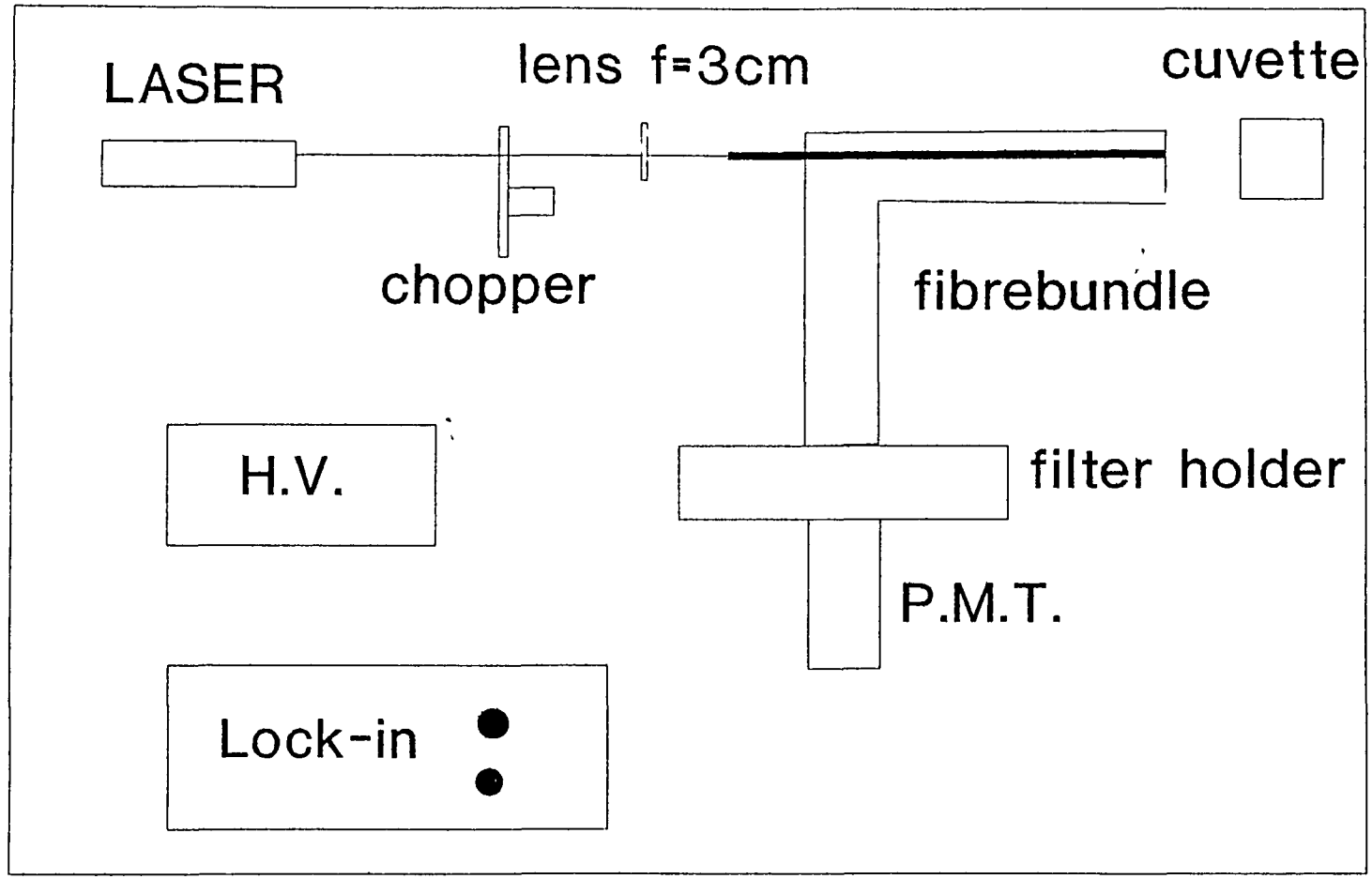


Fig 3 1 Schematic diagram of the fluorescent detection apparatus

3 2 Apparatus

A simplified diagram of the experimental apparatus utilised in this chapter is presented in fig 3 1 A 5mW He-Ne laser is used to excite a Hp solution contained within a glass cuvette The laser light is first passed through an optical chopper which modulates the light at a frequency of 200Hz Experiments on the system reveal little variation in detected Hp fluorescence with chopping frequency For this reason a convenient frequency of 200Hz was chosen As all experiments were carried out in a dark room stray frequency components from overhead fluorescent lights did not interfere with the detection electronics

In order to simulate the use of a fluorescent endoscope the laser light is conveyed to the Hp solution via a single 600$\mu$m diameter excitation fibre The light is focussed onto the fibre by means of a lens (focal length = 3cm). By placing a photo-diode alternately at the optical chopper and at the distal end of the fibre a fibre-coupling efficiency of 0 8 was measured The light leaving the distal end of the fibre is coupled directly into a 1cm thick cuvette containing the Hp + $H_2O$ solution The resultant fluorescent and backscattered excitation light fluxes are collected by the fibre-bundle and conducted to a filter-holder which is located between the fibre-bundle and the photocathode of the photomultiplier tube (PMT). Two optical filters are then used to alternately transmit these light fluxes to the PMT

The light signals are detected by the PMT and passed

to a lock-in amplifier The lock-in receives a reference signal from a slotted opto-switch located on the chopper and amplifies only those signals in phase with the chopped laser light The amplified signals can then be read from the digital display of the lock-in In this manner a ratio of scattered fluorescent signals is obtained It was decided to monitor this dimensionless ratio as a means of fluorescent detection as many problems that would otherwise be encountered in clinical work are thus eliminated (see 3 2 6)

In assembling the apparatus used in this experimental set-up the cost and availability of equipment was a consideration In the detection system boxcar averaging or photon counting techniques can equally be used to obtain a ratio of scattered fluorescent light signals The choice of a lock-in together with the other pieces of equipment used in the instrument represent the use of common and readily accessible pieces of laboratory equipment In the following sections the design and performance of the instrument is described in more detail

### 3 2.1 The Fibre-Bundle

A fibre-bundle was constructed for experimental use in this chapter The bundle consists of a single 600$\mu$m diameter excitation fibre surrounded by a cluster of 200$\mu$m diameter collection fibres (core diameters are 570 and

190$\mu$m respectively) The numerical aperture (NA) of both the excitation and collection fibres is 0 44

A theoretical examination of the detection efficiency of the fibre-bundle was undertaken in order to estimate the amount of fluorescent light sampled by the fibre-bundle

The He-Ne laser light leaving the distal end of the excitation fibre will define a cone as it enters the sample

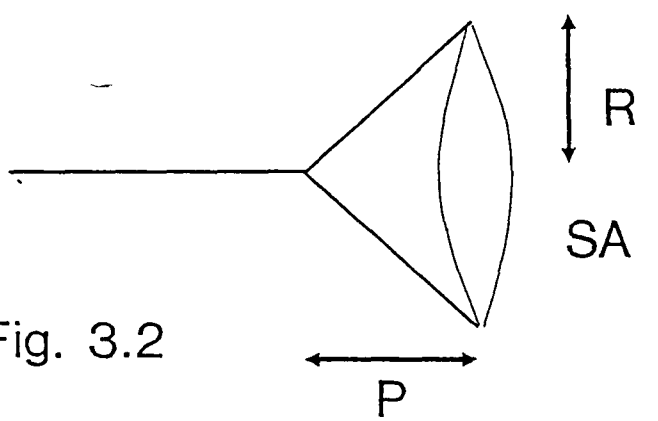


Fig. 3.2

Fig 3.2 Light cone leaving excitation fibre

where SA = area of illumination (area at base of the cone)

R = radius of circular area SA

P = height of cone (i e distance from fibre-tip)

n = refractive index of medium (for $H_2O$ n = 1 33)

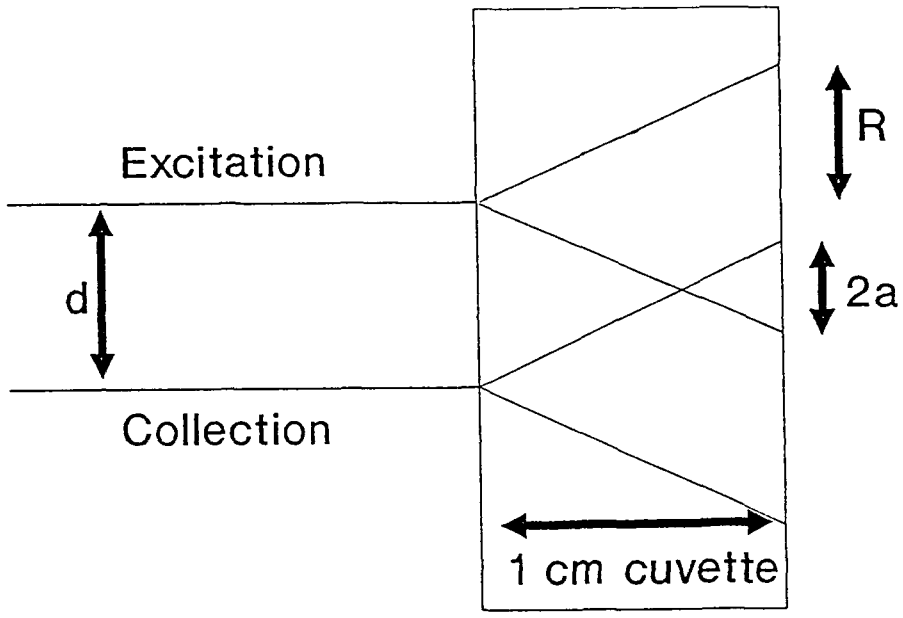


Fig 3.3 Schematic Representation of excitation and collection light cones within the cuvette

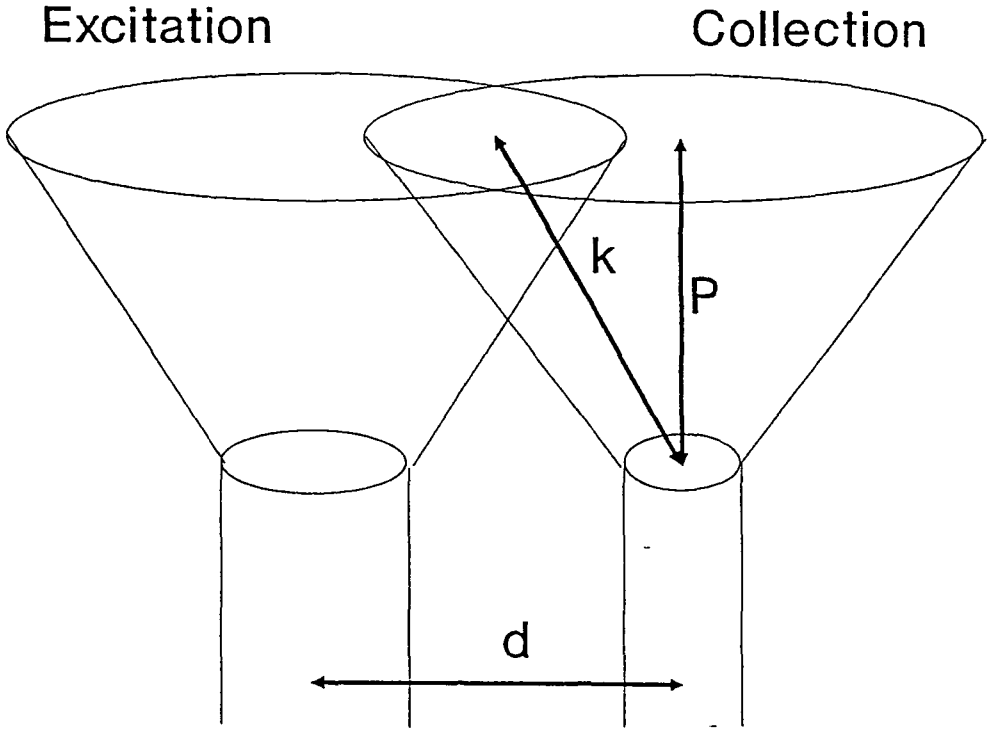


Fig 3 4 Excitation and collection light cones with corresponding overlap volume

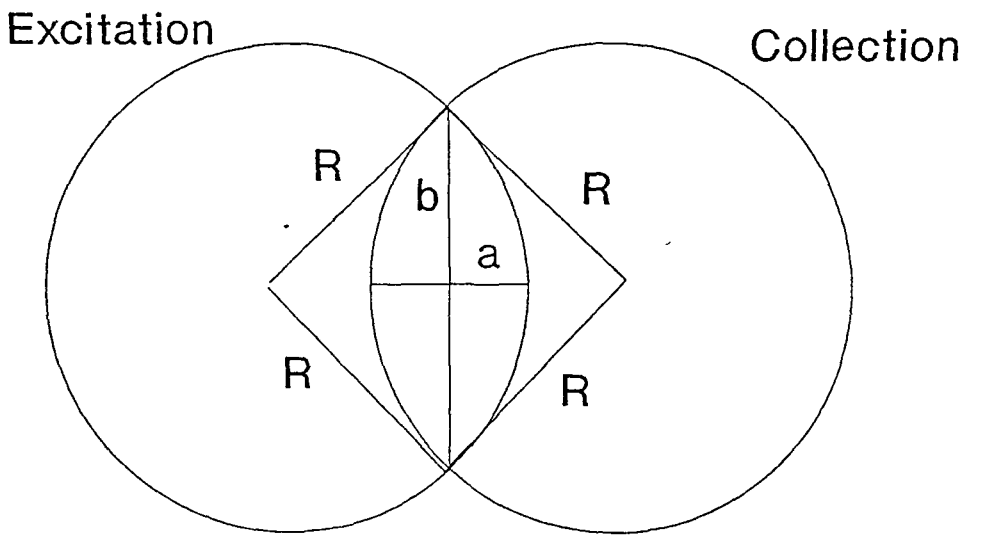


Fig 3.5 Head-on view of excitation and collection cones at any point within the cuvette

The solid angle ($\Omega$) of this cone is defined as the surface area at the base of the cone divided by its distance from the fibre-tip squared The solid angle can be expressed as a function of the numerical aperture of the fibre and the refractive index of the medium into which the light is coupled i e

$$\Omega = \left( \frac{NA}{n} \right)^2 \Pi = \frac{\Pi R^2}{P^2} = \frac{SA}{P^2} \quad \text{(Steradians)} \qquad (1)$$

$$\Rightarrow SA = \Omega P^2 \quad (cm^2) \qquad (2)$$

Similarly there is a cone at each collection fibre from which fluorescent and backscattered excitation light will be collected into the fibre The overlap between the input and collection cones is the region of solution from which fluorescent light is sampled by the fibre-bundle The geometry of the situation is shown in fig 3 3

In order to gain an expression for the amount of fluorescence produced in the overlap region the region is divided into thin slices of equal thickness The amount of fluorescence stimulated within a thin slice of solution can be shown (33) to be approximated by the equation

$$F = I_o\ (2\ 3\epsilon c\Delta x)\ \phi \qquad (3)$$

where

$I_o$ = excitation irradiance ($mW/cm^2$)

$\epsilon$ = molar extinction coefficient ($cm^{-1}$ per $\mu g/ml$)

c = concentration of Hp in solution ($\mu g/ml$)

$\Delta x$ = thickness of slice (cm)

$\phi$ = fluorescence efficiency

The fluorescent irradiance emitted from each slice can be calculated from (3) and the total fluorescence produced in the overlap region obtained by summing the contributions from each slice

The surface area at any point within the slices is assumed to be elliptical (see fig 3 4) In order to calculate the excitation laser irradiance ($I_o$, $mW/cm^2$) within each of these slices the surface area at the centre of each of these slices must be obtained

The surface area of an ellipse is defined as $\Pi ab$ where ,

a = point where the ellipse intersects the horizontal axis and

b = point where the ellipse intersects the vertical axis (see fig 3 5)

From fig 3 3 it is apparent that

$$a = \frac{d - 2(d - R)}{2} = \frac{2R - d}{2}$$

also from fig 3 5

$$b^2 = R^2 - (R - a)^2$$

$$\Rightarrow \quad b = (R^2 - (R - a)^2)^{1/2}$$

$$= \quad b = (R^2 - d^2/4)^{1/2}$$

where

R = radius of the circle at the base of the collection and excitation fibre cones at any point P from the fibre-tips

d = distance between the excitation and collection fibre centres.

Thus the surface area at the centre of any slice within the overlap region can be expressed as

$$S = \Pi \left( \frac{2R - d}{2} \right) \quad X \quad \left( (R^2 - d^2/4)^{1/2} \right) \quad (cm^2) \qquad (4)$$

Po is the laser power (mW) leaving the distal end of the excitation fibre It is assumed constant over the thickness of the sample, light absorption is ignored as the sample is dilute The excitation laser irradiance ($mW/cm^2$) within each of the slices can therefore be expressed as

$$I_o = \frac{Po}{S} \qquad (mW/cm^2)$$

The value for $I_o$ thus obtained can be slotted into equation (3) in order to obtain the amount of fluorescence produced in each slice. The total fluorescence produced in the overlap region is then obtained by summing the contributions from each slice

Not all the fluorescence emitted in the overlap region however will be detected by the fibre-bundle In order to calculate the amount of fluorescence sampled by the bundle the solid angle which each slice within the overlap region subtends to the collection fibres must be considered

The fluorescent emission from each slice is assumed to be constant over all angles from 0 to 2Π steradians The fluorescent irradiance from each slice expressed in $mW/cm^2$ per steradian is thus F/2Π

Thus the fluorescent power (mW) incident on the fibre from each slice in the overlap region can be expressed as

$$P_c = \frac{F}{2\Pi} \quad \frac{\Pi R_f^2}{k^2} \quad (\Pi R_f^2)$$

where $R_f$ = radius of collection fibre cone

$k$ = distance between the centre of the slice and the collection fibre face

$(k = (P^2 + d^2/4)^{1/2})$

$\Pi R_f^2 / k^2$ = solid angle of the collection fibre in steradians as viewed from the centre of the slice

Pc must be calculated for each of the slices in the overlap region and the contributions summed in order to gain an expression for the total fluorescent power incident on the collection fibre i e

$$P_{(TOT)} = \sum_{0}^{\text{no of slices}} P_c$$

A computer program has been developed which calculates $P_{(TOT)}$ by means of the technique outlined above Fig 3 6 is a plot of $P_{(TOT)}$ as a function of d, the separation between the centre of the excitation and collection fibre

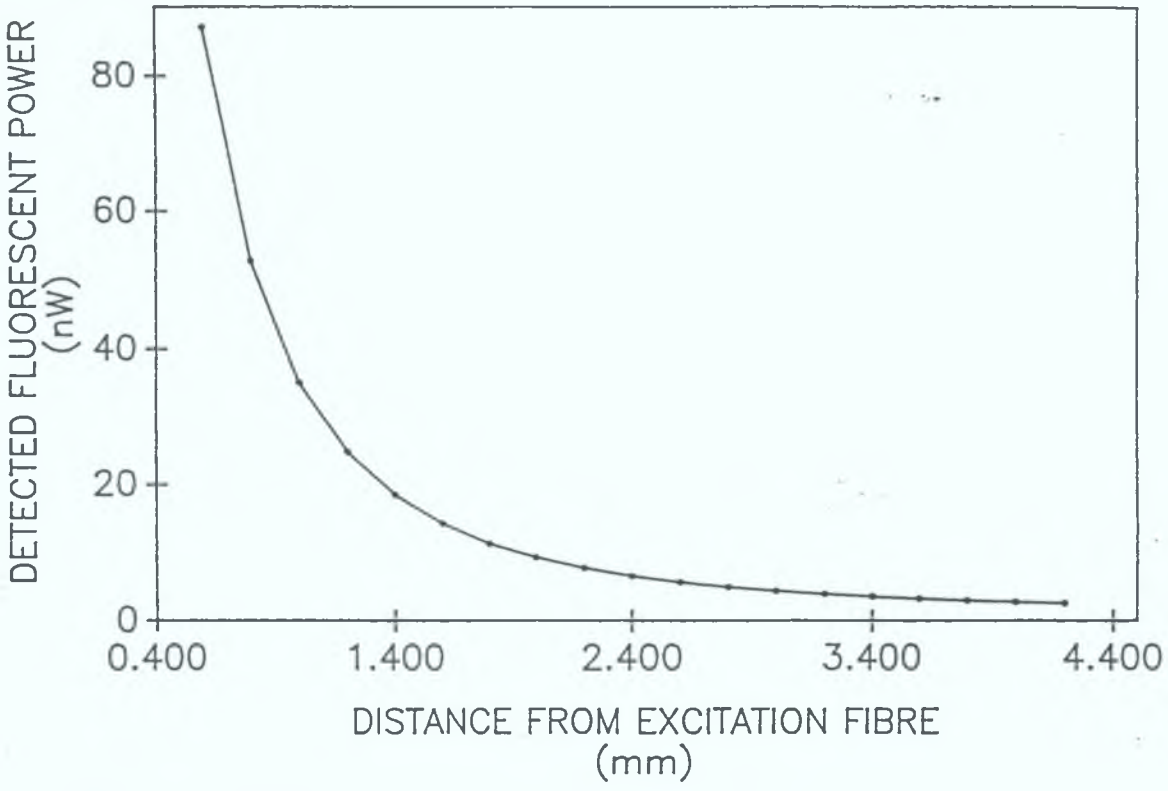


Fig 3.6 A plot of detected fluorescent power versus distance from the excitation fibre

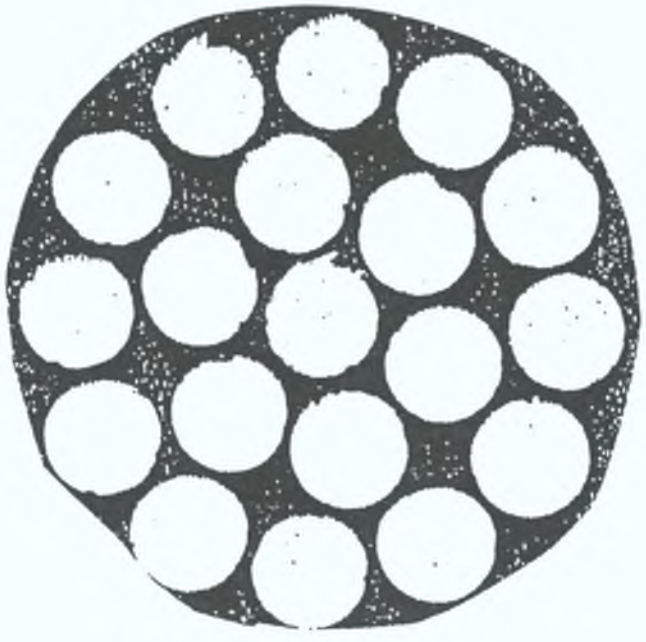

Fig 3.7 A head-on view of light leaving a fibre-bundle exactly similar to the one described above.

A head-on view of light emerging from a fibre-bundle similar to the one described in this chapter is presented in fig 3 7 In the analysis heretofore the collection efficiency of only one collection fibre has been discussed From fig 3 7 it is apparent that there are 6 fibres in the inner ring of the fibre-bundle Thus the total fluorescent power sampled by the inner ring of the fibre-bundle is 6 x $P_{(TOT)}$ From fig 3 7 values of $P_{(TOT)}$ for each of the outer rings of fibres can be obtained Finally by summing the contributions from each of the rings a value for the total fluorescent power sampled by the fibre bundle can be obtained For the sake of simplicity the effects of oversampling i e one collection fibre cone sampling a region of the excitation cone that has already been sampled by another collection fibre is ignored

For an incident light power of 4 mW coupled directly into a 1cm cuvette, containing a solution of Hp + $H_2O$ (concentration 1$\mu$g/ml), a sampled fluorescent power of 2 8 x $10^{-4}$ mW is obtained The design of the bundle was based on the principle of maximising $P_{(TOT)}$ by minimising the distance between excitation and collection fibres d Thus 200$\mu$m diameter collection fibres were used Fibres of a smaller diameter were considered too brittle for use

3.2 2 Filter Characteristics

The collection fibres in the fibre-bundle serve to convey the fluorescence and backscattered excitation light to the filter-holder This filter-holder alternately holds

(i) a narrow band-pass interference filter centred at 633nm and which transmits only the backscattered excitation signal

(ii) a wratten gel no 35 filter which only transmits the fluorescent signal

In fig 3 8 the transmission spectra of these filters are presented The interference filter allows 60% transmission at 632 8nm , and no transmission after 650nm The no 35 filter allows 10% transmission at 655nm (the fluorescent peak of Hp) , but continues to allow transmission up to 710nm This allows for the detection of the integrated fluorescence emission from 650-710nm After 660nm it is only the tail of the fluorescent peak that is detected The fluorescent light power transmitted through the no 35 filter and incident on the photocathode of the PMT can be expressed as the fluorescent power sampled by the fibre-bundle multiplied by the transmission of the collection fibres (80%) and the transmission of the no 35 filter at the fluorescent wavelength (10%) i e.

$$F = 0\ 1 \times (0\ 8 \times 2.8 \times 10^{-4}) = 2\ 2 \times 10^{-5} mW$$

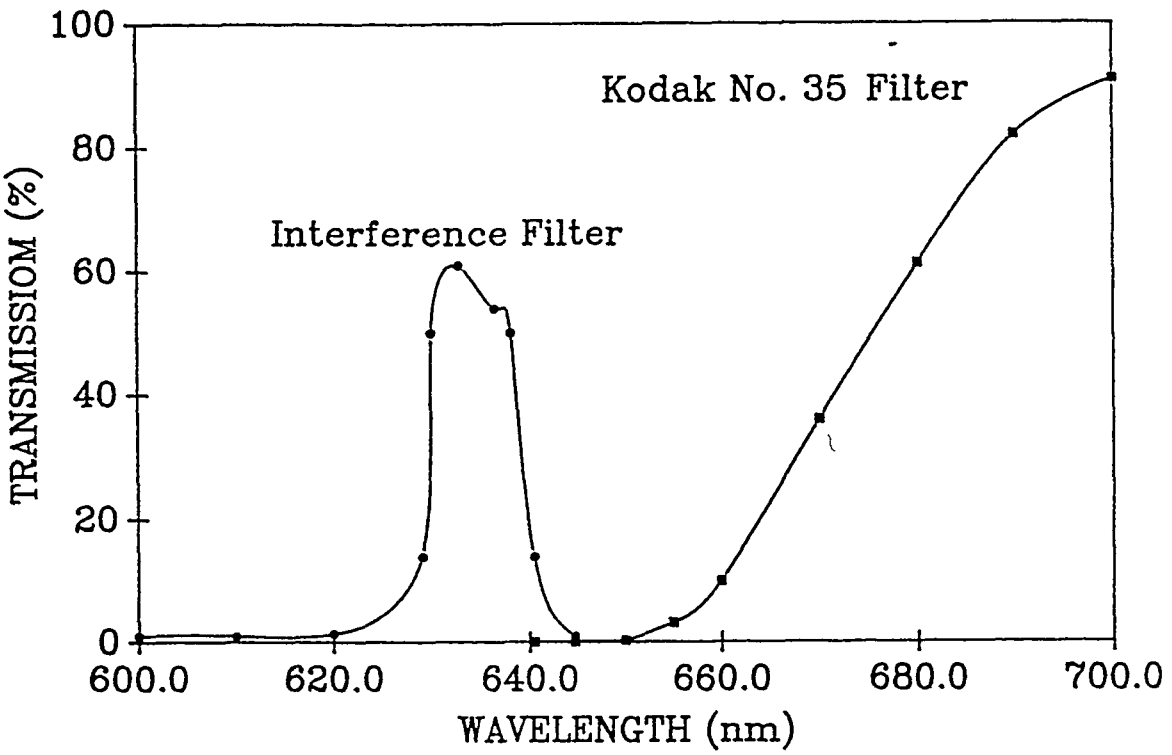


Fig 3 9 Visible light transmission (%) plotted against wavelength for (1) Interference filter (2) No.35 Wratten Gel filter

3 2.3 Detection In choosing a photodetector for the system it must be borne in mind that the fluorescent signal is very small Thus the appropriate detector must combine the following factors

(1) good response in 600-700nm region of the spectrum,

(2) high Cathode Radiant Sensitivity (CRS),

(3) high gain,

(4) low dark current;

(5) high Signal to Noise ratio (S/N).

Other factors to be considered are cost, ease of

incorporation into the experimental set-up, and power supply requirements PMT's were chosen over solid state detectors such as avalanche photo diodes because of their low dark currents typically compared to the latter devices. Typical values for PMT dark currents are of the order of 1-10nA

In Table 3.1 the response of a number of commercially available PMT's are assessed The figures used are all from manufacturers specifications, and the PMT's assessed are all chosen because of their good response in the 600-700nm region of the spectrum The anode currents are calculated for an incident light power of 2 2 x $10^{-5}$mW i e the fluorescent light power calculated as incident on the photodetector from our model calculations

| MAKE | R S (mA/W) | $I_k$ (mA) | GAIN | $I_a$ (mA) | COST |
|---|---|---|---|---|---|
| TE 9798 | 28 4 | 2 6$e^{-6}$ | 1.3$e^{-6}$ | 3 3 | 549 |
| TE 9828 | 28 4 | 2 6$e^{-6}$ | 1 0$e^{6}$ | 2 6 | 582 |
| TE 9973 | 20 | 3 5$e^{-6}$ | 1 3$e^{6}$ | 4 6 | 356 |
| TE 9658 | 44 | 1 3 $^{-5}$ | 0 6$e^{6}$ | 7 8 | 950 |
| TE 9659 | 46 | 1 9$e^{-5}$ | 0 7$e^{6}$ | 11 2 | 1067 |
| HAM R928 | 34 | 1 6$e^{-6}$ | 1 0$e^{7}$ | 16 | 148 |
| HAM R758 | 65 | 2 9$e^{-6}$ | 1 6$e^{5}$ | 0 47 | 401 |

$I_a$ = Anode Current $I_k$ = Cathode Current

R S = Radiant Sensitivity TE = Thorn EMI HAM = Hamamatsu

For our application the HAM R928 seemed the best option because of its low cost, low power supply requirements and its high gain and high anode current

The resultant anode current from the PMT is sent to a Stanford Research Systems SR510 lock-in amplifier where the signal is converted to a voltage and amplified The lock-in output can then be read from a digital display

### 3.2.4 Ratio Method of Fluorescent Detection

The ratio method of Hp detection is a novel concept in fluorescent endoscopy (20) It is reported (20,2) that it should eliminate the effects of certain parameters on the detection of fluorescence The use of the filter-holder in this system allows for the separate detection of Hp fluorescence and back-scattered He-Ne light The ratio of these two signals is recorded and used as the basis for fluorescent detection The main advantages of the ratio method appear to be that fluorescent detection becomes independent of

(i) fibre-bundle to sample distances

(ii) variations in sample topography

(iii) variations in the efficiencies of the detection and excitation systems

By placing the appropriate filter in the filter-holder a reading can be obtained from the digital display of the lock-in for each of the light signals The ratio is then expressed as a percentage as follows

$$R\ (\%) = \frac{\text{Fluorescent Signal}}{\text{Backscatter Signal}} \times 100$$

From the filter characteristics it is estimated that 60% of backscattered laser light is transmitted through the interference filter while 10% of the fluorescent light is passed through the no 35 filter Thus in order to obtain an appropriate value for the ratio of fluorescent to backscattered light at the sample the ratio obtained from the lock-in was multiplied by 6

## 3.3 Experiments

It has been reported that in-vivo HpD concentrations as low as 1μg/ml have been measured in tumourous areas (27). Thus if the use of He-Ne excitation light is to become a valid alternative in fluorescent endoscopy, detection systems must be developed which detect He-Ne induced HpD fluorescence from concentrations of the dye less than 1μg/ml. In order to determine the sensitivity of our system for the detection of Hp fluorescence a series of experiments were carried out The objective was to obtain the lowest signal ratio which could be identified by the system and thus determine the lowest concentration of Hp which could be detected Hp was utilised in these experiments as a convenient model for the clinically popular HpD for the reasons outlined in chapter 2 In this way the efficiency of using a He-Ne laser as excitation source can be assessed

### 3 3 1 Procedure

In these experiments the system was used to detect fluorescence from solutions of Hp and methanol (MeOH) and Hp and $H_2O$ The experimental set-up is as described in section 3 2 and outlined in fig 3 1 .The He-Ne laser light is coupled directly from the fibre-bundle to a cuvette containing Hp in solution Fluorescent detection is by means of the ratio method as outlined in section 3 2 4

The solutions of Hp + $H_2O$ and Hp + MeOH were prepared according to the procedures described in chapter 2 in order to preserve a uniformity of photophysical properties throughout the experiments. The concentration of Hp in solution was progressively lowered and the ratio of backscattered laser light to fluorescence is noted from the lock-in amplifier. In this way plots of signal ratio versus Hp concentration for both Hp in methanol and Hp in $H_2O$ were obtained.

3.3.2 Results and Discussion :

In fig 3.8 and 3.9 typical results obtained from these experiments are plotted. Each point on the plots represents the average of three separate measurements and error bars are included for accuracy. Both plots display a rapid fall-off of signal ratio with Hp concentration. In general the signal ratio for concentrations of Hp in MeOH is higher than that of similar concentrations of Hp in $H_2O$. This is due to the superior solubility of Hp in MeOH resulting in an increased fluorescent quantum efficiency for Hp in MeOH. Both plots exhibit a marked tailing off at a ratio of 0.04%. This ratio can be considered to be the lowest signal ratio that can be distinguished by the system. For the case of Hp + MeOH this corresponds to a concentration limit of 0.01 $\mu$g/ml while for Hp + $H_2O$ it corresponds to 0.1 $\mu$g/ml. The sensitivity limit of 0.1 $\mu$g/ml obtained for Hp + $H_2O$ is lower than the 0.36$\mu$g/ml limit obtained for 632nm

excitation using the spectrophotometer in chapter 2 The sensitivity limits obtained illustrate that very low concentrations of Hp can be detected by this technique Similarly the use of a He-Ne laser as excitation source in the system results in the detection of Hp concentrations well below the 1$\mu$g/ml concentration of HpD measured to accumulate in tumourous areas (27)

3 4 Other Experiments

The use of a fibre-bundle in this system limits the amount of detected fluorescence Concentration curves were obtained for the system without the fibre-bundle A lens was used to focus the fluorescence from the cuvette onto the photocathode of the PMT Sensitivity levels of 1 x $10^{-4}\mu$g/ml were obtained for Hp + $H_2O$ Thus the use of the fibre-bundle reduces the sensitivity level of the system by a factor of 1 x $10^3$

In another set-up a scanning monochromator was placed between the sample-holder and the PMT Again fluorescent detection was undertaken without the fibre-bundle and a lens focussed the fluorescent light from the cuvette onto the entrance slit of the monochromator The monochromator scanned between 600 and 700nm and a dual peaked spectrum obtained with the excitation peak at 632nm and an emission peak at 655nm The peak-height of the emission peak was recorded for progressively dilute solutions of Hp + $H_2O$ and a sensitivity limit of 8 x $10^{-5}\mu$g/ml obtained. This is a factor of 1 2 x $10^3$ times more sensitive than the system

with the fibre-bundle This scanning monochromator system could also utilise the ratio method of fluorescent detection as outlined in this chapter by recording the ratio of the excitation peak height to that of the emission peak If a fibre-bundle were added to this set-up the sensitivity would be reduced, by a factor of $1 \times 10^{-3}$ and would thus equate to the system described in this chapter The use of a scanning monochromator detection system in clinical situations would be infeasible however as for each point sampled in (for example) the trachea, the monochromator would have to scan across the region of the spectrum 600-700nm This would make the duration of a typical examination intolerable

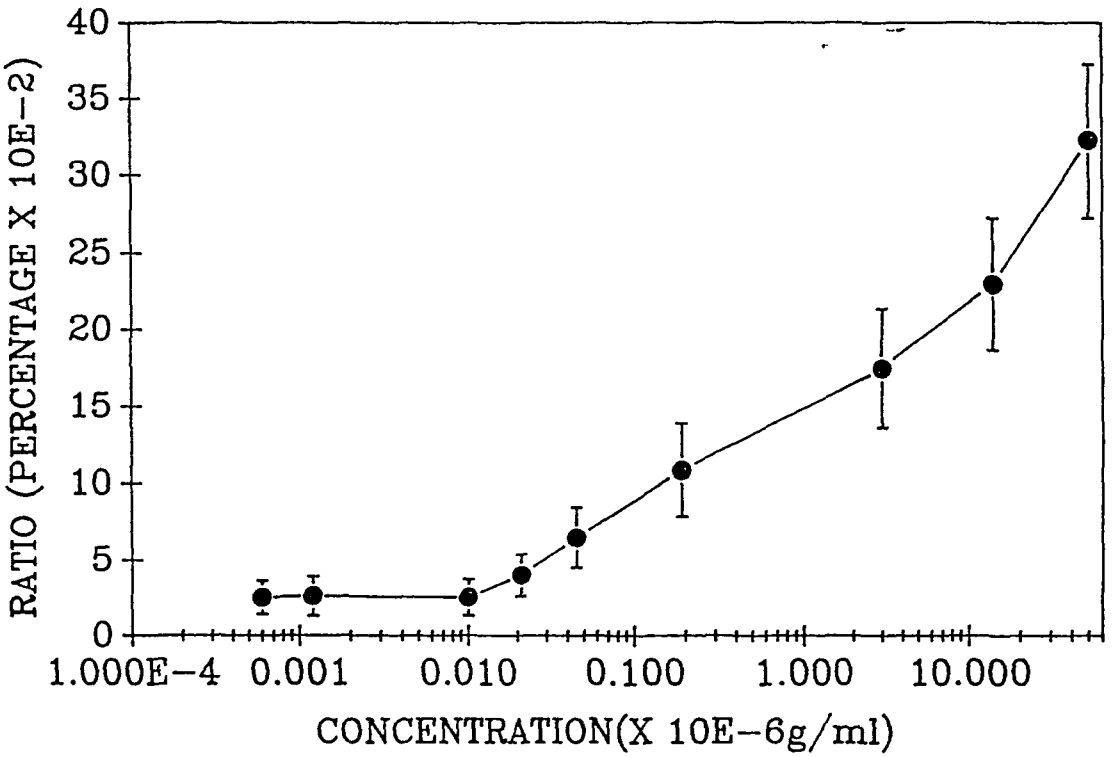


Fig 3 8 Concentration of Hp in a solution of Methanol plotted against signal ratio

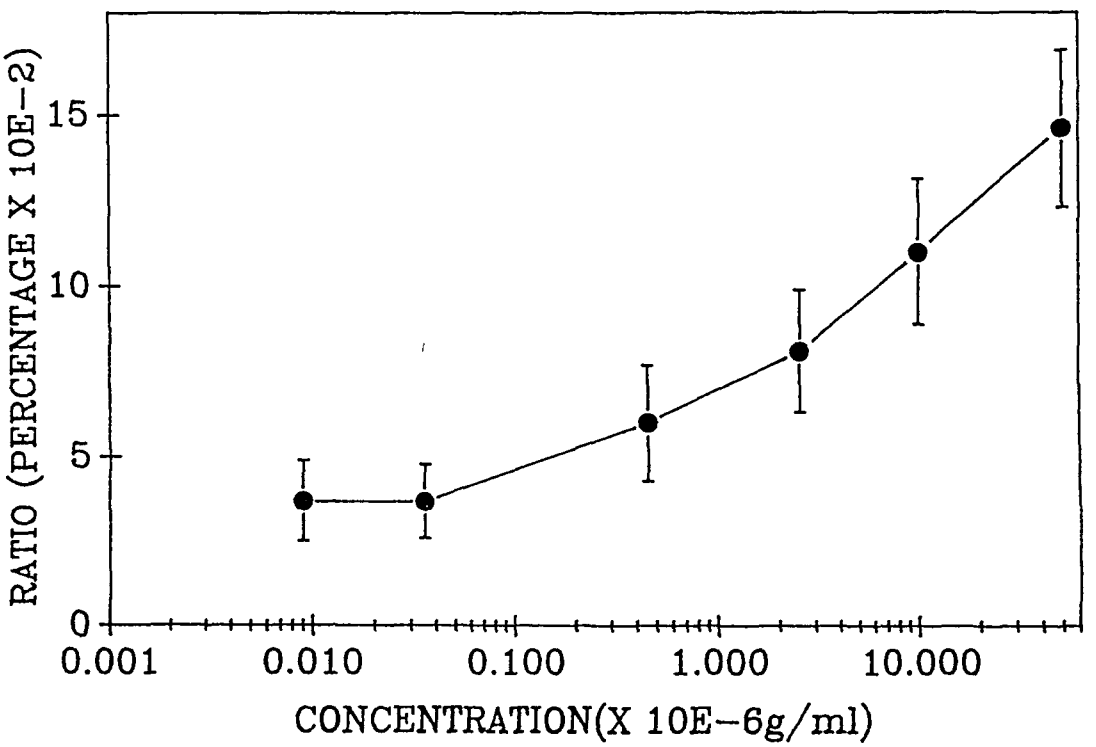


Fig 3 9 Concentration of Hp in a solution of $H_2O$ plotted against signal ratio

## 3 5 Conclusion

The purpose of this chapter was to investigate the use of a He-Ne laser in fluorescence endoscopy For this reason a system was developed for the in-vitro detection of Hp fluorescence

In order to simulate endoscopic conditions a fibre-bundle was used in the system to both transmit the excitation signal and collect the resultant fluorescence In designing the fibre-bundle careful consideration was taken of both fibre-bundle geometry and fluorescent collection efficiency. A theoretical examination of these factors lead to the design of a bundle which minimised d, the distance between the excitation and collection fibres, in order to maximise the detected fluorescence. For convenience the fibre-bundle used in this system was 30cm in length however its diameter of 0 9cm was chosen in order that the bundle could fit adequately into most clinical endoscopes

In this system, fluorescent detection is quantified by means of the ratio method (see 3 3 5) This technique of fluorescent detection should prove of great benefit in clinical circumstances as it predicts the irradication of temporal variations in fluorescent detection due to changes in topography, tumour to bundle distance and system excitation and detection efficiencies

Experiments on this system have shown that in-vitro concentrations of 0 01 $\mu$g/ml for Hp in methanol and 0 1 $\mu$g/ml for Hp in $H_2O$ can be detected. These limits are below

the 1 μg/ml concentration of HpD quoted (27) to have been measured in tumourous areas 48 hours post injection This seems to indicate that this system which incorporates a He-Ne laser as excitation source may be effective for the detection of tumours via fluorescent endoscopy It must be stressed , however, that the sensitivity limits of the system were obtained for the detection of in-vitro Hp fluorescence from a glass cuvette and that in-vivo conditions may be significantly different However the detection of low concentrations of Hp in solution using a He-Ne laser as excitation source is encouraging

In conclusion a system has been developed which uses a He-Ne laser as excitation source and can detect low concentrations of Hp in solution The system was designed for the detection of in-vitro fluorescence however it could easily be adapted to form the basis of an instrument for the detection of intra-cavitary tumours via fluorescence endoscopy In this regard the use of the He-Ne laser and the ratio method of fluorescent detection could present the clinician with significant advantages over conventional techniques of fluorescent endoscopy

Chapter 4

# LIGHT-TISSUE INTERACTION

## 4.1 Introduction

A knowledge of how light behaves in biological tissue is fundamental to a number of areas in photomedicine e.g. laser surgery, PDT, fluorescence endoscopy etc. In order to fully characterize the clinical performance of the apparatus described in chapter 3, it is necessary to take account of the interaction of light with tissue. In this chapter an overview is given of the main models used to describe the interaction and an appropriate choice is made to describe the propagation of He-Ne laser light through tissue. This will then form the basis in chapter 5 for a comprehensive model of the performance of the apparatus in a simulated clinical setting.

## 4.2 Tissue Optics

Biological tissue is a complex scattering and absorbing medium with a higher refractive index than air (35). Thus when a light beam reaches an air/tissue boundary a small portion of the flux will be reflected. The remainder of the light (typically 95-96%) penetrates the

tissue and encounters multiple absorption and scattering centres The extent of scattering and absorption depends on the wavelength of the incident light and the type of tissue involved Most tissues are highly scattering and a large portion of the light flux is backscattered from the tissue

An accurate description of the propagation of light within tissue is difficult An estimate of the light distribution in tissue can be obtained by solving the radiative transport equation This poses a formidable mathematical problem for which Chandrasekhar (37) has proposed a general solution

## 4 3 Transport Theory

Radiative transport theory has proved a popular and effective method for the study of scattered light in turbid materials In the past it has been used to describe such widespread phenomena as atmospheric optics, oceanic optics and astrophysics (36) The theory involves the general solution of the transport equation which, if we assume the light incident on a slab geometry, has been defined by Chandrasekhar (37) as (see overleaf)

$$\mu \frac{dI(z,\mu)}{dz} = -(\sigma_a + \sigma_s)I(z,\mu) + \frac{(\sigma_a + \sigma_s)}{2} \quad (1)$$

$$X \int d\mu^1 I(z,\mu)p(\mu,\mu^1)$$

where $I(z,\mu)$ = radiance at depth z

$\mu$ = Cos $\theta$

$\theta$ = angle between the direction of scattering and the normal (see fig 4 1)

$p(\mu,\mu^1)$ = phase function for light scattering from the direction $\mu^1$ = Cos $\theta^1$ into $\mu$ = Cos $\theta$ The phase function is assumed to depend on the angle between $\mu$ and $\mu^1$ only The normalization condition imposed on $p(\mu,\mu^1)$ is ·

$$\frac{1}{2} \int_{-1}^{1} p(\mu,\mu^1)\, d\mu^1 = \frac{\sigma_s}{\sigma_a + \sigma_s}$$

where $\sigma_a$ = the absorption coefficient of the medium and $\sigma_s$ = the scattering coefficient.

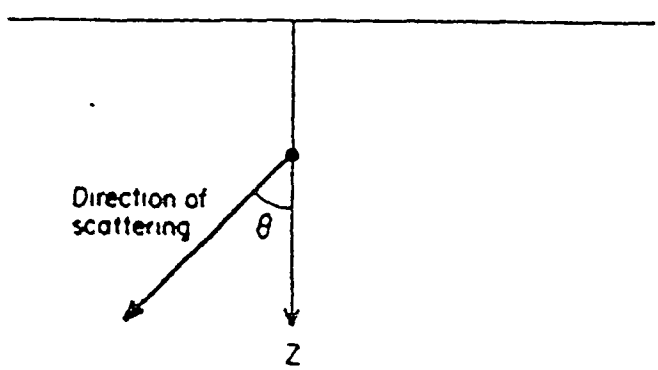


Fig 4 1 $\theta$ - angle between direction of scattering and the normal

Although this equation provides a very accurate description of tissue optics the general solution of the equation is not known In photomedicine simplified but plausible approximations of the equation have been applied to light-tissue interaction In this chapter three such models are discussed and their results compared These are Beers Law, the Kubelka-Munk theory and the diffusion approximation The quantity of interest in these models is the light energy fluence rate within the tissue This is defined as *the total energy of the photons incident per second on a small sphere centred at that point and divided by the cross sectional area of the sphere* (38) These models are discussed in depth below

4.3 1 Beers Law· This is the simplest of the models and states that light intensity is exponentially attenuated as it passes through tissue and is given by

$$I(z) = Io\ e^{-T(z)} \qquad (2)$$

I(z) = intensity at depth z

Io = incident intensity (i e at z = 0)

T = attenuation coefficient

T can be easily calculated by measuring the total transmission through a sample of tissue. Despite its simplicity Beers Law has been applied successfully to

several tissue Its inherent disadvantage lies in the fact that the calculation of T does not distinguish between scattering and absorbing events For this reason, the general rule of thumb when applying Beers Law is that it is only valid when the absorption coefficient is much larger than the scattering coefficient This is true for most applications of the $CO_2$ , Excimer and Er.YAG lasers when the penetration depth is less than 40$\mu$m (35)

4 3 2 Kubelka-Munk

The Kubelka Munk (KM) theory (39) is an extension of Beers Law to take account of light scattering It is named after the authors of a 1931 paper which proposed the theory for the description of the optical properties of paint Since then it has been used to model a wide variety of processes In the field of light-tissue interactions van Gemert and Hulsbergen-Henning (40) have used it to describe light interaction in port-wine stains while Wan et al (41) have applied it to skin scattering and absorption in a general sense

In the KM theory a diffuse light is incident on a tissue slab and the irradiance throughout the tissue is assumed constant in all directions (i e isotropic) Two light fluxes, one travelling in the forward direction (F+(z)) and one in the backward direction (F-(z)) are used to describe the energy fluence rate at depth The rate of change of forward flux with depth is defined as the amount

of scattered backward flux less the amount of forward flux which has been either scattered or absorbed Similarly the rate of change of backward flux is given by the scattered forward flux less amount of scattered or absorbed backward flux These fluxes can be defined by the differentials (39)

$$\frac{dF+(z)}{dz} = -(K+S)F+(z) + SF-(z) \qquad (3)$$

$$-\frac{dF-(z)}{dz} = -(K+S)F-(z) + SF+(z) \qquad (4)$$

and the energy fluence rate defined as

$$\psi(z) = 2(F+(z) + F-(z)) \qquad (5)$$

K and S are the KM coefficients of absorption and scattering and are not the same as the absorption and scattering coefficients of tissue They have been shown to be related to the diffuse reflectance (Rd) and transmission (Td) properties of tissue (54) As it is difficult to measure the diffuse reflectance and transmission through tissue information on K and S for biological tissue, is scarce and often has to be estimated with considerable inaccuracy Other problems with the model are that it is only valid when dealing with diffuse irradiance in a 2-D geometry The model is popular, however, because it is simple and convenient to use and provides an approximate solution Van Gemert and van der Putten (42) used the method to model the detection of subcutaneous tumours by HpD fluorescent detection

### 4.3.3 Diffusion Theory·

The diffusion approximation of the transport equation has been widely used for light propagation in biological media especially where scattering dominates absorption (35, 36, 43) It is the only one of the models mentioned here which can accommodate a collimated light source If the case of a collimated laser beam incident on a slab of tissue is considered then the diffusion theory makes the assumption that the radiance at any point in the tissue can be expressed as

$$I(z,\mu) = Ic(z)\delta(x) + Id(z,\mu) \qquad (6)$$

where

Ic(z) = collimated radiance at depth z

Id(z,$\mu$) = diffuse radiance at depth z and

$\theta$ = angle between the direction of scattering and the normal

$\delta$(x) = delta function with x = 1-$\mu$ Thus $\delta$(x) = 0 everywhere except at x = 0 where $\delta$(0) = 1

$\mu$ is defined as Cos $\theta$ where $\theta$ is the angle between the direction of light scattering and the normal Equation (6) thus states that the radiance at any depth z is given by

the collimated radiance at that point, which is zero in every direction except $\theta = 0$, plus the diffuse radiance at that point The diffuse radiance at depth is given by

$$Id(z) = \phi(z) + \mu\Psi(z) \qquad (7)$$

where

$\phi(z)$ = isotropic part

$\Psi(z)$ = anisotropic part

These assumptions make it possible to solve equation (1) (see van Gemert (43)) yielding the following coupled differential equations (seeoverleaf)

$$\frac{dFc(z)}{dz} = - DFc(z)$$

$$\frac{dF+(z)}{dz} = - EF_{+}(z) + F\ (F-(z)) + BFc(z)$$

$$\frac{dF-(z)}{dz} = - F\ (F_{+}(z)) + EF-(z) - CFc(z)$$

F+(z) and F-(z) are the forward and backward photon fluxes respectively , while Fc(z) represents the collimated flux within the tissue The constants B, C, D, E, F are defined as follows .

$$B = \sigma_s(2 + 3g)/4$$

$$C = \sigma_s(2 - 3g)/4$$

$$D = (\sigma_a + \sigma_s)$$

$$E = \left[2\sigma_a + 0\ 75\ \{\sigma_a + (1-g)\sigma_s\} - \sigma_a\right]$$

$$F = \left[0\ 75\{\sigma_a + (1-g)\sigma_s\} - \sigma_a\right]$$

Where

$\sigma_a$ = absorption coefficient ($m^{-1}$)

$\sigma_s$ = scattering coefficient ($m^{-1}$)

g = anisotropy factor

The anisotropy factor g is introduced to allow for a slight anisotropic scattering of the diffuse flux and is defined as the mean cosine of the scattering angle This scattering angle $\theta$ is the angle between the z-direction of propagation and the direction into which the light flux has been scattered upon impinging on a scattering centre (see fig 4 1) g can be varied to describe backward peaked (g = -1), isotropic (g = 0) or forward peaked (g = 1) scattering (Groenhuis et al (44))

In order to get an expression for the energy fluence rate, the three flux differential equations must be solved These equations were reduced (see appendix 1) using linear algebra to the following three simultaneous equations We acknowledge the assistance of Dr E Bouffet of DCU Mathematics Dept. in these calculations

$$F+(z) = \alpha e^{-Dz}(G) + \beta e^{Lz}(F) + \gamma e^{-Lz}(F) \qquad (8)$$

$$F-(z) = \alpha e^{-Dz}(H) + \beta e^{Lz}(J) + \gamma e^{-Lz}(K) \qquad (9)$$

$$Fc(z) = \alpha e^{-Dz}(I) + 0 + 0 \qquad (10)$$

D, F, G, H, I, J, L, K are all constants defined in appendix 1 $\alpha$, $\beta$ and $\vartheta$ are constants and are determined by means of applying the appropriate boundary conditions to (8), (9) and (10). Star et al (38) proposed the following boundary condition for light incident on a tissue slab of thickness Z

$$F+(0) = 0 = F-(Z)$$

This states that no nett scattered light flux enters the medium at the boundaries To these can be added the condition that

$$Fc(0) = Io = \text{incident light intensity of the laser}$$

By obtaining expressions for $\alpha$, $\beta$, and $\vartheta$ readily solvable equations are obtained for the light fluxes and the energy fluence rate at any distance z in the medium is obtained as follows

$$\Psi(z) = 2(F+(z) + F-(z)) + Fc(z) \qquad (11)$$

The diffusion approximation of the transport equation is valid for optically dense and highly scattering media. As this appears to be the case for a wide variety of biological tissue its use for the description of light-tissue interaction is well-documented in the literature The inclusion of a collimated flux term in the

model makes it suitable for modeling laser irradiation of tissue However at the tissue boundaries the model has been shown to be inaccurate This is because the model requires the presence of diffuse light fluxes within the tissue and at the boundary scattering is not dominant resulting in a strong collimated flux Equation (11) can be readily solved with the unknown factors being $\sigma_a$, $\sigma_s$ and g being obtained from the literature

## 4 4 Numerical Solutions

In order to chose the most effective model for the description of the propagation of He-Ne laser light through tissue, the models described in the previous sections were implemented in computer programs and numerically solved for different simulated tissues These programs were written in BBC Basic, compiled in RiscBasic and run on an Archimedes PC with maths co-processor installed

These programs were used to generate plots in which the three models are compared for the description of light propagation in tissues with

(i) dominant absorption

(ii) equal absorption and scattering

(iii) scattering much greater than absorption.

The optical coefficients used in these programs are obtained from the literature In obtaining optical coefficients for these situations, however, it is important to note that the KM coefficients are not the same as the transport coefficients used in the diffusion approximation and Beers law. However, Welch et al (35) have provided equivalent values for both sets of coefficients for the situations described above Fig 4 2 tabulates these values $\sigma_a$ and $\sigma_s$ are the transport coefficients with Beers Law attenuation coefficient given by $T = \sigma_a + \sigma_s$ K and S are the absorption and scattering Kubelka-Munk coefficients respectively All values are expressed in $cm^{-1}$

| $\sigma_a$ | $\sigma_s$ | T | K | S | Condition |
|---|---|---|---|---|---|
| 10 | 1 | 11 | 10 8 | 0 33 | Dominant Absorption |
| 10 | 10 | 20 | 14 7 | 5 1 | Equal Scatt & Abs |
| 1 | 100 | 101 | 2 0 | 75 | Dominant Scattering |

Fig 4.2 Table of equivalent values for transport and KM coefficients

As the diffusion approximation model is the only model which allows for a collimated flux term it is examined in more detail than the Kubelka-Munk or Beers Law models. Plots are generated of the three photon fluxes and the resultant energy fluence rate as calculated by the model. $\sigma_a$(0.0013 $mm^{-1}$) and $\sigma_s$(1 $mm^{-1}$) are chosen in order that $\sigma_a <<< \sigma_s$ and the scattering is considered to be predominantly forward peaked with g = 0 71 These conditions have been chosen in order to replicate the

conditions reported (35) as being prevalent for red light passing through tissue

The influence of the anisotropy factor g on the diffusion equation is investigated Plots are generated of fluence rates for g varied between 0 and 1 From the plot the performance of the model for the description of isotropic (g = 0) to highly forward scattering (g = 1) light propagation can be assessed

In figs 4 8 and 4 9 fluence rates are plotted for varying $\sigma_a$ and $\sigma_s$ respectively This yields an indication as to in which types of tissue the diffusion approximation represents a realistic description of the propagation of light.

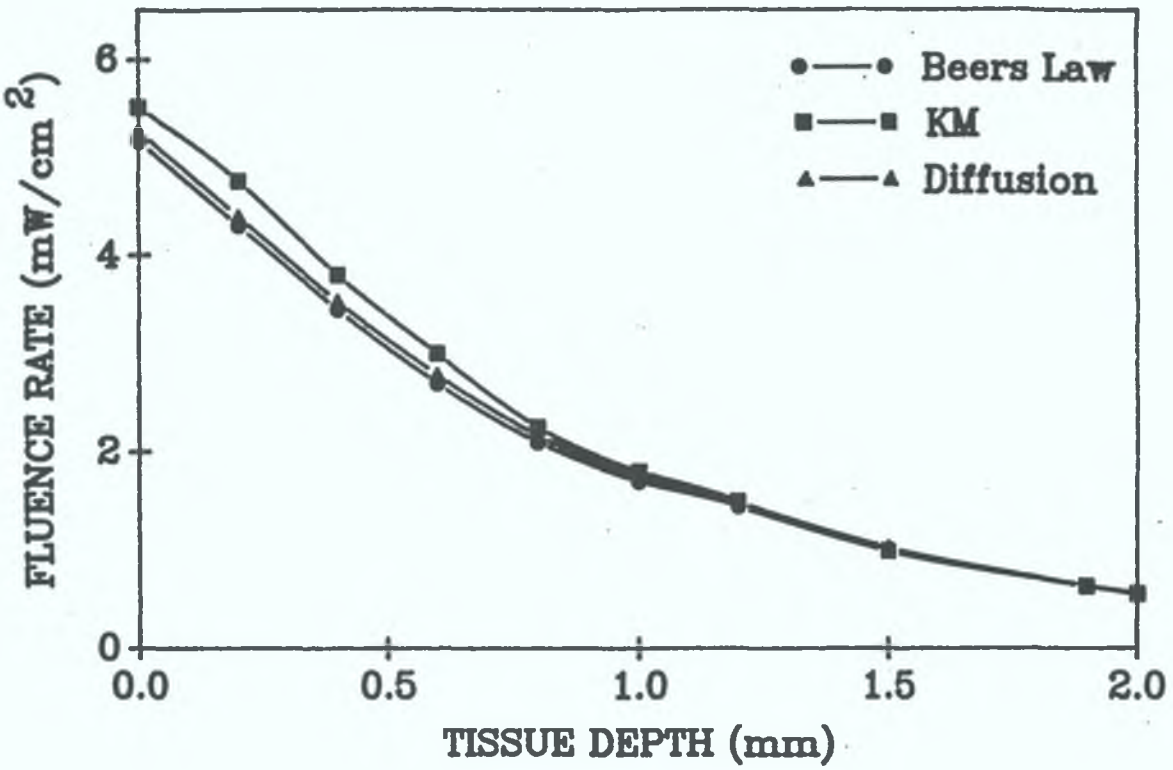


Fig 4.3 Beers law, KM, and diffusion models plotted against tissue thickness for dominant absorption (see fig 4.2).

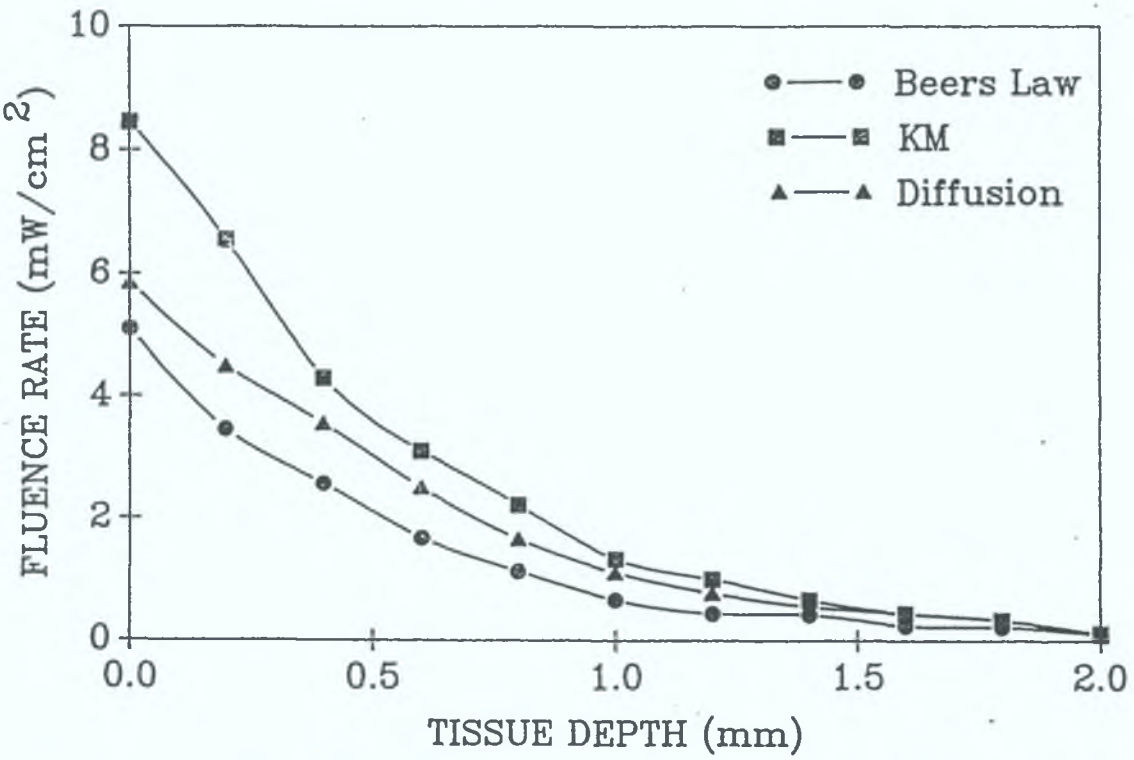


Fig 4.4 Beers law, KM, and diffusion models plotted against tissue thickness for equal scattering and absorption

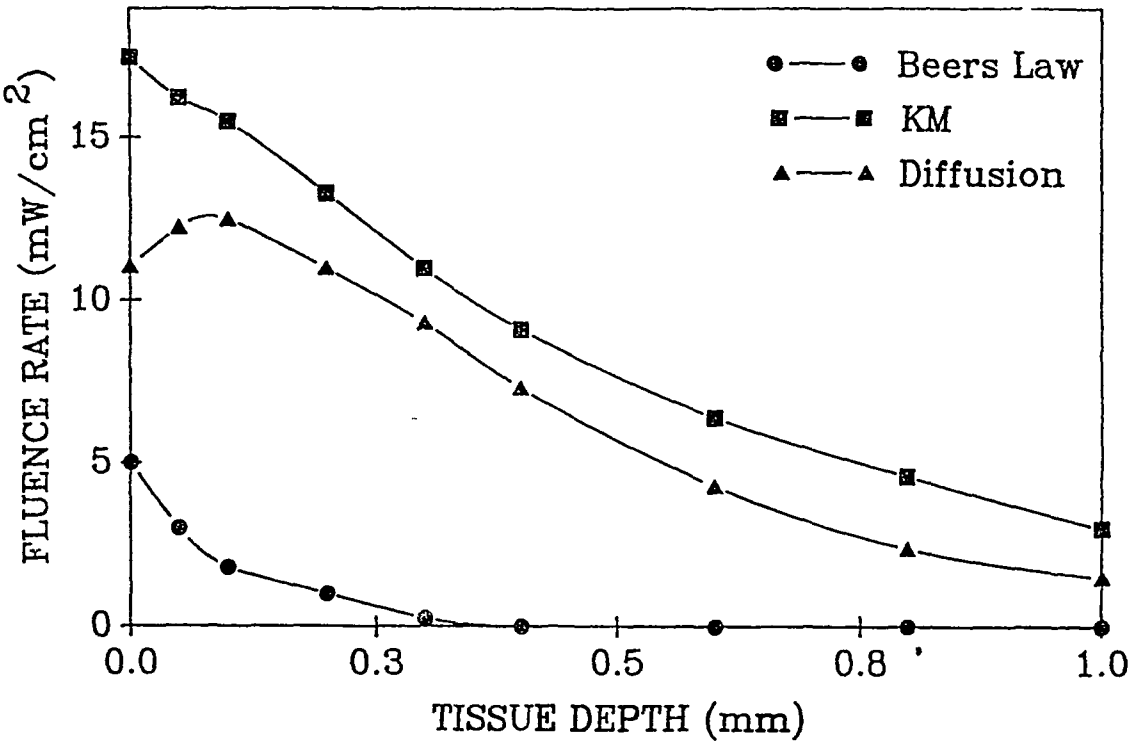


Fig 4.5 Beers law, KM, and diffusion models plotted against tissue thickness for scattering dominant (see table 4 2)

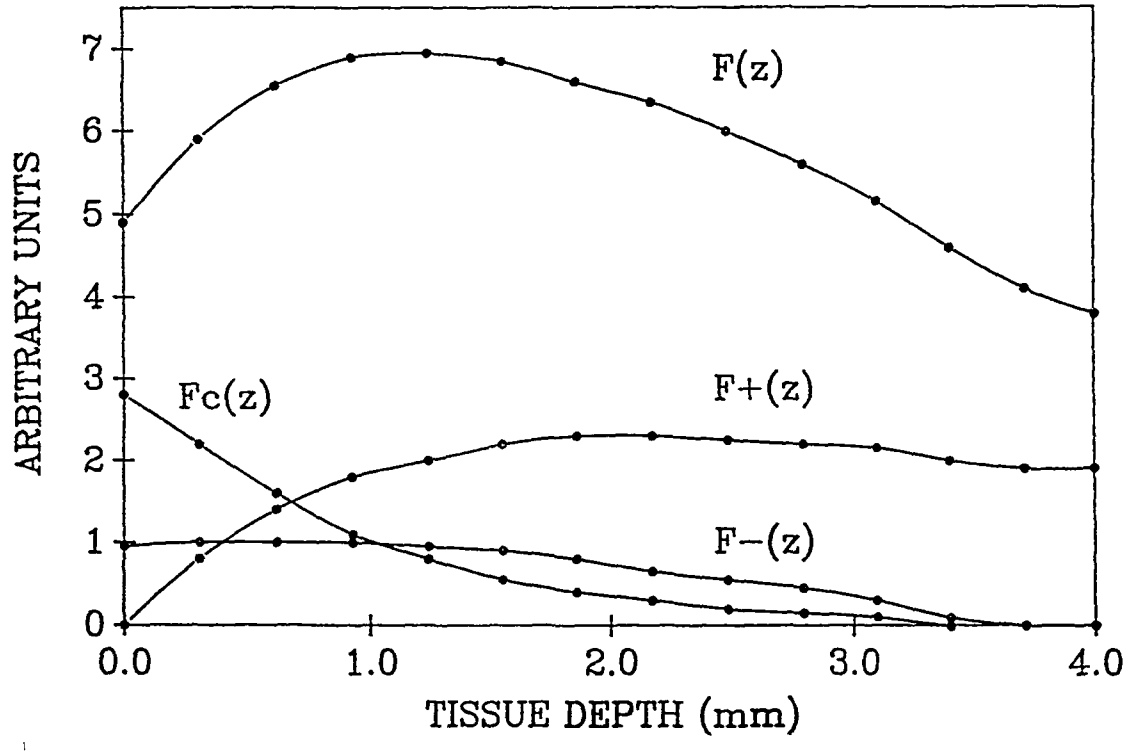


Fig 4.6 Energy fluence rate and the three photon fluxes plotted against tissue depth where $\sigma$ >>> $\sigma$ and g = 0.71

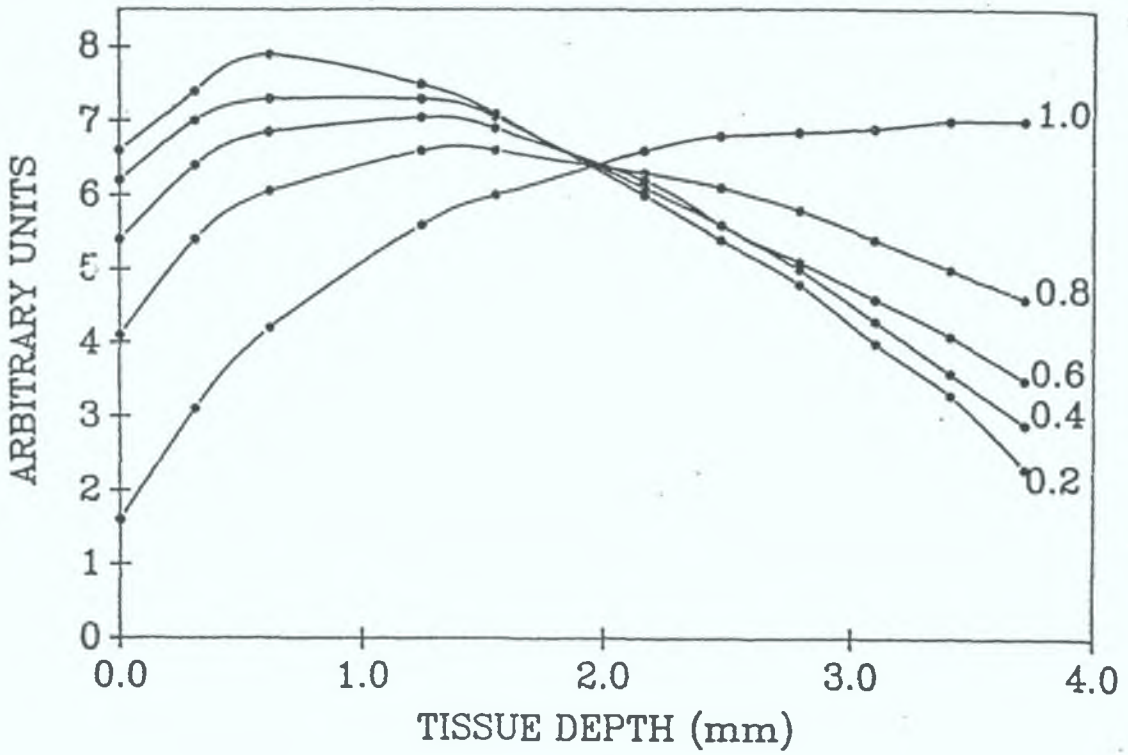


Fig 4.7 Energy fluence rate plotted against tissue depth for g varied between 1 and 0.

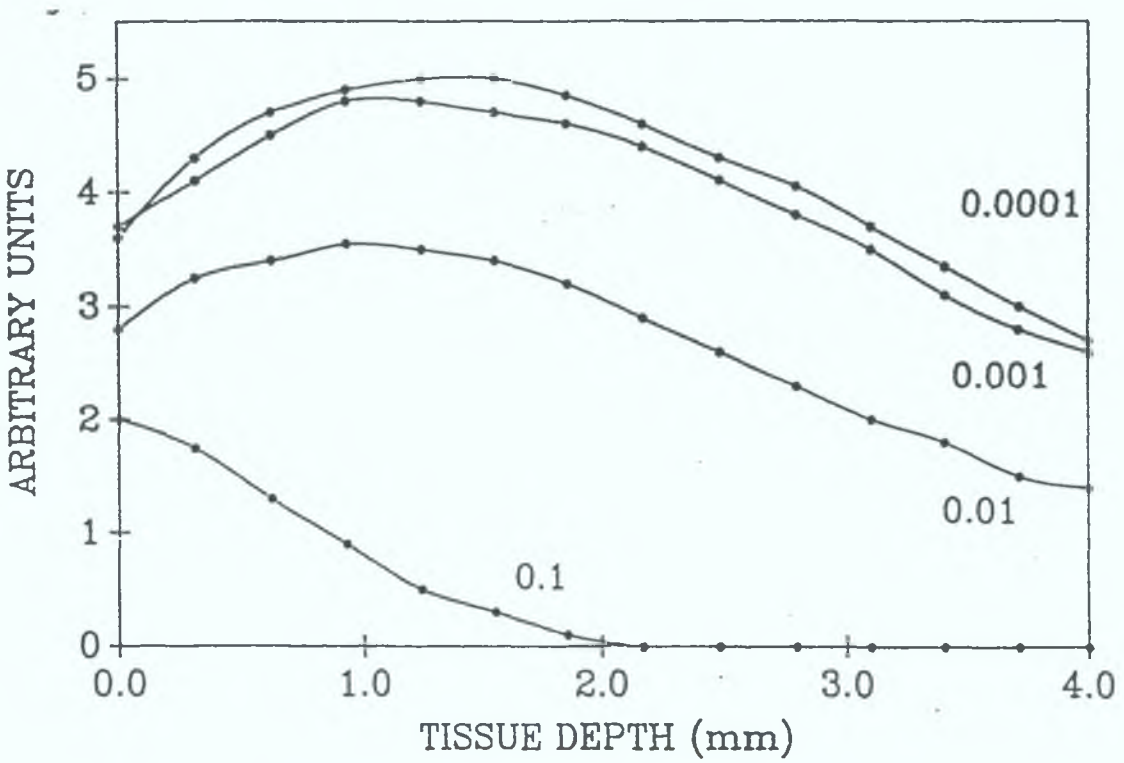


Fig 4.8 Energy fluence rate plotted against tissue depth for $\sigma_a$ varied between 0.1 and 1 x $10^{-4}$

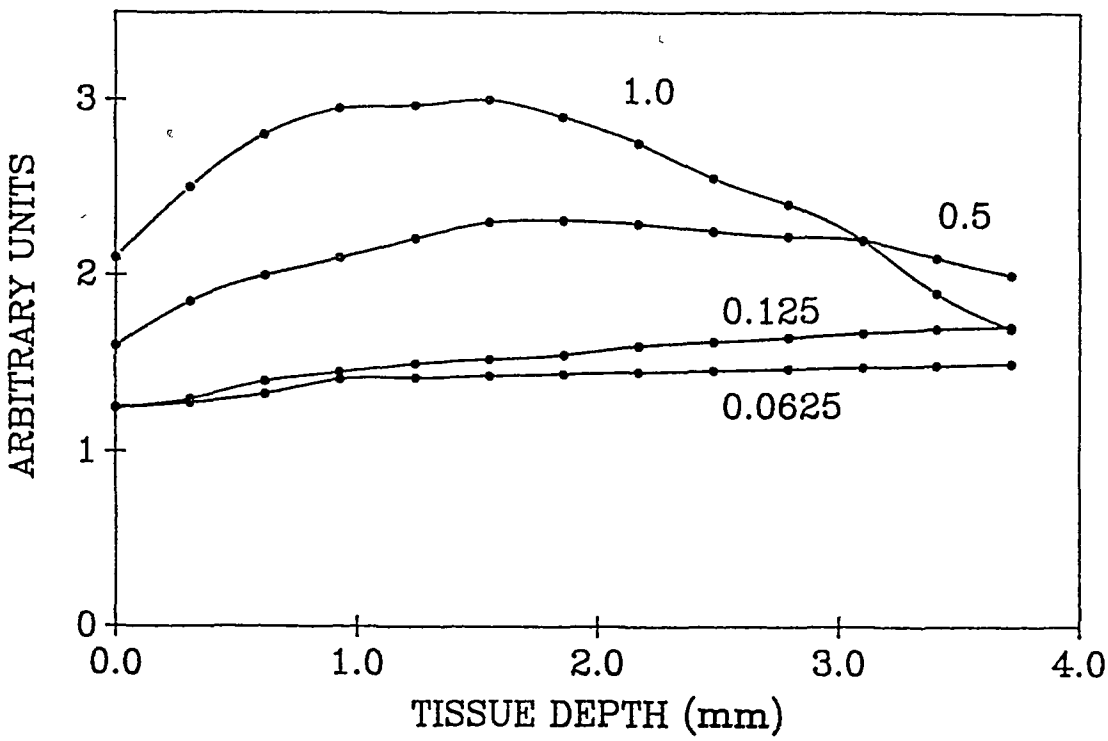


Fig 4 9 Energy fluence rate plotted against tissue depth for $\sigma_s$ varied between 1 0 and 0 06 $mm^{-1}$

4.5 Results and Discussion

From fig. 4 3 it is apparent that when absorption dominates there is very good agreement between the models Beers Law then provides a very simple and effective technique for the description of light propagation in highly absorbent tissue When scattering and absorption begin to equalize (fig 4 4), however, discrepancies between the models begin to appear. In fig 4.5 where scattering is dominant Beers Law is shown to be increasingly inadequate for the description of light distribution This is because it fails to account for the broadening of the light beam within the tissue and it does not include a component to

cater for backscatter The Kubelka-Munk theory similarly does not account for beam broadening and it cannot accommodate a collimated flux term This causes it to overestimate fluence rates when scattering dominates Compared to Beers Law and the Kubelka-Munk theory the diffusion approximation appears to be the best of the three models for highly scattering tissue Its collimated flux term makes it suitable for describing laser-tissue interaction and it allows for beam broadening and backscatter

From fig 4 6 it can be seen that for highly scattering tissue the energy fluence rate within the tissue is greater than the incident irradiance (i e incident irradiance = Fc(0)). This phenomena is well documented and has been reported by Star (38) and Motamedi (45) amongst others It is due to diffuse internal reflection and backscattering at the tissue surface and is dependent on the absorption coefficient as can be seen from fig 4 8 where the fluence rate just inside the tissue is seen to drop markedly with increasing $\sigma_a$ This phenomenon can be compared to the well-known "build-up" effect in Radiotherapy where the fluence rate of external beam radiation is observed to be greater just inside the tissue

In fig 4 6 the fluence rate is seen to reach a maximum within the tissue In fig 4 7 it is shown that this peak shifts further into the tissue with increasing g The reason for this is that as g increases transmission (forward scattering) increases and the local absorption

as this propagation becomes more forward scattering the fluence rate peaks further into the tissue and decays more slowly when compared with a more isotropic medium At g = 1 the light is totally forward scattered resulting in a fluence rate peak which extends up to 7mm inside the tissue, with the fluence rate at the tissue surface approximating the incident irradiance

Fig 4.9 indicates that as $\sigma_s$ decreases to the magnitude of $\sigma_a$ the fluence plot collapses to a straight line and total transmission is predicted as would be expected These plots seem to indicate that the diffusion approximation presents a cogent and logical description of laser-tissue interaction The shape of the plots obtained are confirmed theoretically by Yoon et al (1989) (46) and experimentally by Moes (1989) (47).

## 4.6 Conclusion

In this chapter an analysis was presented of several methods for the modeling of light propagation in tissue All three methods prove effective for specific applications The simplest method, Beer's Law, is applicable where absorption dominates scattering and has been used effectively for the description of the transmission of visible light below 600nm travelling through blood The KM theory is a more robust technique and has been used extensively in light-tissue modeling Problems with the method include the fact that it only allows for diffuse irradiance and 2-D geometries It is also difficult to obtain accurate values for the K and S coefficients The diffusion theory is able to accommodate a collimated flux which makes it suitable for laser-tissue modeling It has been shown to be very effective for the description of conditions where scattering dominates absorption The main drawback of the model is that it has been shown, both by phantom studies and when compared to other models, to be inaccurate at tissue boundaries The reason for this is that in highly scattering tissue propagation is strongly forward peaked (e g g = 0 71) Thus at tissue boundaries or at local inhomogeneities the model is unable to account for large backscattered signals caused by differences in refractive indices

The three models described in this chapter are not the only models currently in use for the description of light propagation in tissue. Several other techniques have

recently appeared in the literature These include the discreet ordinate approximation (45) of the transport equation and models which trace photon migration in tissue in a probabilistic fashion such as the lattice (55) and Monte-Carlo (56) techniques. These models are relatively complex and prove prohibitive in terms of computing time

In chapter 5 the diffusion theory is used to model the propagation of He-Ne laser light through bronchial tissue The diffusion theory is chosen because of its ability to describe laser interactions and situations where $\sigma_s >> \sigma_a$ (which has been shown (35) to be the case for red light propagating through tissue) The quantity of interest in the model is the radiant energy fluence rate at depth and thus accuracy limitations at the tissue boundary have only a limited effect on the efficiency of the model

# Chapter 5

# A THEORETICAL DESCRIPTION OF A SYSTEM FOR THE PERFORMANCE OF FLUORESCENCE ENDOSCOPY

## 5.1 Introduction

In chapter 3 the design of a system for the detection of Hp fluorescence was described. This system utilises a He-Ne laser as excitation source and introduces a novel method of fluorescence detection involving the determination of a ratio of fluorescent : backscattered excitation light. The aim of this project is to investigate whether this system can be used as the basis of an instrument for the effective performance of fluorescence endoscopy.

Fluorescent endoscopy, as outlined in chapter 1, involves the location of intra-cavitary tumours via the detection of fluorescence from a tumour bound photosensitising dye. It has been shown (chapter 3) that the system is capable of detecting fluorescence from very low concentrations of Hp in solution. Also the ratio method assumes certain advantages over other techniques of clinical fluorescence detection. In this chapter a comprehensive mathematical model is presented which predicts the behaviour of an instrument, based on the

system described in chapter 3, for the detection of small intra-cavitary tumours This model serves to assess the effectiveness of the instrument for tumour detection and presents a detailed sensitivity analysis in terms of such parameters as tumour size, concentration of photosensitiser, and thickness of overlying tissue. This should prove of great benefit in predicting clinical results and in the analysis of such in-vivo results The model is also designed to be adaptable to other systems and instruments of tumour fluorescence detection Similarly the model could be applied to light dosimetry considerations in photodynamic therapy, general laser surgery and other applications of lasers in medicine

5 2 Model

In this section the detection of a tumour using a clinical instrument based on the system described in chapter 3 is modelled The model assumes both the same excitation source (He-Ne laser) and the same detection apparatus ( PMT, lock-in amplifier and ratio method of fluorescent detection) as used in chapter 3 A clinical endoscope is used to transmit the excitation light to the site of the tumour and collect the resultant fluorescence This endoscope is assumed to comprise of a fibre-bundle exactly similar to the bundle designed in chapter 3. The only difference is that this bundle must of necessity be over 1 metre in length in order to access an inter-cavitary tumour.

The target or model tumour is assumed to be cylindrical in shape and embedded in a mass of healthy tissue (see fig 5 1) The dimensions of the tumour are taken as diameter = 5mm, thickness = 0 5mm and overlying tissue thickness = 1 5mm These dimensions are chosen to represent the likely dimensions of early small cell carcinoma of the tracheo-bronchial (TB) tract Such carcinomas develop initially in the submucosa and are thus separated from the lumen of the body tract by several layers of epithelial tissue HpD is assumed to have selectively accumulated in the tumour with a concentration of 1$\mu$g per gram of tumour while being totally absent in the surrounding tissue. The fibre-optic endoscope is assumed to

be located in the lumen of the of the body cavity with the excitation fibre positioned directly adjacent to the tumour (see fig 5 1)

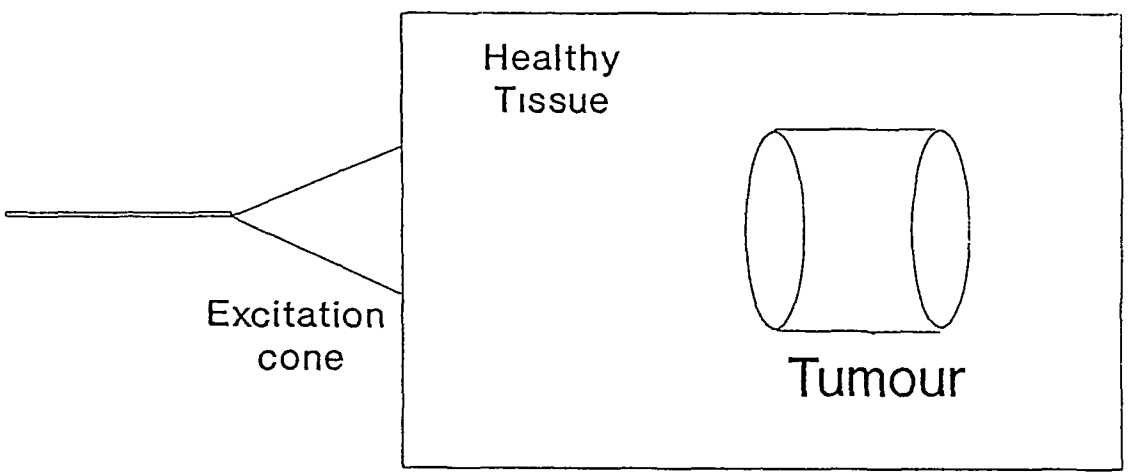


Fig 5 1 Schematic representation of a tumour embedded in healthy tissue

For the sake of simplicity the process of tumour detection with the instrument can be broken down into the following sections

(1) The coupling of the excitation light from the He-Ne laser to deep within the tissue
(2) The propagation of excitation light through the overlying tissue to the tumour site
(3) The stimulation of the HpD within the tumour and the subsequent return of the fluorescence from the tumour to the tissue surface.
(4) The collection of the fluorescence that reaches the tissue surface, by the fibre-bundle and the detection system

In this chapter these sections will be dealt with separately

5 2 1 Excitation

In order to access locations deep within the body cavities a fibre-bundle of over 1 metre long must be used This fibre-bundle is assumed to be positioned within the lumen of the body tract 1 cm from the epithelial wall The epithelial wall of both the main body tracts (i e the tracheo-bronchial and the gastro-intestinal) are coated with a thick layer of mucus , secreted from ducts at the base of the cilia. Thus the light leaving the excitation fibre may be considered to be coupled into an aqueous

environment This excitation light describes a cone as it 'leaves the excitation fibre The surface area of this cone (SA) , at the epithelial wall determines the irradiance ($mW/cm^2$) of the excitation light which enters the tissue If the fibre-bundle is assumed to be identical in all things but length to the one described in chapter 3 then from chapter 3 we have the surface area at the tissue wall given by ·

$$SA = \left(\frac{0\ 44}{1\ 33}\right)^2 \Pi \times (1\ 0)^2 \qquad (1)$$

Where 0 44 is the numerical aperture of the excitation fibre and 1 33 is the refractive index of the medium into which the light leaving the fibre is coupled

Doiron reported a 25% light loss when coupling a Krypton-ion laser down a 1 metre length of fibre. Assuming a similar "worst case" coupling efficiency then if a 5mW He-Ne is used as excitation source the excitation light intensity entering the tissue is given by

$$I_o = \frac{5 \times 0\ 75}{SA} = 10\ 9\ mW/cm^2 \qquad (2)$$

Generally, coupling efficiencies for red light will however be higher

5 2.2 Light-Tissue Interaction

In equation (2) the light intensity entering the tissue is calculated In order to detect the tumour the light must travel through the overlying epithelial tissue before exciting fluorescence in the HpD marked tumour In chapter 4 several models for the description of light propagation ın tissue were outlined The diffusion approximation of the transport equation is considered the most appropriate model for the description of the progress of He-Ne laser light through the epithelial tissue for the following reasons

(1) It includes a collimated flux term whıch makes it suıtable for the description of laser-tissue interaction

(2) It has proved the most accurate model in the case of tissues with scattering coefficient ($\sigma_s$) significantly larger than the absorption coefficient ($\sigma_a$) This is the case for a wide variety of biological tissues at 630nm , including bronchial epithelium tissue (see fig 5 2)

(3) $\sigma_a$ and $\sigma_s$ are easily measured for epithelial tissue and values are well-documented in the literature (48).

(4) The model allows for the anisotropic perturbance of ırradiance at depth. This makes it suitable for thick tissue slabs

In chapter 4 the diffusion approximation is broken down to

the following three equations for the forward , backward and collimated photon fluxes respectively

$$\frac{dFc(z)}{dz} = -(\sigma_a + \sigma_s)Fc(z)$$

$$\frac{dF+(z)}{dz} = -[2\sigma_a + 0\ 75\{\sigma_a + (1-g)\sigma_s\} - \sigma_a]F_+(z) + [0\ 75\{\sigma_a + (1-g)\sigma_s\} - \sigma_a]F_-(z) + \sigma_s(2 + 3g)\frac{Fc(z)}{4}$$

$$-\frac{dF_-(z)}{dz} = -[2\sigma_a + 0\ 75\{\sigma_a + (1-g)\sigma_s\} - \sigma_a]F_-(z) + [0\ 75\{\sigma_a + (1-g)\sigma_s\} - \sigma_a]F_+(z) + \sigma_s(2 - 3g)\frac{Fc(z)}{4}$$

These equations can be solved by recourse to linear algebra as outlined in appendix 1 In this way a general solution to the three simultaneous equations is obtained By applying the boundary conditions

$$F+(z = 0) = 0 = F-(z = Z)$$

(Z is the thickness of the slab of tissue in which the light is propagated) expressions for Fc(z), F+(z), and F-(z) are obtained These fluxes are expressed as functions of $\sigma_a$ , $\sigma_s$ and g the anisotropy factor The light fluence rate can be calculated as in chapter 4 by means of the expression

$$\Psi(z) = Fc(z) + 2(F+(z) + F-(z))$$

In order to obtain the fluence rate of He-Ne light as it passes through tissue appropriate values of $\sigma_a$ , $\sigma_s$ and g must be obtained. The anisotropy factor g is commonly taken as 0 71 for a variety of tissue types and wavelengths (47) Values of $\sigma_a$ and $\sigma_s$ were obtained from the scientific literature Wilson and Peterson (48) have published a table of tissue coefficients for a range of light wavelengths Fig 5 2 tabulates the coefficients quoted for 630nm light

| $\sigma_a (cm^{-1})$ | $\sigma_s (cm^{-1})$ | Tissue |
|---|---|---|
| 0 4 | 7 9 | Cow Muscle |
| 0 3 | 4.0 | Chicken Muscle |
| 1 0 | 17 0 | Human Dermis |

Fig 5 2 Optical coefficents of tissue at 630nm

The backscattered excitation light can be calculated by recording the value of the backward photon flux at a tissue thickness of zero (i e F-(z = 0)) Fresnel reflection at the tissue surface is neglected as identical refractive indices inside and outside the tissue are assumed

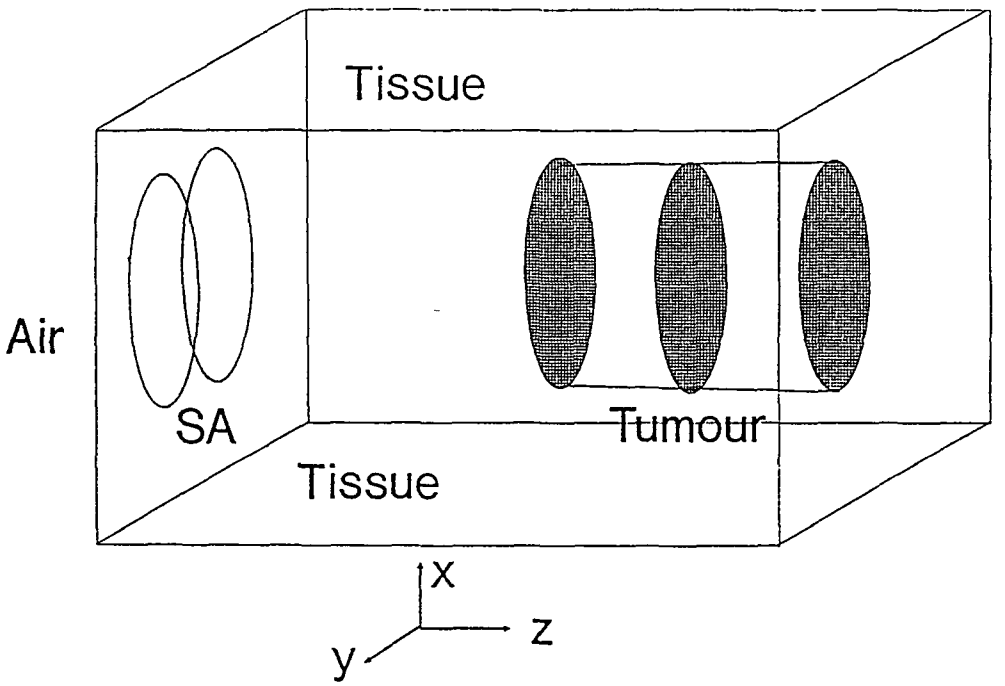


Fig 5 3 Model of tumour as x-y lattice of point sources and corresponding lattice structure of the surface area of intersection (SA)

5 2.3 Tumour Fluorescence

In the last section it was shown how the energy fluence rate of He-Ne light is calculated as it passes through the tissue In this section we will examine what happens when the He-Ne light strikes the HpD marked tumour The first thing to be determined is the He-Ne energy fluence rate within the tumour It is assumed in this model

that the tumour and the overlying tissue both have the same optical properties Thus if the location of the tumour within the tissue is known then the fluence rate can be determined at each point within the tumour

It is assumed that with respect to the excitation light the problem can be treated in a 1-D fashion and that the fluence rate only varies with z The tumour is divided into thin slices of thickness corresponding to a unit z co-ordinate (see fig 5 3) The fluence rate of excitation light for each of these slices is recorded and assumed constant for all x and y co-ordinate values of the tumour corresponding to each unit z value When excitation light strikes each slice of tumour , fluorescence is emitted in all directions The total yield is given by

$$Y = I_{ex}\ QE\ Ct \quad (mW/cm^2) \quad (3)$$

where ·

$I_{ex}$ = energy fluence rate of the excitation light

QE = quantum efficiency of HpD marked tumour slice

Ct = concentration of HpD in tumour

In order to simulate the fluorescent process each of the tumour slices is considered to be an x-y lattice of point sources (see fig 5 3) The emission from each of these point sources is given off in all directions and its propagation back through the overlying tissue to the skin surface has been described by McKenzie (49) as

$$\phi(z) = \frac{\text{Pow} \times (\sigma_a + \sigma_s)^2 \exp - (\sigma_a - \sigma_s)}{8\pi \times \sigma_a \times z} \quad \text{(mW)} \qquad (4)$$

where $\phi(z)$ = power at distance z from point source

Pow = Y x L (area of each unit x-y lattice)

Due to the fact that there is only a small difference in wavelength both for excitation and emission wavelengths the optical properties of tissue are considered to be identical From equation (4) the amount of fluorescent light which reaches the tissue surface from each of the point sources within the tumour can be obtained By summing the contributions from each of these point sources the total amount of fluorescent light which reaches the tissue surface from a single slice of tumour can be calculated Subsequently the contribution from each slice is added

5 2 4 Collection Efficiency .

In the previous section it was shown how the amount of HpD fluorescence which reaches the tissue surface can be calculated Not all of this fluorescence will be detected by the fibre-bundle In chapter 3 a detailed analysis of the collection efficiency of the fibre-bundle was presented Equation (4) defined the surface area of intersection (SA) between the excitation light cone and the detection light cone of the first collection fibre In this model equation (4) is used to calculate the intersection surface area (SA) at the tissue surface It is considered that only light which emerges from the tissue within SA will be sampled by the collection fibres. In fig 5 3 the format of the tumour-tissue structure used in this model is outlined For It is assumed that SA is positioned directly above the tumour on the tissue surface SA is divided in the x-y plane, into a lattice structure similar to that of the tumour The contribution from each point source in the tumour volume, to each point within the SA of intersection on the skin surface is then summed and a value for the total fluorescent light contribution within the SA, obtained

The fluorescent photons which emerge within the intersection area can be assumed to be emitted in all forward directions This emission is assumed constant over all angles from 0 to Π steradians Thus the fluorescent

power leaving the intersection area can be expressed in mW/steradian as

$$\dot{P} = \frac{\text{total fluorescent power in intersection area}}{2\Pi}$$

The total fluorescent power collected by the first collection fibre can thus be expressed as

$$F = P \times \frac{\Pi R_f^2}{k^2} \quad \text{(mW)}$$

where $R_f$ = radius of collection fibre

$k$ = distance between SA and collection fibre face

There are 6 collection fibres in the inner ring of the fibre-bundle thus the fluorescent power sampled by the inner ring is 6F. In order to obtain the total fluorescent power sampled by the fibre-bundle F is calculated for each of the rings of fibres in the bundle and multiplied by the number of fibres in each respective ring The contributions from each of the rings are then summed The effects of oversampling by the collection fibres are ignored

The laser excitation light backscattered from the tissue can be calculated by obtaining the value of the backward photon flux F-(z) at the tissue surface i e at z = 0 This can be obtained from the general solution to equations (8) (9) and (10) (see section 5 3). The value obtained is a light fluence rate expressed in $mW/cm^2$ If this is multiplied by the intersection area (SA) then the total backscattered excitation light power leaving SA can be obtained The quantity of backscattered light sampled by the fibre-bundle can be calculated in the same way as the sampled fluorescent light is calculated above The detected fluorescence is then calculated as a percentage of detected backscattered excitation light and forms the basis of all tumour detection predictions generated by the model

## 5.3 Results

The above calculations and assumptions were implemented in a computer program which was developed and which generates predictions as to the sensitivity of the instrument for the detection of tumours embedded in the tracheo-bronchial wall. This program was written in Basic compiled in RiscBasic and run on an Archimedes PC with a Floating Point Emulator installed (see appendix 2). In figs 5.5 to 5.11 typical results obtained from this program are presented. The graphs take the form of fluorescent : backscattered signal ratios (expressed as a percentage) plotted as a function of different parameters i.e. tumour dimensions , tumour depth , HpD concentration or distance of fibre-bundle from tissue. The dimensions of the design or model tumour considered in this chapter are chosen to represent the dimensions of early small cell carcinomas of the TB tract. Thus a cylindrical tumour of dimensions ; diameter 5 mm, thickness 0.5mm, concentration 1$\mu$g of HpD per gram of tumour, embedded in healthy tissue 1.5 mm from the lumen of a body cavity, is assumed. The fibre-bundle is assumed to be positioned directly above the tumour 1 cm from the tissue wall. Small cell carcinomas can be present as a small plaque several millimetres thick or as a large sheet type condition thin and spread out. Figs 5.5 to 5.11

investigate the feasibility of tumour detection as the tumour dimensions change as the endoscope to tumour distance changes and as the concentration of HpD in the tumour changes. They present an example of the predictions which can be obtained from this model.

One of the assumed advantages of the ratio method of fluorescent detection is that tumour detection is independent of fibre-bundle to sample distance. This claim is investigated in fig 5.5 where the distance of the fibre-bundle from the TB wall (P) is plotted against signal ratio for the model tumour. The plot shows that signal ratio has a marked dependence on P . In order to investigate this anomaly fig 5.6 shows a plot of P versus signal ratio for two different tumour diameters. All other parameters are identical as in fig 5.5. It is shown that for the larger diameter P is shown to be independent of signal ratio.

In fig 5.7 the effect of HpD concentration on detection of the model tumour is investigated. Concentrations of up to 1$\mu$g of HpD per gram of tumour have been quoted (27) to accumulate. Fig 5.7 predicts that there is a linear relationship between concentration and signal ratio at concentrations around 1$\mu$g/g. This is as expected. The distance between fibre-bundle and tissue wall is taken to be 1cm.

One of the advantages of using red instead of violet excitation light is that it penetrates more deeply into tissue and thus can access more deeply embedded tumours In order to investigate how deep a tumour can be detected by the instrument the overlying healthy tissue thickness of the model tumour is increased and tissue thickness plotted as a function of signal ratio (fig 5.8) From fig 5 8 it is apparent that signal ratio decreases rapidly with tissue thickness up to a thickness of circa 2 5mm beyond which increasing tissue thickness has little effect on signal ratio

As has been mentioned above, early small cell carcinoma can present itself as a large sheet of minimal thickness and large diameter or as a plaque of small diameter and several millimetres thickness For this reason the cylindrical shape of the model tumour is ideal for assessing the feasibility of tumour detection In fig 5 9 a tumour plaque is simulated and the affect of increasing the thickness of the tumour is investigated The signal ratio is seen to increase linearly with tumour thickness to a thickness of 0 6mm after which tumour thickness becomes independent of signal ratio In fig 5 10 the tumour diameter is varied in order to simulate sheet-like small cell carcinoma. For small diameters increasing the tumour diameter has little effect on signal ratio For diameters above 2mm however the signal ratio increases linearly with

increasing diameter The implications of these plots are that in clinical situations, if factors such as HpD concentration distance of bundle from tissue etc are known, tumour dimensions can be ascertained from detected signal ratios within certain limits i e for tumours with a diameter greater than 2 mm and thickness less than 0 6mm

In fig 5 11 the tumour diameter is varied again but this time as the diameter is increased the thickness of the tumour is decreased proportionally in order to maintain a constant tumour volume This plot investigates the feasibility of tumour detection as the model tumour gets longer and thinner From the plot it is apparent that when the tumour dimensions represent those of a plaque of small cell carcinoma (i e small diameter, large thickness) the signal ratio rises sharply with diameter As the tumour dimensions begin to represent sheet-like carcinoma (i e large diameter, negligible thickness) the signal ratio drops sharply and for diameters greater than 1cm the signal ratio is independent of diameter

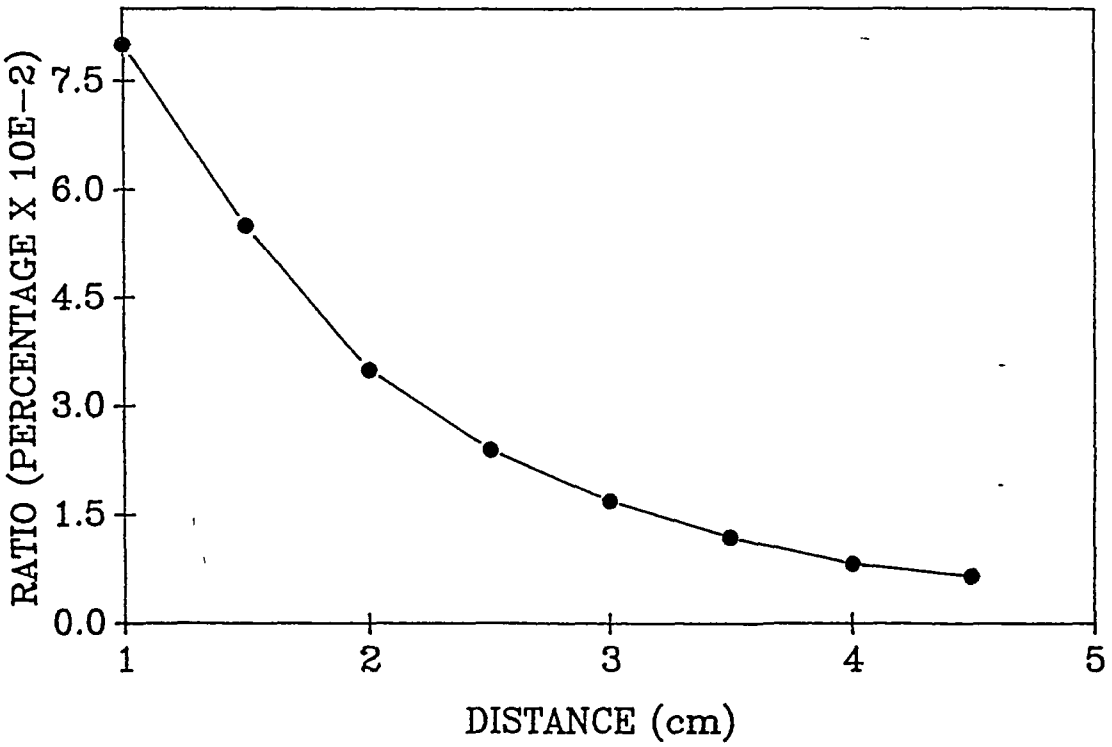


Fig 5 5 Distance from sample versus signal ratio for the model tumour.

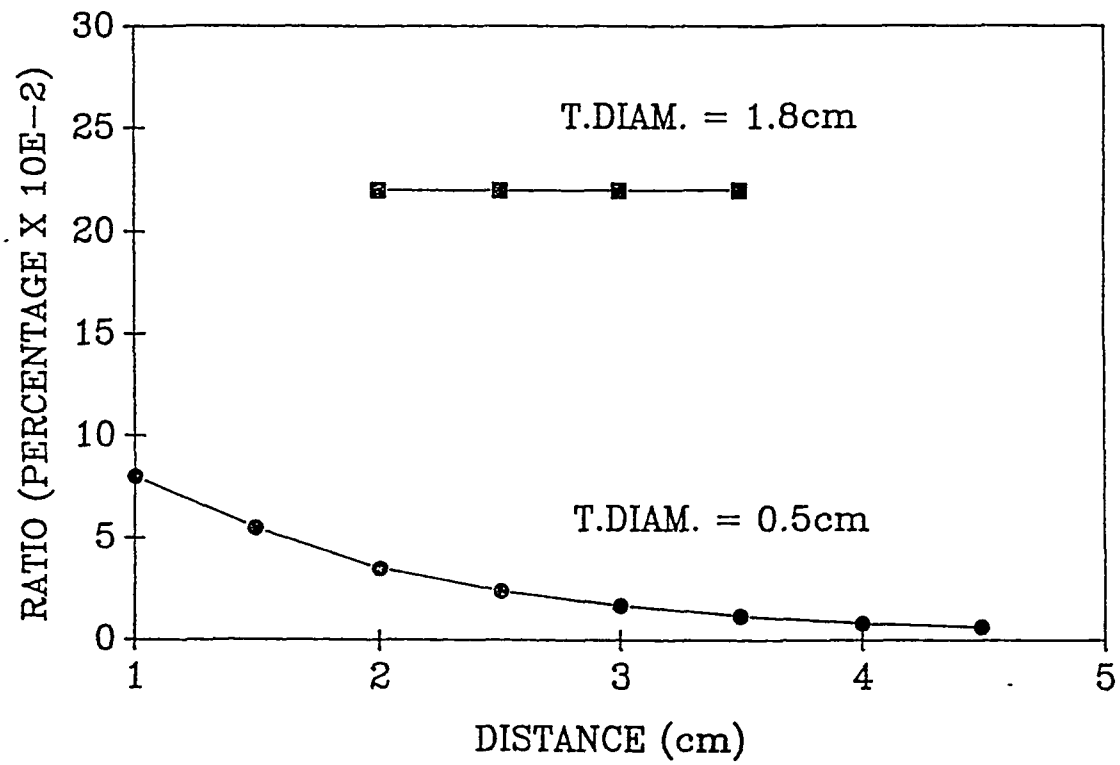


Fig 5 6 Distance from sample versus signal ratio for tumour surface diameters 0.5cm and 1 8cm

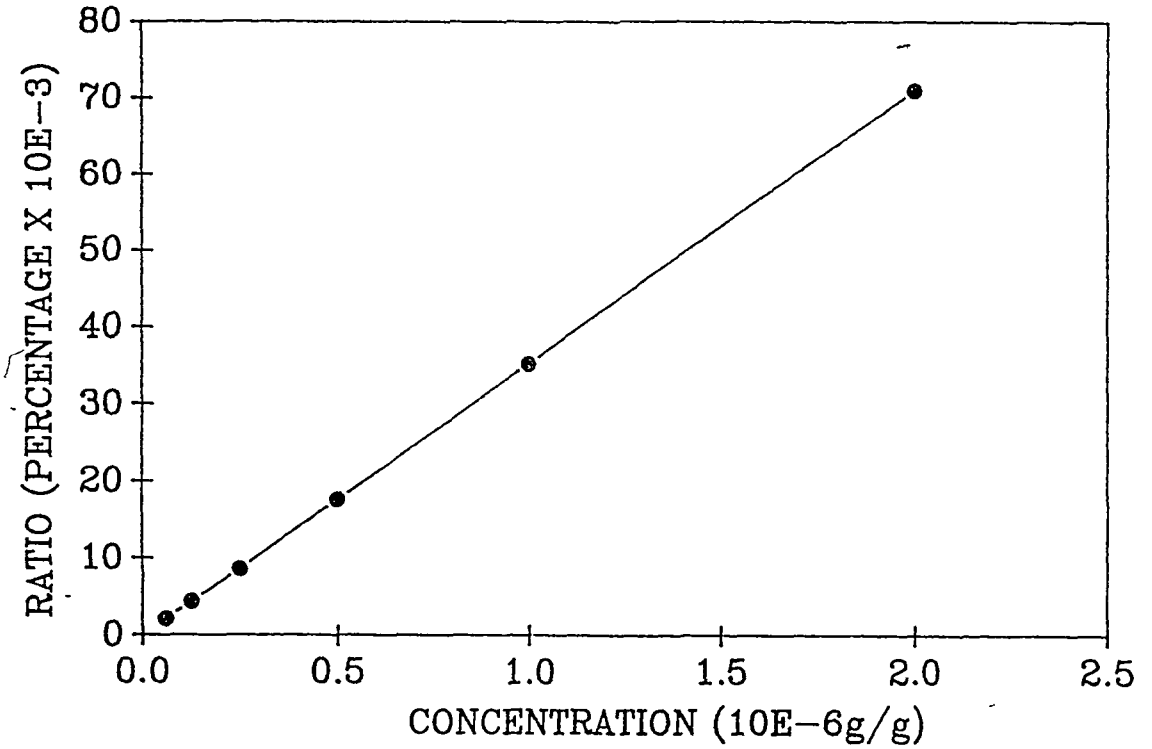


Fig 5 7 Concentration of localised HpD versus signal ratio for the model tumour

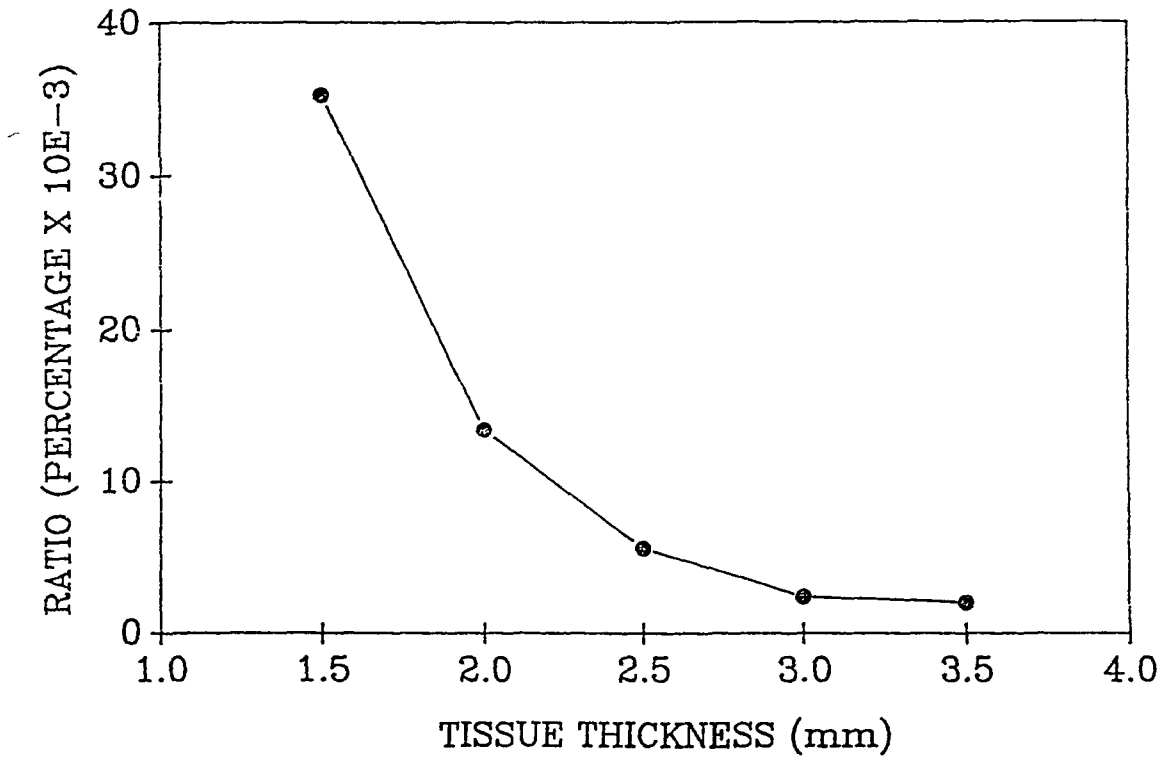


Fig 5 8 Overlying healthy tissue thickness versus signal ratio

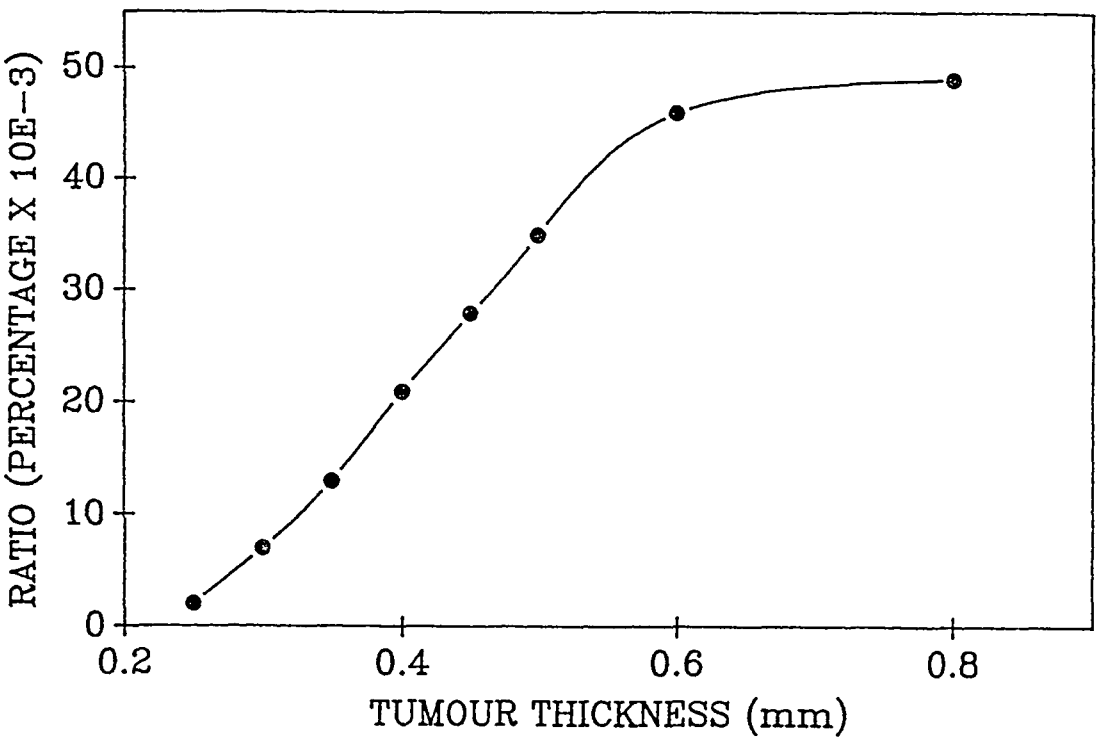


Fig 5 9 Tumour thickness versus signal ratio

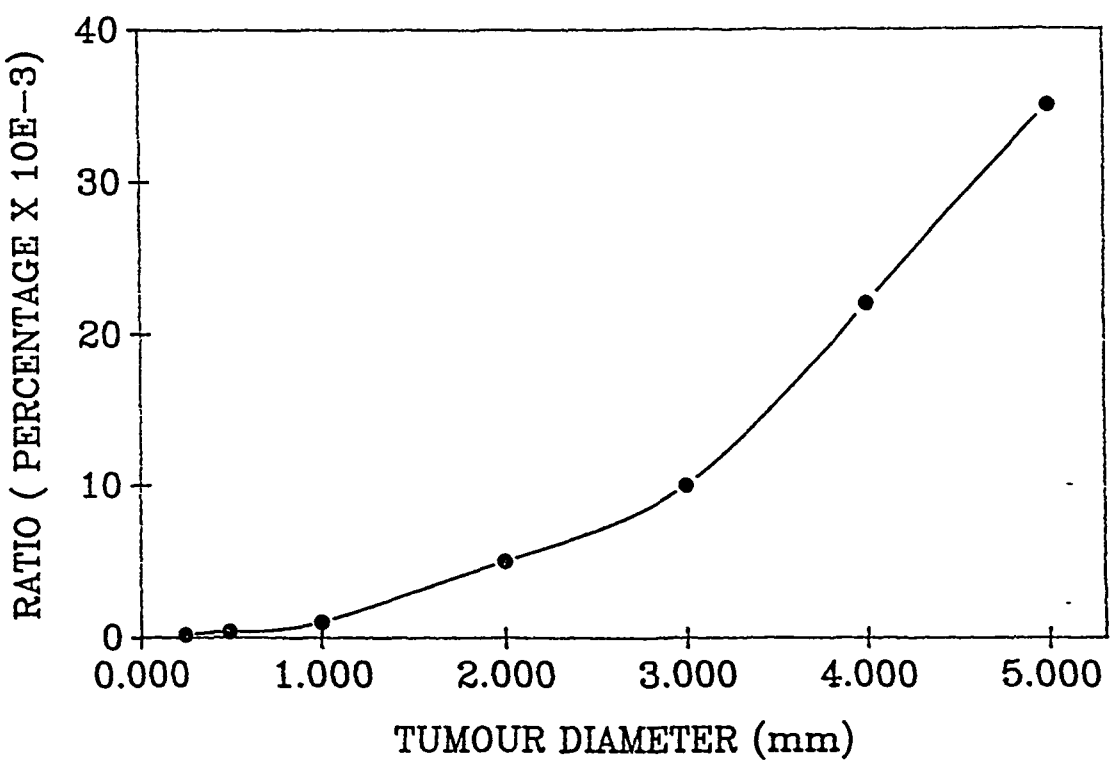


Fig 5 10 Tumour diameter versus signal ratio

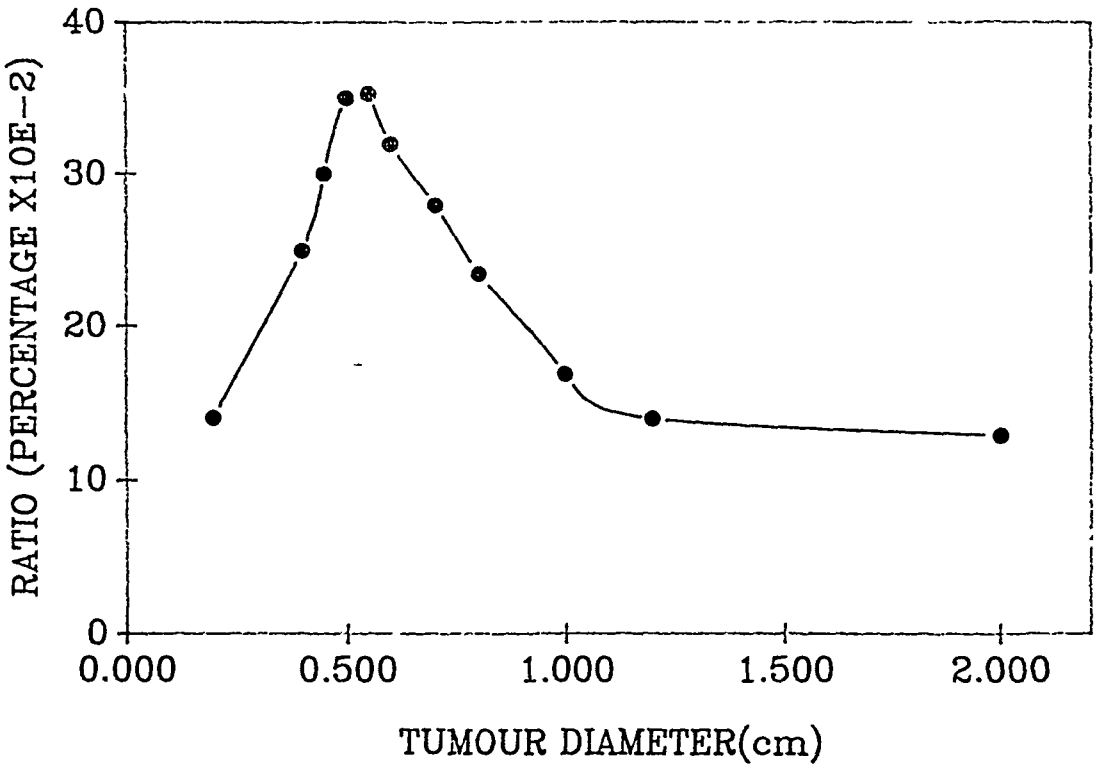


Fig 5 11 Tumour diameter with constant tumour volume plotted against signal ratio

## 5.4 Discussion

One of the assumed advantages of the ratio method of fluorescent detection is that the signal ratio is independent of fibre-bundle to sample distance (P) (2,20) This assumption is shown to be erroneous in fig 5 5 Signal ratio is seen to fall off markedly with distance for the model tumour (i e tumour diameter 0 5 cm) In contrast Fig 5.6 shows that for tumours of much larger diameter the assumption holds This anomaly is explained in terms of the collection efficiency of the fibre-bundle If the area on the tissue surface sampled by the collection fibres is greater than the tumour surface area then the fibre-bundle will collect proportionally more backscattered excitation light than fluorescence This causes the signal ratio to drop with distance on account of the fact that the collection area on the tissue surface increases with P However a tumour with a large surface area will show a signal ratio unaffected by variations in P This is because its surface area will always be bigger than the collection area and the same proportion of backscattered to fluorescent light will be detected by the fibre-bundle Hence the assumed distance invariance will hold

In fig 5 7 a linear plot is obtained as the concentration of HpD in the tumour is decreased In chapter 3 in-vitro fluorescent detection of Hp fluorescence in solutions of $H_2O$ and MeOH reveal a slow tail-off of signal ratio at low concentrations This discrepancy is probably

due to the experimental difficulties involved in the handling of low concentrations of Hp In particular Hp has a tendency to stick to the sides of the cuvette causing experimental inaccuracy Alternately there is some evidence to suggest that the fluorescent quantum yield of Hp in solution changes with concentration On account of the lack of available data this phenomenon was not accounted for in the model and may explain the difference between experimental and theoretical data at low concentrations Aside from this anomaly, experimental (chapter 3) and theoretical data show very good agreement

The variation of signal ratio with the thickness of overlying healthy tissue is plotted in fig 5 8 In chapter 3 it has been observed experimentally that the lowest signal ratio that can be detected by the endoscopic instrument is approximatly $6 \times 10^{-3}$% If this criteria is applied to fig 5 8 it can be predicted that the instrument will detect the model tumour beneath an overlying tissue thickness of up to 2 4mm The implication of this in clinical terms is that the instrument is sensitive enough to detect the model tumour deep into the submucosa of the tracheo-bronchial tract

Fig 5 9 examines what happens when the tumour thickness is increased The plot rises steadily but levels off after a thickness of 0 6mm An explanation for this may be because the excitation signal drops significantly inside

the tumour and thus after 0 6mm the localised HpD is not stimulated to fluoresce therefore the increased tumour thickness does not contribute to the fluorescent signal If $6 \times 10^{-3}$% is taken as the lowest signal ratio that can be detected by the system then from fig 5 9 it is apparent that model tumours with thicknesses less than 0 3mm will not be detected

Variation of the tumour diameter in fig 5 10 shows very little change in signal ratio for small diameters As the diameter increases to the point where the tumour surface area approaches that of the collection surface area on the tissue surface, the signal ratio increases significantly The signal ratio is expected to reach a saturation level beyond which increasing the tumour diameter will have no effect on the signal ratio A signal ratio of $6 \times 10^{-3}$% corresponds to a tumour diameter of circa 2 5mm in fig 5 10 The implication of this is that small cell model tumour plaques with diameters less than 2 5mm will go undetected by the system However such tumours are very small in size (i e diameter = 2 5mm and thickness = 0 5mm) and could be considered to be in a very early stage of development and in no danger of becoming invasive i.e spreading to other parts of the body

In fig 5 11 the diameter is varied but the tumour volume is kept constant Thus as the diameter is increased the thickness is decreased in order to maintain the volume. This plot gives us an indication of the system's detection limit for small and spread out sheet-type tumours In fig 5 11 the signal ratio rises initially as the tumour diameter approaches that of the detection overlap area This is because the energy fluence rates at the deeper levels of the tumour are very low and these levels do not contribute significantly to the fluorescent process As these deeper levels are cut away the tumour becomes longer and thinner and eventually the levels with significant energy fluence rates are disregarded causing the signal to drop sharply All points on the plot are above the 6 x $10^{-3}$% limit of detection This implies that all model tumours with a thickness of 0 5mm will be detected irrespective of their diameter and that thickness is the deciding factor in terms of whether the tumour will be detected or not

## 5 5 Conclusion

A theoretical analysis of the clinical behaviour of our instrument has been presented in this chapter A mathematical model which incorporates fibre-geometry, light-tissue interaction, tumour fluorescence and collection efficiency considerations, has been developed This model is then incorporated in a computer program which then serves to generate predictions as to the performance of the instrument for the detection of a model or target tumour The target tumour is assumed to be cylindrical in shape with dimensions , diameter = 5mm , thickness = 0 5mm , with an overlying overlying healthy tissue thickness of 1 5mm and a concentration of 1$\mu$g of HpD per gram of tumour This model or target tumour mirrors the dimensions of early small cell carcinomas of the tracheo-bronchial (TB) and gastro-intestinal (GI) tracts The model can be easily adapted to describe other systems with, maybe a different excitation wavelength and source or a different fluorescent detection technique

The model predictions presented in this chapter do not constitute a full analysis of the clinical performance of the instrument They rather provide an indication of the kind of data that can be obtained from the model In clinical procedures the model should play a role in tandem with the sensitivity analysis carried out on the instrument in chapter 3 Such a comparison could be used to plan light doses and determine whether detection is feasible in a

given situation.

The model predictions are presented in figs 5 5 to 5 11 From fig 5.5 it is seen that tumour detection is not independent of fibre-bundle to tissue distance for the target tumour, as assumed by the ratio method of fluorescent detection In fig 5 6 however independence is found for tumours of larger diameter This anomaly is explained in terms of the geometry of the fibre-bundle In clinical situations the dimensions of the tumour will not be known and thus endoscope to tissue signal ratio invariance cannot be assumed as an advantage of the ratio method

From the sensitivity analysis carried out on the system in chapter 3 we know that the smallest signal ratio detectable by the system is $6 \times 10^{-3}$% This criteria is applied to the model results in order to ascertain the limits of tumour detection From fig 5 8 it is apparent that model tumour detection can occur below a maximum healthy tissue thickness of 2 4mm The extent of epithelial tissue (where small cell carcinomas originate) in the TB and GI tracts is approximately 1.5-2 0mm Thus the system is sensitive enough to detect the model tumour throughout the extent of the epithelial layer

From fig 5 9 the model predicts a minimum detectable model tumour thickness of 0 3mm As the diameter of the

model tumour is 5mm the minimum cylindrical tumour volume that can be detected is thus 5 8 $mm^3$. This represents the minimum volume of sheet-like small cell tumour that can be detected In fig 5 10 a minimum detectable diameter of 2 5 mm is predicted for the model tumour (i e thickness = 0 5mm) This results in a minimum detectable volume of 2 4 $mm^3$ for a plaque-like small cell tumour. These predictions indicate that the system can detect small cell carcinomas while still contained in the epithelial layer. X-ray and nuclear medicine techniques quote a tumour detection resolution of $1cm^3$ at which point the tumour has either invaded the lumen of the body-cavity or become invasive (i e entered the sub-mucosa and possibly the bloodstream) Thus the system outlined in this project may prove valuable in screening sections of the population known to be at high risk for the development of small cell carcinomas

The model predictions in this chapter are observed to be of the same order of magnitude as the concentration curves obtained for the system in chapter 3. This is encouraging but the accuracy of the model's predictions can not be fully assessed until they are compared with clinical experimental results. At present there is no clinical application of fluorescence endoscopy or photodynamic therapy in this country In the absence of any such clinical trial results experiments are carried out on a tissue-tumour phantom in chapter 6 and the results obtained compared with those of the model

# Chapter 6

# EXPERIMENTS ON A TISSUE-TUMOUR PHANTOM

## 6 1 Introduction

In chapter 3 an instrument for tumour detection using fluorescence endoscopy was described Several experiments on the in-vitro detection of Hp fluorescence were then conducted, and it was found that the instrument was capable of detecting fluorescence from low concentrations of Hp in solution In vitro samples can be expected to have different optical properties from in vivo samples For this reason, in chapter 5 the instrument was modelled for the in vivo detection of small cell carcinomas of the tracheo-bronchial tract In order to investigate the accuracy of the model's predictions a tumour-tissue phantom with readily tunable optical properties was developed The phantom was constructed in order to approximate as near as possible the dimensions of the model tumour investigated in chapter 5 In this chapter the design of the phantom is described Experiments are carried out on this phantom and the response of the system to variations in

(1) Hp concentration

(2) fibre-bundle to phantom distance

(3) overlying tissue thickness

are compared with the results obtained in the model

## 6 2 Theory

The use of phantoms for dose estimation and therapy planning is well established in the fields of radiotherapy and diagnostic imaging. Very little work has been done on the development of realistic tissue phantoms in photomedicine Such phantoms would allow the testing of models of light propagation and the determination of light flux distributions for various treatment techniques In the related fields of PDT and fluorescence endoscopy such phantoms would amongst others permit the investigation of such questions as the effect of photosensitiser concentration on fluorescent yield Wilson and Patterson (48) have suggested the following four criteria for the ideal tissue phantom

(1) the ability to simulate optical properties of a range of tissue types
(2) the ability to offer stable and reproducible optical properties
(3) the ability to have selectable geometry
(4) the capability of incorporating tissue boundaries and interfaces

There are currently two schools of thought relating to the development of tissue phantoms in light dosimetry One school advocates the use of actual excised human or animal tissue as the phantom material (52) While this approach has the advantage of realism a number of problems arise in the handling of such tissue Firstly it has been shown that the optical properties of this post-mortem tissue can be radically different from those of living tissue due to deoxygenation and blood drainage (50) Secondly the properties of excised tissue change with time causing irreproducible results (52)

The second school advocates the use of inert materials to replicate the properties of tissue in vivo In order to fabricate "tissue" in this way account must be taken of the relative mixture of scattering and absorption centres within a specific tissue type For this reason most such phantoms consist of mixtures of scattering and absorbing materials Marynissen and Star (51) reported the design of a liquid phantom of polyvinyl acetate particles (pure scatterers) suspended in India ink ( a pure absorber) Similar phantoms have been described by Takatani (52) who used blood (absorber) and milk (scatterer) and Wilson (50) who choose blood and agar By varying the relative concentrations of these materials the optical properties of different tissue types could be obtained These phantoms have the advantage over excised tissue in that they can be easily tuned to simulate a wide range of tissue and that the optical properties obtained are reproducible Moes et

al (47) have recently used a mixture of the dye Evans Blue (absorber) and a 10% Intralipid solution (scatterer) as a phantom medium for the investigation of energy fluence rates at 633nm This mixture forms the basis for the tissue phantom described in this chapter This solution was chosen partly because the materials were readily available and partly because an accurate account of the relationship between optical properties and the relative concentrations of scatterer and absorber is available in the literature

Fig 6 1 Schematic representation of the "tumour-tissue" phantom

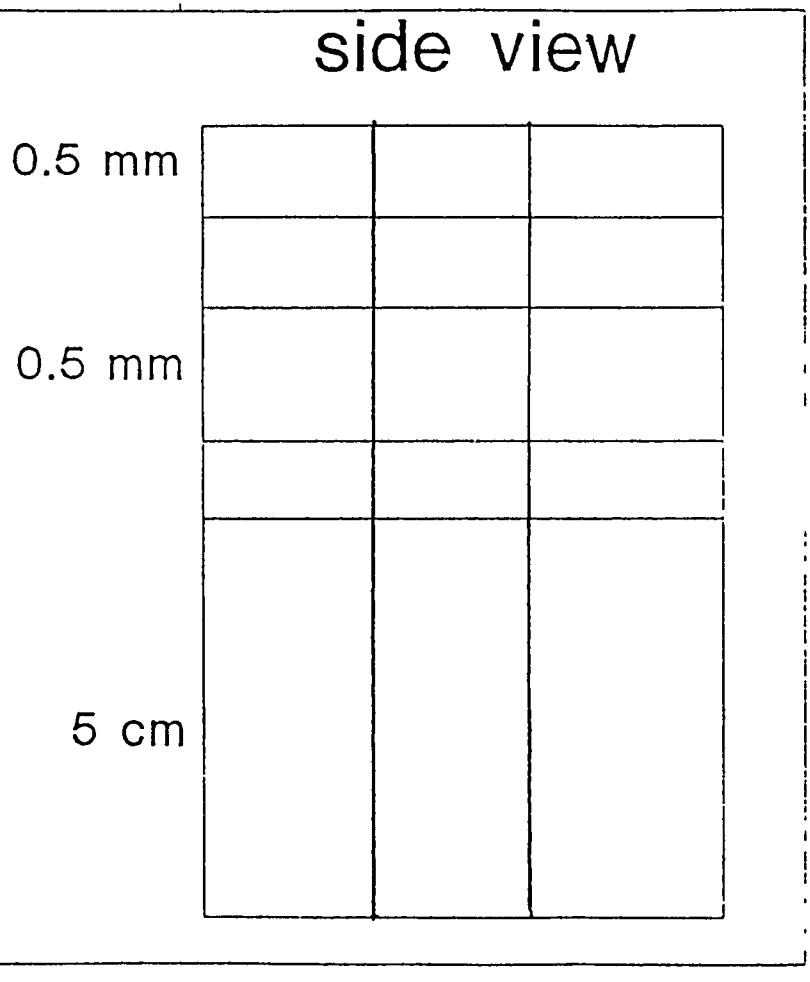
side view
0.5 mm
0.5 mm
5 cm

## 6 3 Phantom Design

The main aim of this chapter is to check the accuracy of the mathematical model as described in chapter 5 For this reason it is essential that the tissue phantom will have the same optical properties as those assumed in chapter 5 Thus the phantom must have the following properties .

Scattering coefficient $\sigma_s = 7\ 9\ cm^{-1}$

Absorption coefficient $\sigma_a = 0\ 4\ cm^{-1}$

Anisotropy factor $g = 0\ 71$

The tissue phantom described by Moes et al (47) consists of a mixture of Evans Blue and Intralipid Moes carried out a series of absorption and scattering measurements and was able to report that with g = 0 71 the scattering coefficient of a 10% solution of Intralipid and water yields a scattering coefficient of

$$\sigma_s = 38\ 6 \times 10^{-3} mm^{-1}/ml \text{ of solution/litre of water}$$

Similarly Evans blue, the absorbing medium, at a concentration of 515mg/litre of water has an absorption coefficient of

$$\sigma_a = 7\ 6 \times 10^{-3} mm^{-1}$$

These two substances were then mixed accordingly in order to obtain a tissue simulating phantom with

$$\sigma_a = 0\ 4\text{cm}^{-1},\ \sigma_s' = 7\ 9\text{cm}^{-1} \text{ and } g = 0\ 71$$

In order to simulate a HpD marked tumour embedded in healthy tissue a "phantom tumour" is introduced into the tissue simulating phantom The "phantom tumour" consists of a solution of Hp + $H_2O$. By means of a specially designed container the tissue and tumour phantoms can be positioned to simulate a HpD marked tumour with over and underlying layers of healthy tissue

A schematic view of the phantom container is presented in fig 6 1 and its construction is described below

A cylindrical shaft 4 5cm in depth and with a diameter of 0 8cm was drilled in a 5 x 5 x 4cm perspex block A similar 0 8cm diameter hole was drilled in a number of 0 5mm thick glass slides The sides of the perspex block were painted matt black The shaft in the perspex block can be filled with the tissue phantom in order to simulate a thick slice of tissue Similarly the tissue or tumour phantoms can be placed in the centre of the glass slides The liquid phantom material is enclosed within the slides by means of microscope cover slips It was assumed that the thickness of the microscope cover-slips did not affect

light propagation within the phantom This container allows the position of the tumour phantom to be varied within the layers of tissue phantom

## 6.4 Experiments

In this chapter the response of the fluorescent detection system, described in chapter 3, is measured using the tissue-tumour phantom Several experiments were carried out and the results obtained are compared with those obtained from the clinical model outlined in chapter 5 In this way an indication of the accuracy of the model's predictions can be obtained

In all three sets of experiments were carried out. Firstly the sensitivity limit of the system is determined and compared with that obtained in chapter 3 for the in-vitro detection of Hp fluorescence from a cuvette containing a solution of Hp + $H_2O$. Secondly the relationship of fibre-bundle to sample distance is investigated and compared with the model predictions Finally the relationship between overlying healthy tissue thickness and signal ratio is investigated by varying the depth of the tumour phantom within the tissue phantom and recording the signal ratio. The resultant plot is again compared with that generated by the clinical model. The experimental procedures carried out in these three sets of experiments are outlined below

6 4.1 Procedure

The sensitivity limit of the instrument for detection of fluorescence from the phantom was determined by filling the shaft of the perspex block with the tissue simulating substance and covering the shaft with a microscope cover slip A drop of Hp solution was placed in the centre of one of the glass slices and enclosed front and back by a cover slip Fluorescent detection was via the ratio method and the signal ratio was measured for successively more dilute solutions of Hp + $H_2O$ . A plot of signal ratio versus concentration of Hp in solution was obtained and the lowest concentration of Hp for which fluorescence could be detected (i e the sensitivity limit) was measured.

The perspex block was again filled with the tissue simulating phantom and the tumour phantom (consisting of a glass slice containing 1$\mu$g/ml of Hp + MeOH) was placed on top of the block The distance of the fibre-bundle from the phantom was then increased in steps of 0 5cm and the signal ratio measured for each step A plot of distance from phantom versus signal ratio was thus obtained

In this experiment a glass slip containing 1$\mu$g/ml of Hp + MeOH was placed on top of the perspex block (containing the tissue simulating material). The glass slip was considered to represent a HpD marked tumour. Slips of

0.5mm thickness containing the tissue simulating material were then successively placed on top of the "tumour" and the signal ratio noted as a function of overlying tissue thickness. A plot of signal ratio versus thickness of overlying "tissue" was thus obtained. This plot could be directly compared to that generated by the clinical model (chapter 5) in order to assess the accuracy of the model's predictions.

## 6.5 Results

In figs 6.2 - 6.4 representative results obtained from some of these experiments are plotted. In fig 6.2 a plot of signal ratio versus concentration of Hp in $H_2O$ is presented. The plot falls sharply with concentration for concentrations greater than 10 $\mu$g/ml. Below 10$\mu$g/ml the plot begins to tail off yielding a lowest detectable concentration of Hp (i.e the sensitivity limit ) of circa 0.7$\mu$g/ml. For each of the points displayed on the plot four measurements were taken and the average value recorded.

In fig. 6.3 the signal ratio is plotted against distance of fibre-bundle from sample for both the results obtained from the phantom experiments (square points) and those obtained from the model predictions (circular points). The experimental phantom points all represent the average of three separate measurements and error bars are included for accuracy. When the experimental error bars

are included the plots show good agreement underlining the fact that the ratio method of utilised in our system does not result in the previously assumed independence of fluorescent detection with fibre-bundle to sample distance

In fig 6 4 the model predictions (circular points) and phantom results (square points) are presented together for the variation of signal ratio with overlying healthy-tissue thickness. The phantom results are again the result of the average of three measurements and the inclusion of error bars indicates good agreement between the model and the experimental results Both plots show a rapid fall off of signal ratio with tissue thickness for thicknesses less than 1 5mm Increasing the tissue thickness above 2mm for the phantom and circa 2 5mm for the model has no effect on the signal ratio This is because the signal ratio at these thicknesses is below the noise level and thus no tumour detection can occur

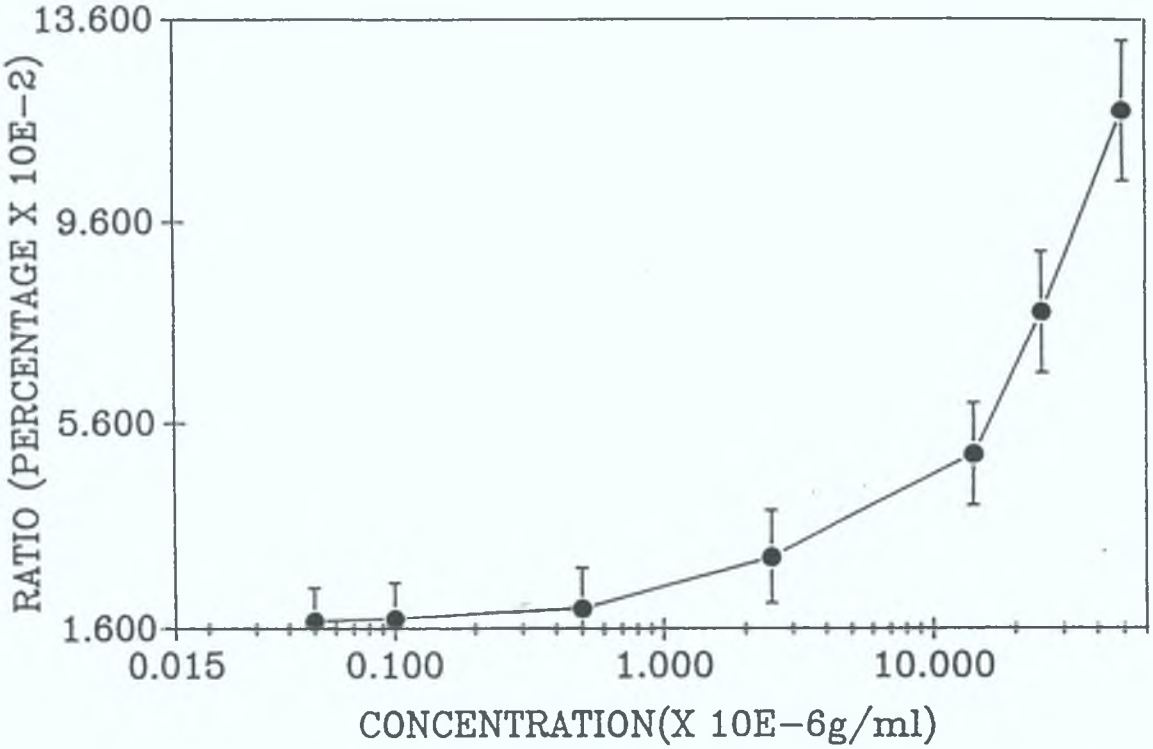


Fig 6.2 Concentration of Hp in $H_2O$ versus signal ratio for the tumour phantom.

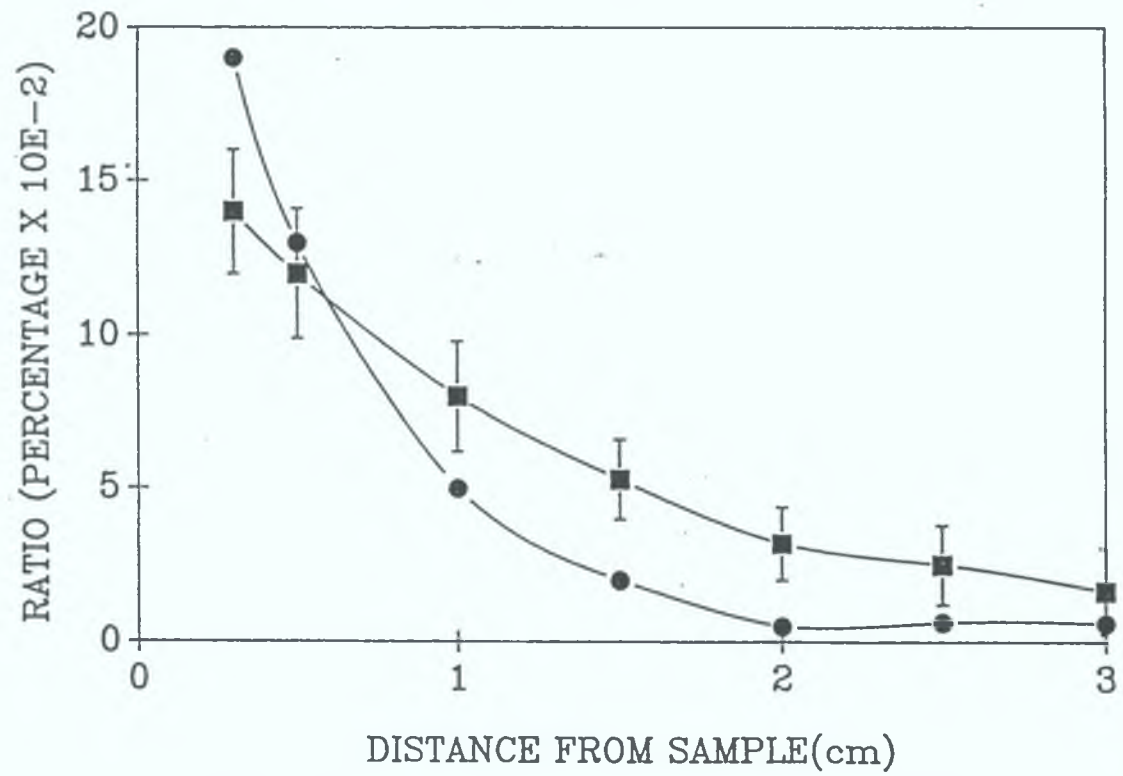


Fig 6.3 Distance of fibre-bundle from sample plotted against signal ratio for both phantom (square points) and model (circular points) results.

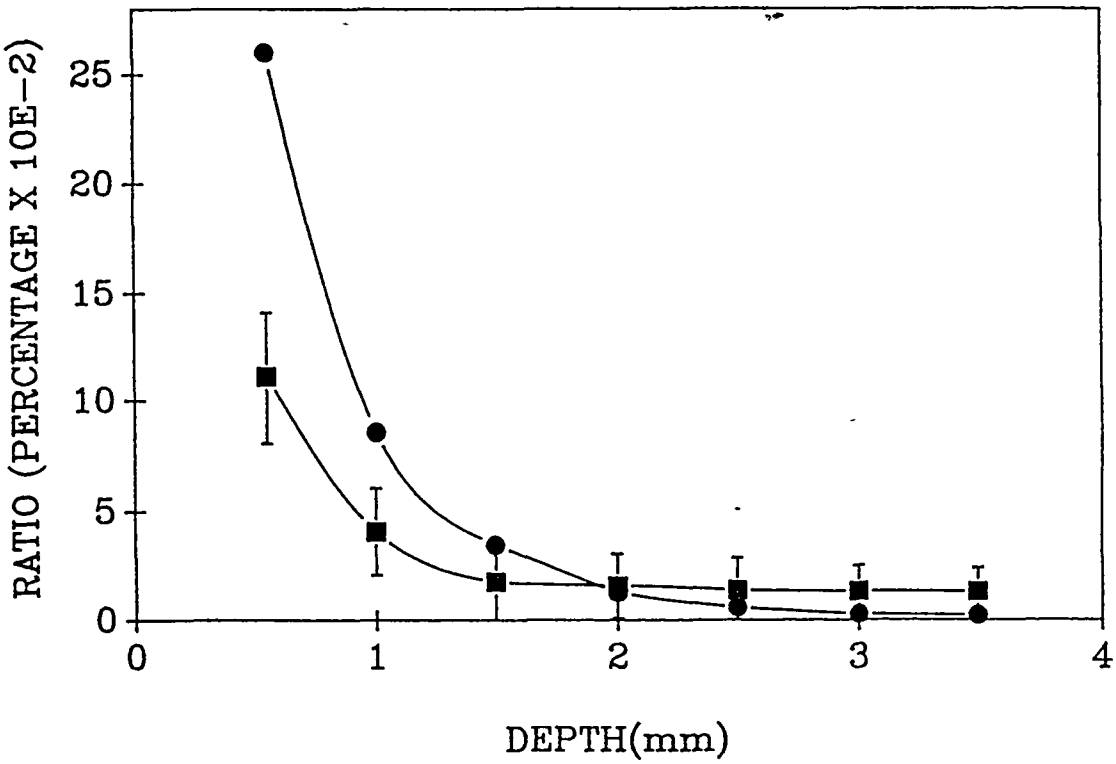


Fig 6 4 Healthy tissue depth plotted against signal ratio for both phantom (square points) and model (circular points) results.

## 6 6 Discussion

From fig 6 2 it is found that the sensitivity limit for the detection of Hp fluorescence from the tissue-tumour phantom using the detection system described in chapter 3 is circa 0.7$\mu$g of Hp per ml of $H_2O$ A similar experiment carried out on a solution of Hp and methanol (MeOH) yielded a sensitivity limit of just under 0 1$\mu$g/ml. These concentration sensitivity limits for the detection of Hp fluorescence are a factor of 10 less than those obtained in chapter 3 This is to be expected as in chapter 3 fluorescence is detected from Hp solutions contained in a 1 cm thick cuvette. This results in an excited volume of solution of 0 35 $cm^3$ The total tumour phantom volume (i e the glass slip containing the Hp solution ) is 0.08 $cm^3$ Thus the greater excited volume in chapter 3 would be expected to produce the most fluorescence

The dimensions of the tumour phantom were chosen to approximate the dimensions of the model tumour outlined in chapter 5 The design of the model tumour in turn was based on the common dimensions of early small cell carcinomas of tracheo-bronchial tract Thus the sensitivity limits obtained with our system for the detection of fluorescence from the tumour phantom can be considered to approximate clinical sensitivity limits for the detection of HpD marked tumours

One of the assumed advantages of the ratio method of fluorescent detection is that detection is independent of variations in fibre-bundle to sample distance Model predictions (chapter 5) indicate that this is only true for tumours of large diameters Fig 6 3 confirms this prediction The model and phantom results show a marked fall off with increasing distance The two plots are reasonably similar in both shape and magnitude with the phantom results showing a slightly higher signal ratio for distances greater than 1 cm This is due to the fact that in this experiment tissue simulating phantoms were not placed over the phantom tumour while in the model an overlying healthy tissue thickness of 1 5mm was assumed

In fig 6 4 the the effect of tumour depth on signal ratio is shown The plot shows good agreement between the experimental results and the model predictions are almost identical for tissue thicknesses greater than 1mm Clear differences in magnitude are apparent however at small tumour depths (i e overlying tissue thicknesses of less than 1 mm) The reason for this disparity is still unclear, but could possibly be due to limitations in the diffusion model at low depths (i e close to the tissue surface)

## 6 6 Conclusion

In this chapter a tumour-tissue phantom was designed in order to measure the response of the endoscopic instrument in simulated in vivo conditions The response of the instrument was then compared with theoretical predictions from chapter 5 in order to test the accuracy of the mathematical model

The phantom was designed to come as close as possible to the four criteria for the ideal tissue phantom as outlined in 6 2 The use of a liquid phantom of Evans blue and Intralipid fulfilled the first two criteria i e that the phantom should be capable of simulating the optical properties of a range of tissues and that these properties were stable and reproducible The use of the perspex block and the multiple glass slices makes it possible to control the geometry of the phantom Also the introduction of the "tumour slice" at selectable positions incorporates a tumour-tissue interface within the phantom These features go some way to fulfilling the two last criteria

A concentration of 1$\mu$g/g has been quoted as the concentration of HpD which has been observed to accumulate in tumourous tissue In this chapter a sensitivity limit of 0 7$\mu$g/ml has been obtained for a cylindrical tumour phantom consisting of a solution of Hp + $H_2O$ of dimensions diameter 8mm , and thickness 0.5mm The dimensions of the phantom were chosen to simulate clinical conditions. These results indicate that He-Ne excitation can excite

fluorescence from concentrations of Hp in solution (in simulated clinical conditions) lower than the concentrations of HpD measured to have accumulated in tumourous tissue. This implies that the He-Ne laser could represent an effective and improved excitation source for the detection of early tumours by means of fluorescence endoscopy

Figs 6 3 and 6 4 indicate good agreement between model predictions and results obtained using the phantom Similarly the dependence of signal ratio on fibre-bundle to tissue distance was not initially expected It was however predicted by the model and confirmed by the phantom experiments This seems to demonstrate that the assumptions made in the model are valid and that it is an accurate theoretical analysis of the use of our instrument for the excitation and detection of fluorescence through a turbid material

Finally this chapter confirms the validity of the model developed in chapter 5 and establishes a unique and effective tumour-tissue phantom for use in treatment and therapy planning for both fluorescence endoscopy and PDT To my knowledge this is the first complete tumour-tissue phantom described

# Chapter 7

# CONCLUSION

## 1 1 Summary and Discussion

The clinical use of fluorescence endoscopy for the detection of intra-cavitary cancer tumours is a quite recent development Early clinical trials using violet light excitation have disappointed researchers on account of the large numbers of false diagnosis obtained. The use of red excitation light has been proposed in order to alleviate some of these difficulties In this project the use of red He-Ne laser light (632 8nm) as excitation source in fluorescence endoscopy was investigated

The choice of red over violet light excitation is based on the facts that red light has greater penetration in tissue and its transmission is unaffected in the presence of blood Similarly the auto-fluorescence signal from healthy tissue is much lower at red than at violet wavelengths The main disadvantage of using red light is that it corresponds to one of the minor excitation peaks of HpD In chapter 2 an analysis of the photophysical properties of a solution of Hp + $H_2O$ was carried out using

a spectrofluorimeter Excitation spectra revealed that the excitation efficiency of Hp at 410nm is approximately 75 times greater than that obtained at 632nm Analyses of the fluorescent emission spectra for 410nm excitation revealed the presence of 3 emission bands centred at 585, 615, and 680nm respectively The emission spectra obtained for excitation at 632nm revealed a single emission band centred at 685nm.

Sensitivity limits i e the lowest concentration of Hp in solution for which fluorescence can be detected by the spectrofluorimeter, were obtained for both 410 and 632nm excitation. Comparison of these limits revealed a sensitivity limit for 410nm excitation 300 times lower than that obtained for 632nm excitation The limit for 410nm excitation was 1 x $10^{-3}\mu g/ml$ while for 632nm excitation a limit of 0 36$\mu g/ml$ was obtained This demonstrates why 410nm light has been the preferred excitation wavelength in fluorescent endoscopy The use of red excitation light however offers the possibility of detecting bloody tumours and cancers deeply embedded in healthy tissue It was shown in chapter 2 that 632nm light can excite fluorescence in a Hp solution, with a sensitivity limit of 0 36$\mu g/ml$ This limit is below the 1$\mu g/ml$ concentration of HpD quoted (27) to accumulate in tumourous areas and indicates that He-Ne laser excitation could be effective for the detection of remote tumours inaccessible to violet excitation

In chapter 3 a system was designed for the detection of Hp fluorescence incorporating a He-Ne laser as excitation source. The careful choice of photomultiplier tube and the use of an optical chopper and lock-in amplifier renders the system sensitive to low level fluorescent signals. The use of optical filters in the ratio method of fluorescent detection eliminates stray signals from the detection process. A fibre-bundle was introduced into the system in order to simulate tumour detection using a fibre-optic endoscope. The design of the fibre-bundle proved of crucial importance in terms of the efficiency of signal collection. In experimental tests the system attained a lowest measurable signal ratio of 6 x $10^{-3}$% . This corresponded to a sensitivity limit of 0.01$\mu$g/ml for solutions of Hp and Methanol and a limit of approximately 0.1$\mu$g/ml for a solution of Hp + $H_2O$. The sensitivity limit for Hp + $H_2O$ is lower than that obtained in chapter 3 for 632nm excitation using the spectrofluorimeter. This demonstrates the effectiveness of the system for the detection of Hp fluorescence.

The system designed and tested in chapter 3 could easily form the basis of a clinical instrument for the performance of fluorescence endoscopy. In this regard the ratio method of fluorescence detection offers the solution to some of the problems inherent in clinical measurements i.e. variations in surface topography and changes in efficiencies of exciting and detecting apparatus. However

as shown in chapters 5 and 6 it does not solve the problem of the variation in signal with fibre-bundle to tissue distance. The solution to this problem would be of great benefit to the clinician.

Of the methods reviewed in chapter 4 the diffusion theory seems to be the best method of describing laser interaction with highly scattering tissue as it allows for the presence of a collimated light flux within the tissue. Other techniques have been recently mentioned in the literature including the discreet ordinates and Monte-Carlo techniques. These methods are complex and prohibitive in terms of the computing time and power required. The diffusion theory is used as the basis for the clinical model described in chapter 5. Despite several simplifying assumptions in particular those concerning the 2-D grid-like structure of the tumour and the collection efficiency of the bundle the model generates predictions which are similar in magnitude to the in vitro results obtained in chapter 3. A target or model cylindrical tumour is assumed of diameter 5mm and thickness 0.5mm positioned 1.5mm beneath the surface of the tissue. The position and dimensions of the target tumour are chosen to model those of early small cell carcinoma of the tracheo-bronchial (TB) tract. By applying the lowest detectable signal ratio for the system (i.e. $6 \times 10^{-3}$%) to the plots generated by the model, predictions were made as to the size of tumour which could be detected. In this way

the model predicts that the target tumour can be detected to a distance of 2 4mm below the lumen of the TB tract Small cell carcinomas can present as a plaque of cells or as a thin sheet-like condition The model predicts that detection will occur for sheet-like small cell tumours as thin as 0 3mm and for plaques with diameters as small as 2 5mm

The model predictions obtained in chapter 5 are compared with the results of tests carried out on the tissue-tumour phantom with the endoscopic apparatus The construction of the phantom and the results obtained are discussed in chapter 6 Reasonably good agreement is found between phantom and model results Tests carried out on the phantom confirm the model prediction that signal ratio is not always invariant of fibre-bundle to sample distance Sensitivity levels for "superficial tumours" using the phantom are obtained at circa 0 5$\mu$g/ml for solutions of Hp + $H_2O$

The endoscopic system designed in this project has proven a cheap simple and effective instrument for the excitation and detection of Hp fluorescence It has been shown that fluorescence can be detected from quite low concentrations of Hp upon He-Ne laser excitation The sensitivity limit of 0 5$\mu$g/ml obtained from the phantom test is still below the 1$\mu$g/ml quoted by Doiron as the concentration of HpD that localises in tumourous areas It

remains to be seen if the phantom results obtained here are reproducible for HpD in clinical circumstances Similarly the accuracy of the model predictions and the "reality" of the phantom will not be determined until rigorous clinical testing of this type of endoscopic apparatus is undertaken The ratio method of fluorescent detection seems to have eliminated some of the clinical difficulties of performing fluorescence endoscopy. The most troublesome problem for the clinician i.e the variation of fluorescent signal with endoscope to tissue distance, remains unresolved. It is hoped that further investigation will eliminate this problem

## 1 2 Future Research and Development

The work carried out in this project is intended as an initial assessment of the use of He-Ne light for the detection of small tumours via fluorescence endoscopy Much further investigation is required before this technique becomes a viable clinical tool

From a design point of view attention should be focused on improving the collection efficiency of the fibre-bundle This may be achieved by increasing the number of collection fibres within the bundle The limiting factor in this regard is the ease with which the bundle can be manipulated within the endoscope Further research could also consider the addition of a small collecting lens to the bundle tip

The theoretical description of the instrument's performance, outlined in chapter 5, utilises the diffusion approximation for the description of light-tissue interaction While the results obtained from this model seem quite realistic other authors have shown it to be inaccurate at tissue interfaces and at local inhomogeneities This may cause serious inaccuracies in calculating the fluence rate at the tumour-tissue boundary For this reason other models of light-tissue interaction should be investigated Monte-Carlo simulation and the discreet ordinate method are possibilities as they allow for sudden changes in the scattering profile These models

may prove too complex however and a modified version of the diffusion approximation may be sufficient

The tumour-tissue phantom provides a quick and simple way of testing the efficiency of the instrument Ultimately the accuracy of the results obtained from the phantom depend on how closely it simulates biological tissue Very little work has been reported on the design of tissue phantoms for use in photomedicine Further research should be concentrated on the incorporation of local irregularities within the phantom and in the closer investigation of the in-vivo properties of tissue Results obtained from any future improved phantom should be compared with the predictions of a theoretical model (either the model outlined in chapter 5 or perhaps a more accurate model) The phantom should be developed to the point where model and phantom results coincide. The phantom could then be used in confidence to calibrate the instrument and predict its accuracy prior to clinical procedures Such a "realistic" phantom would also find many other applications in the field of photomedicine

The problem of signal ratio variation with bundle to tissue distance is one that must be resolved if fluorescence endoscopy is to become a viable clinical procedure For tumours with a surface area smaller than the surface area of intersection between the excitation and first collection fibres the ratio is seen to drop off with

distance This is due to increased detection of backscattered light This problem might be solved by using the excitation light reflected off the tissue surface as a reference This reflected signal should fall off with distance. If an accurate value for the refractive index of the tissue was known, detection of this signal would give the distance between the bundle and the tissue (P). Further measurements would yield whether P varied or not in each particular case. A scaling factor calculated from the model predictions could then be applied to the measurements in order to compensate for the fall off in detected signal ratio Techniques such as this should be investigated in order to alleviate the problem of signal ratio dependence on P

Finally, HpD is not the ideal photosensitiser. Its fluorescent emission upon He-Ne excitation is low and its ability to localise in tumourous tissue is erratic What is needed is a compound which has a strong fluorescence upon red light excitation and a good ability to localise. The development of such a compound is still under active investigation

References


1. Spikes, J.D. Porphyrin Localization and Treatment of Tumours. Ed. Doiron, D. and Gomer C. Liss Publications New York p.209-27 (1984).
2. Svanberg, S. Physica Scripta T26 p. 90-97 (1988).
3. Bonnett, R. New Scientist 28 Jan. 1989.
4. Raab, O. Z.Biol. Vol. 39 p.524 (1900).
5. von Tappeiner, H and Jesionek, A. Muench. Med. Wochschr. Vol. 1 p. 2042-4 (1903).
6. von Tappeiner, H and Jodblauer, A. F.C W Vogel Leipzig (1907).
7. Copeman, S.M. Brit.Med. J. Vol.2 p. 233 (1929).
8. Auler, H. and Banzer G. (1942) For reference see (1).
9. Figge, F.H. Proc. Soc. Exper. Biol. Med. Vol. 68 p. 640-1 (1948).
10. Lipson, R. and Baldes, E. Arch. Dermatol. Vol. 82 p. 508-16 (1960).
11. Lipson, R. and Baldes, E. J. Nat. Can. Instit. Vol. 26 (1961).
12. Lipson, R. and Baldes, E. Cancer Vol. 20 p. 2255-57 (1967).
13. Doiron, D. and Profio, E. Chest Vol. 76 p. 27-32 (1979).
14. Profio, A. and Doiron, D. Med.Phys. Vol 35 No. 10 (1982)
15. Mattielo, J. and Hetzel, F. Rev. Sci. Instrum. Vol. 57 p. 2339-2341 (1986).

16. Andersson, et al Med. Phys. Vol. 14 p. 633-636 (1987).

17. Lenz, P. Rev. Sci. Instrum. Vol. 59 p. 930-933 (1988).

18. See reference 14.

19. Cortese, D. and Kinsey J. Mayo Clinic Proceedings Vol. 53 p 594-600, (1978).

20. Zandomenenghi et al, Lasers Med. Sci. Vol. 3 No.2 (1988)

21. Drabkin, D. chapter 2 The Porphyrins Vol I Structure and Synthesis Dolphin, D. Ed. Academic Press Inc., New York, (1978).

22. Kessel, D. Photochem. Photobiol Vol. 851 (1984)

23. Diamond, I. Lancet No.2 Vol.1175 (1972)

24. Turro, N. chapter 3, The Science of Photobiology, Smith, K. Ed. Plenum Press N.Y. Sept. 1977.

25. Mayer-Betz (1913) for reference see (27)

26. Andreoni, A. and Cubeddu, R. Chemical Physics Letters Vol. 100 p.503-6 (1983).

27. Doiron, D. PhD thesis, University of California Santa Barbara 1982.

28. Bonnett, R. and Barenbaum, M. Journal Chemical Society Perkins Edition. Vol 1 p.3135-3139 (1981)

29. Richelli, F. and Grossweiner, L. Photochem. Photobiol. p. 599-06 (1984).

30. Moan, J. and Sommer, S. Photobiochem. and Photobiophysics Vol. 3 p. 93-103 (1981).

31. Pottier, R. Can. J. Chem. Vol. 63 p.1463-67 (1985).

32. Profio, E. and Doiron, D. Phys. Med. Biol. Vol. 5

p. 949-57 (1977).

33. Schenk, G Absorption of Light and Ultra-violet Radiation : fluorescence and phosphorescence emission. Allyn and Bacon Boston USA (1973).

34. Schwab, S. Anal. Chem. Vol. 56 No.12 p. 2199-2210 (1984).

35. Welch, A. Yoon, G and van Gemert M. Lasers in Surgery and Medicine Vol. 6 p. 488-493 (1987).

36. Ishimaru, A. Appl. Optics Vol. 28 No.12 p. 2210-2215 (1989).

37. Chandrasekhar S. Radiative Transfer, Dover Publications New York (1960).

38. Star, W. Marynissen, P. and van Gemert, M. Photochem. Photobiol. p. 151-159 (Jul/Aug 1987).

39. Kubelka, P. J. Opt. Soc. Am. Vol. 38 p. 448-57 (1948).

40. van Gemert, M. and Hulsbergen-Henning J. Arch. Dermatol. Res. Vol. 27 p. 429-39 (1981).

41. Wan, S. et al. Photochem Photobiol Vol. 34 p.493-9 (1981).

42. van der Putten, W. and van Gemert, M.J Phys. Med. Biol. Vol. 28 p. 639-45 (1983).

43. van Gemert, M. et al. Lasers in Med. Sci. Vol. 2 p. 295-302 (1987).

44. Groenhuis, R. Appl. Optics Vol. 22 p.2456-62 (1983).

45. Motamedi, M. et al. Appl. Optics Vol. 28 p.2230-7 (1989).

46. Yoon, G. et al. Appl. Optics Vol. 28 p.2250-5 (1989).

47. Moes, C. et al. Appl. Optics Vol 28 No. 12 p.2292-6 (1989).

48. Wilson, B. and Patterson, M. Phys. Med. Biol. Vol. 31 No.4 p. 327-356 (1986).

49. Mc Kenzie, A. Phys. Med. Biol. Vol. 30 No. 3 p.455-461 (1985).

50. Wilson, et al. Photochem. Photobiol. Vol. 42 p. 153-62 (1985).

51. Marynissen, J. and Star, W. Porphyrin Localization and Treatment of Tumours. Ed. Doiron, D. and Gomer C. Liss Publications New York p.133-48 (1984).

52. Takatani, S. PhD thesis Case Western University (1978).

53. Jori, G. From Photophysics to Photobiology Ed. Favre, Tyrell and Cadet. Elsevier Science Publishers Amsterdam p.373 (1987).

54. van der Putten, W. MSc thesis. The Department of Physics, Eindhoven University of Technology, The Netherlands.

55. Nossal, R. et al. Appl. Optics Vol.28 No.12 p.2238-2244 (1989)

56. Prahl, S. et al. Dosimetry of Laser Radiation in Medicine and Biology SPIE Institute Series Vol IS 5 p. 102-111 (1989).

## Appendix 1

In chapter 4 the three photon flux differential equations which form the basis of the diffusion approximation are outlined. These equations can be expressed as three simultaneous differentials as follows .

$$\frac{dF+(z)}{dz} = Y_1^*(z) = -E\, y_1(z) + F\, y_2(z) + B\, y_3(z)$$

$$\frac{dF-(z)}{dz} = Y_2^*(z) = -F\, y_1(z) + E\, y_2(z) - C\, y_3(z)$$

$$\frac{dFc(z)}{dz} = Y_3^*(z) = \qquad\qquad - D\, y_3(z)$$

$$\text{Let the Matrix A} = \begin{pmatrix} -E & F & B \\ -F & E & -C \\ 0 & 0 & -D \end{pmatrix}$$

The characteristic polynomial is thus

$$\begin{Bmatrix} -E-\lambda & F & B \\ -F & E-\lambda & C \\ 0 & 0 & -D-\lambda \end{Bmatrix}$$

which when the determinant is considered is equal to

$$(-D - \lambda) \left[ (-E - \lambda)(E - \lambda) + F^2 \right]$$

$$= -(D - \lambda) \left[ \lambda^2 - (E^2 - F^2) \right]$$

These equations yield the three eigenvalues - D, +/- $(E^2-F^2)^{1/2}$

Considering the eigenspace for firstly -D we get the equations

$$(-E + D)\, v_1 + F\, v_2 + B\, v_3 = 0$$

$$-F\, v_1 + (E + D)\, v_2 - c\, v_3 = 0$$

This yields by subtraction

$$v_1 (CD - CE - BF) + v_2(CF + BE + BD) = 0$$

therefore we can take

$$v_1 = (CF + BE + BD)$$

$$v_2 = (CD - CE - BF)$$

This gives $Cv_3 = -F\,(CF + BE + BD) + (E + D)(BF + CE - CD)$

$$= -CF^2 + C(E + D)(E - D)$$

therefore

$$v_3 = E^2 - F^2 - D^2$$

This yields an eigen vector for eigen value - D of

$$\begin{pmatrix} CF + BE + BD \\ BF + CE - CD \\ E^2 - D^2 - F^2 \end{pmatrix}$$

In the same way for the eigen value of $+(E^2 - F^2)^{1/2}$ an eigen vector of

$$\begin{pmatrix} F \\ E + (E^2 - F^2)^{1/2} \\ 0 \end{pmatrix}$$

is obtained, and the eigen value of $-(E^2 - F^2)^{1/2}$ yields the eigen vector of

$$\begin{pmatrix} F \\ E - (E^2 - F^2)^{1/2} \\ 0 \end{pmatrix}$$

The general solution of the three simultaneous equations is thus

$$Y_{\substack{i=1,3 \\ 1}}(z) = \alpha e^{-Dz}\begin{bmatrix} CF + B(E + D) \\ BF + C(E - D) \\ E^2 - D^2 - F^2 \end{bmatrix}$$

$$+ \beta e^{z(E^2 - F^2)^{1/2}} \begin{bmatrix} F \\ E + (E^2 - F^2)^{1/2} \\ 0 \end{bmatrix}$$

$$+ \gamma e^{-z(E^2 - F^2)^{1/2}} \begin{bmatrix} F \\ E - (E^2 - F^2)^{1/2} \\ 0 \end{bmatrix}$$

where

$$C = \frac{\sigma_s}{4}(2 - 3g)$$

$$B = \frac{\sigma_s}{4}(2 + 3g)$$

$$D = \sigma_a + \sigma_s$$

$$E = [2\sigma_a + 3/4(\sigma_a + (1-g)\sigma_s) - \sigma_a]$$

$$F = [3/4(\sigma_a + (1-g)\sigma_s) - \sigma_a)]$$

Also let

$$G = CF + B(E + D)$$

$$H = BF + C(E - D)$$

$$I = E^2 - D^2 - F^2$$

$$J = E + (E^2 - F^2)^{1/2}$$

$$K = E - (E^2 - F^2)^{1/2}$$

$$L = (E^2 - F^2)^{1/2}$$

Thus the three photon flux equations can be reduced to three simultaneous and expressed as

$$F+(z) = \alpha e^{-Dz}(G) + \beta e^{Lz}(F) + \gamma e^{-Lz}(F)$$

$$F-(z) = \alpha e^{-Dz}(H) + \beta e^{Lz}(J) + \gamma e^{-Lz}(K)$$

$$Fc(z) = \alpha e^{-Dz}(I) + 0 + 0$$

```
10 REM  A PROGRAM TO CALCULATE LIGHT INTENSITIES
20 REM  AT THE DISTAL END OF THE F/OPTIC CABLE
45 DIM A(10)
50 INPUT "ENTER REFRACTIVE INDEX N";N
60 INPUT"HOW FAR ARE THE FIBRES FROM THE SAMPLE";P
80 INPUT "ENTER NUMERICAL APERTURE"NA
100 SIG=(NA/N)^2)*PI
110 R=SQR(SIG/PI)*P
120 ANG=2*DEG(ATN(R/P))
130 A=PI*R^2
140 INPUT"WHAT IS THE POWER OF YOUR LIGHT SOURCE";POW
150 INPUT"WHAT IS THE COUPLING LIGHT EFFICIENCY";EFF
160 I=POW*EFF/A
170 PR. "NUMERICAL      AREA       INTENSITY       ANGLE"
180 PR." APERTURE        CM2         mW/cm2          DEG "
190 PR. NA ,A   ,I,   ANG
191 A(1)=I
192 A(2)=NA
193 A(3)=R
194 A(4)=P
200 IN."ENTER FILENAME";FILE$
210 X=OPENOUT (FILE$)
215 FOR I=1 TO 4
216 PR.#X,A(I)
217 N.I
240 CLOSE#0
260 END
```

```
10 REM PROGRAM TO CALCULATE THE TRANSMISSION OF LIGHT
20 REM                THROUGH TISSUE
60 DIM FPLUS(200)
70 DIM FPLUS1(200)
80 DIM FMINUS(200)
90 DIM FMINUS1(200)
100 DIM FC(200)
110 DIM A(10)
115 DIM FO(210)
130 DIM FLU (200)
140 PT=0
145 FLU1=0
146 REM ************************************************
147 REM     ENTERING MODEL CONDITIONS
148 REM ************************************************
150 PR."ENTER (1)ABS.(2)SCATT.(3)ANIS.COEFFS"
160 IN.A,S,G
170 IN."ENTER THE DEPTH OF TUMOUR IN TISSUE (mm)";TD
190 IN."ENTER THE TUMOUR THICKNESS (mm)";TT
200 IN."QUANTUM EFFICIENCY OF HP";QE
210 IN."EXTINCTION COEFFICIENT";EX
220 IN."CONCENTRATION OF HP IN TUMOUR";CN
221 REM ************************************************
222 REM      READING EXCITATION LIGHT INTENSITY
223 REM               AT TISSUE SURFACE
224 REM ************************************************
231 IN."ENTER FILENAME";FILE$
232 X=OPENIN(FILE$)
233 FOR I=1 TO 4
234 IN.#X,A(I)
235 N.I
```

```
236 REM **********************************************
237 REM              INITIALISING VARIABLES
238 REM **********************************************


240 Y=2.3*EX*QE*CN*(TT/51)
250 E=(A+3/4*(A+(1-G)*S))
260 F=(3/4*(A+(1-G)*S))
270 B=S*(2+3*G)/4
280 C=S*(2-3*G)/4
290 D=A+S
300 A1=C*F+B*(E+D)
310 A2=SQR(E^2-F^2)
320 A3=B*F+C*(E-D)
330 A4=E+A2
340 A5=E-A2
350 A6=(E^2-F^2-D^2)
360 ALP=A(1)/A6
370 X=TT+TD
380 B1=-ALP*A1/F
390 B2=ALP*((A1*A4/F)*EXP(A2*X)-A3*EXP(-D*X))
400 B3=EXP(A2*X)*A4-EXP(-A2*X)*A5
410 BETA=(B2/B3)+B1
420 GAM=-(B2/B3)
421 REM ******************************************************
422 REM     CALCULATING LIGHT FLUENCE RATE AT DEPTH
423 REM ******************************************************
430 MODE7
431 Z=0.0
440 L=0
470 FOR I= 1 T0 200
480 FPLUS(1)= ALP*A1*EXP(-D*Z)+BETA*F*EXP(A2*Z)+GAM*F*EXP(-A2*Z)
490 FMINUS(I)= ALP*A3*EXP(-D*Z)+BETA*EXP(A2*Z)*A4+GAM*EXP(-A2*Z)*A
500 FC(I)=ALP*A6*EXP(-D*Z)
510 FLU(I)=2*(FPLUS(I)+FMINUS(I)))+FC(I)
560 Z=Z+X/200
570 IF Z < TD THEN GOTO 700
571 REM ******************************************************
572 REM        CALCULATING THE FLUORESCENT YIELD WITHIN THE
573 REM                          TUMOUR AREA
574 REM ******************************************************
580 FO(I)=Y*FLU(I)/2
700 L=L+1
710 P.L
720 N.I
730 REM ******************************************************
731 REM     WRITING TO A DATA FILE
732 REM ******************************************************
740 IN."ENTER FILENAME$";FILE$
750 B=OPENOUT(FILE$)
760 FOR I=150 T0 200
770 PR.#B,FO(I)
780 N.I
785 CLOSE#0
1050 END
```

```
10 REM THIS PROGRAM CALCULATES THE AMOUNT OF FLUORESCENCE
20 REM FROM THE TUMOUR WHICH REACHES THE COLLECTION OVERLAP
30 REM          AREA ON THE TISSUE SURFACE
40 IN."ENTER (1)ABS (2)SCATT COEFFS";A,S
50 DIM P(48,48)
60 DIM A(48,48)
70 DIM F0(55)
71 C*************************************************************
72 C      CALCULATING THE FLUORESCENCE AT ONE POINT ON THE
73 C       TISSUE SURFACE FROM ALL THE POINTS IN THE GRID
74 C          STRUCTURE OF THE TUMOUR


75 C*************************************************************
80 D=A+S
90 IN."ENTER FILENAME";FILE$
100 B=OPENIN(FILE$)
110 FOR F=0 TO 50
120 IN.#B,F0(F)
130 N.F
180 IN."ENTER RADIUS OF TUMOUR";RADI
190 H=RADI/46
200 IN."ENTER HEALTHY TISSUE THICKNESS";L
210 IN."ENTER TUMOUR THICK";THICK
220 FOR F=0 TO 50
230 FOR J=0 TO 45
240 FOR I=0 TO 45
250 R=SQR((L^2)+((I*H)^2)+((J*H)^2))
260 P(I,J)=((H^4)*(1E-7))*(INT(F0(F)*(D^2)*EXP(-D*R)*1E7/(4*PI*A*R)
270 N.I                                                    + P(I,J)
280 N.J
290 L=L+THICK/50
300 N.F
301 C*************************************************************
302 C SHUFFLING THE ARRAY IN ORDER TO CALCULATE THE FLUORESCENCE
303 C  AT EACH POINT ON THE TISSUE OVERLAP AREA
304 C*************************************************************

310 IN."ENTER OVERLAP SURFACE AREA";SA
320 S1=SA/46
330 Z=RADI/S1
340 Y=0
350 FOR K=0 TO 45
360 X=0
370 FOR L=0 TO 45
380 FOR I= 0 TO Z
390 FOR J= 0 TO Z
400 T=ABS(J+X)
410 S=ABS(I+Y)
420 A(K,L)=P(S,T)+A(K,L)
430 N.J
440 N.I
450 X=X-1
460 N.L
470 Y=Y-1
480 N.K
```

```
490 IN."ENTER FILENAME";FILE$
500 B=OPENOUT(FILE$)
510 FOR I= 1 TO 45
520 FOR J= 1 TO 45
530 PR.#B,A(I,J)
540 N.J
550 N.I
560 CLOSE#0
570 END
```

```
40 DIM P(48,48)
50 IN."ENTER FILENAME";FILE$
60 X=OPENIN(FILE$)
70 FOR I=0 TO 45
80 FOR J=0 TO 45

90 IN.#X,P(I,J)
100 SIGNAL = 4*P(I,J)+SIGNAL
110 N.J
120 N.I
130 PR."SIGNAL IS         ",SIGNAL
140 END
```

Acknowledgements

I would like to thank the following people without whom this project would not have come to fruitition. Firstly my supervisor Wil van der Putten whose encouragement patience and enthusiasm were much appreciated. Secondly the staff and post-grads of the Physics Department D.C.U whose comradeship and good humour were an inspiration. In particular I would like to thank the following people : Colin Potter for his help in constructing the fibre-bundle, Charles Markham and Niel O'Hare for use of their much sought after computing facilities and Jean-Paul Mosnier for his help with some of the calculations. Finally I would like to thank my family and friends for the interest and forbearance shown during the course of this project.

The project was partially funded by the Health Research Board.